Biochemical Characterization of the Human m^{6}A-Methyltransferase Complex

DISSERTATION ZUR ERLANGUNG DES DOKTORGRADES
DER NATURWISSENSCHAFTEN (DR. RER. NAT.)
DER FAKULTÄT FÜR BIOLOGIE UND VORKLINISCHE MEDIZIN
DER UNIVERSITÄT REGENSBURG

vorgelegt von

Sam Ringle

aus

Pirmasens

im Jahr 2017

Der Promotionsgesuch wurde eingereicht am:
15.02.2017

Die Arbeit wurde angeleitet von:
Prof. Dr. Gunter Meister

Unterschrift:

Sam Ringle

"In den grundlegenden Fragen muss man naiv sein. Und ich bin der Meinung, dass die Probleme der Welt und der Menschheit ohne Idealismus nicht zu lösen sind. Gleichwohl glaube ich, dass man zugleich realistisch und pragmatisch sein sollte."

Helmut Schmidt

Abstract/Summary

N^6-methyladenosine (m^6A) is one of the most prevalent RNA modifications present within messenger RNAs (mRNAs), with an average of 3-5 modified adenosines per transcript. The methyltransferase-like protein 3 (METTL3) and methyltransferase-like protein 14 (METTL14) have been reported to form a stable dimeric complex that is responsible for the formation of m^6A within mRNAs. The METTL14 subunit of this methyltransferase complex has been proposed to be the catalytic subunit. This conclusion was, however, drawn from analyzing each subunit separately and not within the context of the assembled complex. Here, point mutations within METTL3 resulted in the complete loss of catalytic activity within the binary complex, whereas no such effect was observed when mutating METTL14. In addition to this, cross-linking experiments using tritiated S-adenosyl-methionine (SAM) and recombinantly purified METTL3/14 suggest that METTL3 is also the only subunit that can efficiently bind to the methyl donor. A third aspect that was analyzed in this work was if the METTL3/14 complex can specifically recognize its RNA substrate. Electrophoretic mobility shift assays (EMSAs) that were conducted suggest that the protein complex mostly binds to polyanionic molecules in an unspecific manner and that target specificity is introduced by other means.

During the experimental phase of this work, not much was known about the architecture of the methyltransferase. Here,experiments using truncation constructs of METTL14 provide evidence that the MTA70 domain of this protein is essential for the dimerization with METTL3. An additional protein, namely the Wilms' tumor 1-associating protein (WTAP), has been reported to stably associate with the methyltransferase complex through a direct interaction with METTL3. This interaction between METTL3 and WTAP was also examined in this work. The data collected from immunoprecipitation experiments could demonstrate that the first N-terminal α-helix within METTL3 binds to a small protein region within WTAP's N-terminus. Closer examination of these identified interaction surfaces led to the hypothesis that most likely coiled-coils promote the observed METTL3-WTAP interaction.

All of the above investigated proteins are localized within the cell nucleus. Many nuclear proteins rely on a nuclear localization signal (NLS) for them to be translocated across the nuclear envelope. Here, mutational analysis revealed that WTAP and METTL3 each possess a classical NLS sequence that is functional. For METTL14, this work provides evidence that METTL14 does not have a NLS embedded within its primary sequence and that its localization depends on the heterodimerization with METTL3.

Contents

1. Introduction

1.1 The epitranscriptome

The genetic information encoded in DNA and RNA is build-up by the four different bases adenine, guanine, cytosine and thymine, or in case of RNA, uracil. Early analysis of the total pool of RNA synthesized by the cell, termed the transcriptome, has revealed that other bases besides the canonical ones can be found in large quantities. To date, over 140 different base modifications have been identified in RNA and arise through modification reactions of the "standard" bases that occur post-transcriptionally.[1] Some examples for non-canonical nucleosides present in RNAs are pseudouridine (Ψ), inosine, 5-carbamoylmethyluridine and N^6-methyladenosine (m^6A). Additionally to the presence of a variety of bases, it has been reported that both the ribose and the phosphate moiety within RNA can undergo different modifications as well.[2–6] This collection of different RNA modifications adds a second layer of information onto the transcribed genetic information and has coined the term of the epitranscriptome.[7–9]

It has been proposed that several of these modifications found in different RNA species influence the stability or structure of the RNA. For instance, 5-methylcytosine (m^5C) can be found in several different transfer RNAs (tRNA). Publications have shown that the presence of this modification at the C38 position of the tRNAs Asp^{GTC}, Val^{AAC} and Gly^{GCC}, catalyzed by the protein Dnmt2 (also known as Trdmt1), enhances the stability of the RNA under normal and stress conditions.[10–13] An example for the structural influence of an RNA modification is the pseudouridylation of tRNAs. It has been reported that this modification can rigidify the tRNA structure by locking the ribose of Ψ in the C3'-endo conformation.[14,15]

The importance of RNA modifications is, however, not only confined to the structure and stability of certain transcripts. It has been reported that non-canonical bases are vital for the function of different ribonucleoprotein complexes. Ψ is again a prominent example. This base modification influences the binding affinity of the ribosome towards tRNAs. Therefore, a depletion of pseudouridylation leads to a reduction of translation efficiency and fidelity.[16–18] Another base modification that has an influence on translation is 7-methylguanine (m^7G) that forms the "methyl-cap" of mRNAs.[19–21] This modification is established at the 5' end of mRNAs and is directly and specifically bound by a protein termed eukaryotic initiation factor 4E (eIF4E).[22–24] eIF4E together with eIF4A and eIF4G forms a complex (termed eIF4F) that is essential for the recruitment of the 43S pre-initiation complex to the mRNA.[25–28] m^7G-binding

facilitated by eIF4E is considered the rate-limiting and vital step in the initiation of protein synthesis.[29] Besides translation, the m^7G-cap is also responsible for the nuclear export of mRNAs and is considered a general stability factor for these transcripts.[30–33] Taken together, these examples highlight the necessity and importance of RNA modifications and their contribution to a variety of cellular processes.

Even though the large repertoire of different modifications have been known now for over half a century, the exact molecular modes of action for many of them remain elusive. A great majority of these non-canonical RNA building blocks have been identified and studied in tRNAs and ribosomal RNAs (rRNA). Analysis of RNA modifications was mostly restricted to these two ncRNA species, as these transcripts are highly abundant in the cell and larger quantities can be easily extracted. It was not until recently that more sensitive methods have been developed, allowing the detection and deeper analysis of RNA modifications in all classes of transcripts present in a cell.

1.2 Eukaryotic internal mRNA modifications

It was long thought that eukaryotic mRNAs harbored only a handful of modifications and that their presence was restricted to the 5'- and 3'-end of the transcript. The m^7G-cap and 2'-OH methylation of the first two transcribed nucleotides are the most commonly known representatives of mRNA modifications.[34–39] However, recent publications could show that some of the same modifications found in ncRNAs were also present in mRNAs of different eukaryotes.[40,41] So far the nucleosides inosine, Ψ, m^5C, N^1-methyladenosine and m^6A have been identified in internal sequences of mRNAs (Fig. 1.1).

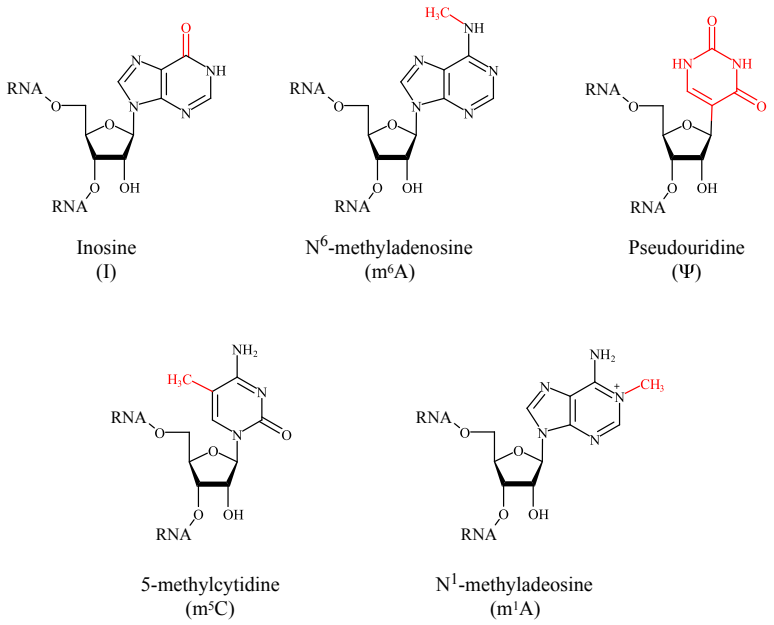

Figure 1.1 Chemical structure of base modifications found in the internal sequences of eukaryotic mRNAs The nucleosides inosine, N^6-methyladenosine, pseudouridine, 5-methylcytidine and N^1-methyladenosine have been found in internal sequences of eukaryotic mRNAs. All modifications are established by highly specialized enzymes that act upon the mRNA posttranscriptionally.

1.2.1 Inosine

Insosine is an RNA modification that has been extensively studied in mRNA during the last two decades. The base adenine is converted into hypoxanthine during a process that has been termed A-to-I RNA editing. This process has been first described to be involved in the unwinding of exogenous double-stranded RNA (dsRNA) in crude extracts derived from *Xenopus laevis* oocytes, embryos or even from mammalian cells.[42–44] This activity was distinct from that observed in the modification of tRNAs and of the purine catabolism. Later, proteins belonging to the adenosine deaminase acting on RNA (ADAR) family were identified as the enzymes responsible for the specific activity observed in *Xenopus*.[45,46] The presence of ADAR-mediated formation of inosine in mRNA remained a matter of controversy until several reports have shown that this RNA modification was indeed harbored in mRNAs and showed a tissue-specific abundance.[47–49] Inosine was later readily mapped within mRNAs via high-throughput sequencing technology and the fact that this non-canonical base is recognized as a guanosine during reverse transcription (RT).[50] Usage of this method led to the identification of 1600 genes.[48] A to I

editing seems to be a stochastic event, as no specific enrichment of this modification can be found within defined regions of mRNA, such as the 5'- or 3'-untranslated region (UTR).

ADAR1 and ADAR2 are the best studied representatives of the ADAR protein family. Investigation of both enzymes have shed light on how mRNA editing is achieved and what are the biological consequences of this event. Both ADAR1 and 2 have been shown to localize in the nucleus and modify messenger transcripts.[51–53] In addition to its presence in the nucleus, ADAR1 can also be found in the cytoplasm.[54,55] Due to this distribution pattern, the event of A-to-I editing can occur in both cellular compartments.[56] A prerequisite for the deamination reaction promoted by ADARs is the presence of a double-stranded region within the mRNA. These double-stranded regions normally span a length of more than 20 base pairs (bp) and can be formed inter- or intramolecularly.[57] This is the minimal requirement towards the target for an efficient removal of the amino group at the C6 position of adenine. However, some sort of specificity is needed to explain substrates that are either edited exclusively by ADAR1 or ADAR2, whereas others are modified by both enzymes.[58–60] The necessity of double-stranded regions make certain transcripts to ideal substrates such as mRNAs that harbor repetitive elements (such as Alu elements) in their UTRs.[61,62] These sequences derived from transposable elements tend to form secondary structures with double-stranded regions and can, therefore, be targeted by ADARs. Other sites have also been identified within the coding region of mRNAs. Editing events in this region can lead to amino acid recoding, as inosine is recognized as a guanine by the translation machinery.[63–65]

Through the event of recoding, some ADAR-targeted transcripts give rise to proteins with a single amino acid substitution. These in return can have a great impact on the function of the protein.[66,67] The presence of inosine within 3'-UTR suggests that these deamination sites might have a regulatory potential. Indeed reports have shown that this type of RNA editing can influence the cellular localization of an mRNA or even its stability.[68–70] Beside the regulation of a single transcript, a single A-to-I editing event can influence multiple transcripts. This can be explained through the modification of mRNA transcripts that give rise to a microRNA (miRNA). A deamination of an adenosine within the seed sequence leads to the regulation of different target transcripts compared to the unmodified miRNA.[71] As these molecular consequences suggest, A-to-I RNA editing can have a significant biological impact. Studies have shown that the inactivation of ADARs can lead to severe phenotypes such as embryonic lethality or death shortly after birth.[58,72,73] Human diseases have been as well associated with the mutations of ADAR proteins which lead to neural dysfunction or alteration of skin pigmentation.[74,75]

1.2.2 5-methylcytidine

Methylation at the C5-position of cytosine is a prominent and well studied modification in the field of epigenetics.[76] The molecular consequence of this DNA modification is mostly repression of gene expression and is essential in several processes such as genomic imprinting, stem cell differentiation and transposon silencing.[77–80] This modification is, however, not restricted to DNA. m^5C has been found and studied in different ncRNAs such as tRNAs and rRNAs. In 2012, this modification has been detected with the help of bisulfite sequencing in different human mRNA transcripts as well.[81] 8495 methylated cytosines were mapped and found to be enriched within the 3'-UTR of messengers. Controversial to this finding, another transcriptome-wide sequencing method could not validate these initial findings.[82] This study involved the treatment of cells with 5-azacytidine coupled with immuno precipitation of the RNA that incorporated the cytidine analog with an anti-azacytidine antibody. The authors did not selectively enrich for mRNAs in their experimental design. Therefore, the absence of these transcripts in their sequencing data could be the result of a reduced sensitivity compared to the mRNA enrichment strategy and the bisulfite sequencing approach used by Squires *et al.*[81] Since these initial publications, there have been no further transcriptome-wide m^5C-sequencing reports published. Therefore, the exact number of transcripts and abundance of this mRNA modification has to be further validated.

The methyltransferase(s) responsible for establishing the cytosine methylation is also a matter of debate. Evidence has been provided that the tRNA methytransferases NSun2 and DNMT2 methylate the 5'- and 3'-UTR of different mRNAs.[81,83] A different study concentrating on NSun2 reported that this protein does not bind mRNAs except for one, namely NSun2.[84] Due to the fact that the methyltransferase(s) has not been clearly identified, little is known about the exact biological function of m^5C in mRNAs. The purposed enrichment of this modification in 3'-UTRs, based on Squires *et al.*, would suggest a regulatory role.[81] So far, only a single study hints to a stabilizing effect on the $p16^{INK4}$ mRNA.[83] A different study using cells that carry a loss of function mutation in one or both known RNA m^5C-methyltransferases (NSun2 and DNMT2) showed no difference in mRNA expression or stability when compared to their wild-type counterparts.[13] This suggests that m^5C does not have a global stabilizing effect on mRNA transcripts. Further investigations are needed in order to identify the exact methytransferase(s) that establishes cytosine methylation. Furthermore, efforts have to be made in resolving the conflicting claims that are present in the field concerning the abundance, presence and function of m^5C within mRNA.

1.2.3 Pseudouridine

Pseudouridine is one of the more recent RNA modifications found within the internal sequences of mRNAs. Three independent studies mapped this modification within mRNAs using a sophisticated high-throughput sequencing protocol.[85–87] All three groups enriched mRNAs and treated the RNA with N-cyclohexyl-N'-(2-morpholinoethyl)carbodiimide metho-p-toluene sulfonate (CMC) to selectively label pseudouridines. The bulky carbodiimide moiety leads to a termination of the reverse transcription reaction one nucleotide after the pseudouridylated site.[88] This approach allowed to map pseudouridines in 41 to 238 protein coding transcripts in yeast and between 89 to 300 mRNAs in humans, depending on the study and the bioinformatic pipeline used to analyze the sequencing data.

These transcriptome-wide mapping studies could also elegantly identify the enzymes responsible for establishing Ψ within messengers. Interestingly, mRNAs share the same modifying proteins as tRNAs and rRNAs, namely the pseudouridine synthase (PUS) enzymes.[85–87] Isomerization of the uridine moiety can be catalyzed by PUS proteins using two different strategies. One arm of this protein family binds snoRNAs of the H/ACA box family that functions as a guide.[89,90] The protein Cbf5p in *Saccharomyces cerevisiae* and NAP57 in humans is the catalytic subunit of this PUS RNP complex.[91–93] The other arm of the PUS family can generate Ψ in a snoRNA independent manner.[94–97] In the transcriptome-wide studies, depletion of either Cbf5p or Nap57 abolish certain pseudouridine sites within mRNAs, whereas other sites were unaffected. The latter suggests that the other sites are modified via the snoRNA-independent mechanism. Deletion strains of *S. cerevisiae* identified the proteins Pus1-4p, Pus6p, Pus7p and Pus9 as the responsible enzymes for the pseudouridylation in mRNA without the necessity of a nucleic acid as a guide.[85,87] In humans, so far only the proteins Pus4 and Pus7 have been linked to the isomerization of uridine in messengers.[87]

Mapping of Ψ could show that the modification is not enriched within a certain region of a mRNA transcript but seem to be evenly distributed.[85] To date, little is known about the biological implications of this mRNA modification. Due to the capacity of Ψ to facilitate unusual base pairing, the presence of this modification within an open reading frame (ORF) could lead to a recoding event similar to those observed for inosine (see 1.2.1). An *in vitro* study using artificial mRNA containing Ψ could show that this non-canonical base can lead to the recoding of a stop-codon into an amino acid and, thus, leads to the synthesis of a longer polypeptide.[98] Interestingly, mRNA pseudouridylation seems to be a regulated process. Schwartz and colleagues could show that upon heat-shock of *S. cerevisiae* cultures, Pus7p is translocated from the nucleus into the cytoplasm. After relocation, Pus7p effectively pseudouridylates

mRNAs leading to a heat shock specific profile.[87] The induction of pseudouridylation has also been shown in human cell lines upon serum starvation, underlining that this modification can be induced via external stimuli and this can be mediated into a biological response.[85] Further studies will be needed to investigate other conditions that induce pseudouridylation, its biological impact and how this modification is translated into a response.

1.2.4 N^1-methyladenosine

N^1-methyladenosine (m^1A) is the youngest member of internal mRNA modifications. All what is known to date about this mRNA base modification has been described by two independent groups in 2016.[99,100] Both groups applied a transcriptome-wide and antibody-based approach to investigate the topology of m^1A within mRNA. Each protocol first enriches for poly-A RNAs that are subsequently chemically fragmented to approximately 100 to 150 nucleotides (nts). RNAs containing m^1A are then specifically enriched using an antibody raised against the modification. After immunoprecipitation, the antibody-bound RNA is retrieved and subjected to a transcriptome-wide RNA sequencing protocol, in order to identify regions containing m^1A. A drawback of this method used in both studies is that the position of m^1A cannot be determined at a nucleotide resolution. Sequencing of anti-m^1A enriched RNA fragments allowed the annotation of "m^1A-peaks", which span a region between 55 and 150 nts. Nevertheless, this approach could identify between 887 and 4151 mRNA transcripts that harbor this modification. Additionally, the authors mapped the methylation at the N1 position of adenine within the 5'-UTR of human mRNAs and/or in close vicinity (approx. 25 nt up- or downstream) of the start codon.[99] On average, only a single m^1A peak is present on a methylated transcript. This typical pattern is also seen in mRNAs from mice suggesting conservation between humans and rodents.[99] This pattern is, however, not conserved in all eukaryotes. Sequencing of the m^1A methylomes from *Schizosaccharomyces pombe* and *S. cerevisiae* revealed a different profile. Within these organisms methylation is mostly found within the ORF of mRNAs, whereas the flanking UTRs display a lower abundance.[99]

The m^1A-methyltransferase(s) for mRNA has not been identified yet. So far, the potential candidates are enzymes that have been shown to methylate ncRNAs such as tRNA or rRNA.[101,102] The transcriptome-wide analysis of m^1A could not reveal a consensus sequence that could narrow down potential candidates. The data provided from the two studies could show that a prerequisite for methylation are GC-rich regions. It has been experimentally demonstrated that the potential enzyme establishing m^1A utilizes S-adenosyl-methionine (SAM) as methyl donor for the methylation reaction.[99] Interestingly, a potential demethylase has already been identified that can revert the reaction. This is an interesting

feature as modifications such as pseudouridylation, cytosine methylation and deamination of adenine have so far been reported to be permanent marks. ALKBH3 is the enzyme responsible for the demethylation of m^1A and is a member of the AlkB protein family and most likely utilizes an oxidation reaction to remove the methyl-group as already described for other RNA demethylases (see 1.5.1.1). A knock-out cell line of this demethylase has revealed numerous m^1A peaks that are normally removed within wild type cells. This in return suggests some sort of specificity as only certain methylation sites/transcripts are targeted by the protein.

The fact that m^1A is a reversible modification and present in the 5'-UTR of mammals suggest that this methylated adenosine could be a regulatory element involved in different biological pathways. It has been shown by the two sequencing studies that the m^1A-methylation patterns respond to different stress stimuli such as heat shock, serum/glucose-starvation and oxidative-stress. This suggests that the methylation profile is differentially regulated during normal and stressed conditions. The direct biological effects of m^1A have yet to be investigated. On a molecular level, this base modification interrupts the Watson-Crick base pairing interface and generates a positive charge at the N1 position under physiological conditions.[103] This modification can therefore facilitate the remodeling of RNA structures, which has already been demonstrated in tRNAs.[104,105] This in return could then lead to a biological response. It is also imaginable that both the positive charge and the methyl group could be a potential binding substrate for certain proteins (see 1.4.3) or repel others that would bind the RNA in an unmethylated state. Future investigation will be needed to explore all the proteins that establish, read and modulate this type of methylation and the biological function they promote.

1.2.5 N^6-methyladenosine

The most prevalent internal modification found within mRNA is m^6A. Using a quantitative liquid chromatography - mass spectrometry approach, it has been shown that this modification contributes to 0.5 to $1\,\%$ of the total adenosine pool incorporated into mRNA.[106,107] The discovery that m^6A is such an abundant mRNA modification lead to a renaissance in the field of RNA modifications. Investigations on this adenosine methylation also coined the term of the epitranscriptome. Due to its importance in the field, the next chapters discuss several points such as the topology, the biological consequence and the proteins that establish, remove and bind to this modification.

1.3 Topology of m^{6}A within mRNA

The presence of m^{6}A in RNA has been known since the nineteen-fifties and -sixties.[108,109] This modification has mostly been detected in different ncRNA species such as tRNAs, small nuclear RNAs (snRNAs) and rRNAs.[110] Studies conducted several years later could show that m^{6}A is also present in mRNAs.[111–114] However, analysis on the distribution of this modification was limited due to the lack of appropriate methods. Until recently, the only known messenger that has been shown to harbor m^{6}Aand which could be biochemically validated was the bovine mRNA encoding for prolactin.[115]

In 2013, a first method was developed to map the presence of m^{6}A on a transcriptome-wide scale.[40,41] The protocol first utilizes an anti-m^{6}A antibody to enrich methylated RNA fragments of about 100 nts. Next, the antibody-bound RNA is retrieved and then submitted to high throughput sequencing to identify m^{6}A-peaks within mRNAs (similar to the approach used to map m^{1}A, see 1.2.4). The combination of immunoprecipitation and RNA sequencing has been termed m^{6}A-seq and allowed the identification of m^{6}A in transcripts derived from more than 7000 human and 3400 mice genes. *S. cerevisiae* and *Arabidopsis thaliana* are two other model organisms whose m^{6}A-profile has been investigated using the same antibody-based approach. A total of approximately 1200 methylated mRNAs could be identified for yeast whereas 6300 transcripts were found to be methylated in *A. thaliana*.[116,117] All transcriptome-wide studies could clearly demonstrate that the presence of m^{6}A in mRNA is a common theme conserved from lower to higher eukaryotes. Due to the low resolution of these transcriptome-wide studies, efforts have been made to improve this antibody-based approach. By cross-linking the m^{6}A-specific antibody with the RNA via UV irradiation either induces point mutations (C to T transitions) or produces truncations during the reverse transcription reaction.[118] These signatures allow to pin-point the exact location of the methylated adenosine within an RNA.

The fact that a great portion of coding transcripts are methylated suggest that m^{6}A is an abundant modification. Strikingly, an average mRNA transcript harbors 3 to 5 m^{6}A-nucleotides.[41,112] This makes m^{6}A a more prominent mRNA modification than the m^{7}G-cap that is a typical mRNA hallmark. Sequencing data from human and mice revealed that m^{6}A could be found around the transcription start (TSS), 5'-UTR, ORF and 3'-UTR. Subsequent normalization of the data to a"standardized" mRNA could show that the distribution of this methylated adenosine is not stochastic. Peaks of m^{6}A were highly enriched around the stop codon and within the 3'-UTR (Fig.1.2).[40,41] A similar enrichment pattern around the stop codon has been observed in yeast as well. However, within yeast m^{6}A-methylation is only present during meiosis and not present during its vegetative state.[116,119] In plants an additional enrichment around

the start codon is observed.[117] In certain mRNA transcripts, a m^6A derivative can be found in close proximity of the methyl-cap (1 or 2 nts away) that additionally carries a methylation at the 2'OH of the ribose. This modification is, however, established by a different machinery than the one catalyzing the formation of m^6A within the internal sequence of the mRNA.[120] Therefore, this derivative represents an independent modification with distinct function(s).

Methylation at the N6-position of adenosine does not occur at random but within a degenerated consensus sequence. The sequence that is recognized by the m^6A-methyltransferase complex is RRACH (A = methylated A; R = purine; H = A, C, or U).[40,41] Even though this sequence is not very well defined and can be found throughout the whole messenger, only methylation sites present in the 3'-portion of mRNAs are readily modified. The underlining mechanism on how only these sites are recognized and preferably methylated is currently debated. The absence of an exact methylation sequence and the fact that not all potential sites are methylated indicate that other factors such as RNA structure or the coupling to a certain biological process might be needed for targeting of the responsible methyltransferase to these site.

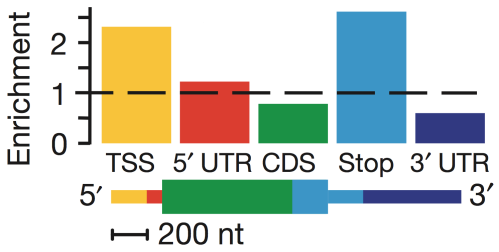

Figure 1.2 Distribution of m^6A within mRNA Normalizing m^6A-sequencing data to a model mRNA reveals that the most methyled adenosines are enriched in close vicinity of the stop codon. This enrichment spans a region of approximately 200 nt up- and down stream of the stop codon (figure adapted from Dominissini *et al.*[41])

1.4 Molecular and biological impact of m^6A in mRNAs

After identifying N^6-methyladenosine as one of the most abundant internal mRNA modifications found in humans, questions have arose concerning the impact of this methylated base within cells. Even though the field on m^6A has only been revived in 2012, some ground breaking work has been conducted linking m^6A methylation to different biological pathways. The next sections are a non-exhaustive list of some important m^6A-dependent mechanisms that have an influence on several cellular processes.

1.4.1 m^7G-independent translation promoted by m^6A

The abundance of m^6A within the 5'-UTR has been reported to be minor compared to the 3' region of a mRNA transcript (see 1.3). Nevertheless, two recent studies could show that even though less frequently deposited in the 5'-UTR the presence of this modification can have a significant cellular impact. These reports demonstrate that a single m^6A within the 5'-UTR can promote cap-independent translation.[121,122] How can m^6A facilitate translation in a cap independent manner? Meyer *et al.* could demonstrate that eIF3 can bind directly to methylated adenosines. As a consequence of this interaction, eIF3 can then recruit the 43S complex to the methylated 5'-UTR of the transcript and initiate translation.[122]

Interestingly, the same group gathered some evidence for the physiological importance of this mechanism in the cell. Upon heat shock, cap-dependent translation is down regulated for most mRNAs within a cell.[123] The expression of a protein termed Heat-shock protein 70 (Hsp70) is normally induced by this stimulus and is translated in a cap-independent fashion.[124] Hsp70 functions as a chaperon and is thought to promote the proper folding of proteins during heat shock.[125] The mRNA of Hsp70 contains an m^6A within its 5'-UTR and translation of this transcript is methylation dependent.[122] In addition to Hsp70, other mRNAs are methylated at their 5'-UTRs during heat-shock. This observation was confirmed by Zhou and colleagues, who demonstrated the *de novo* methylation of 5'-UTRs of different mRNAs during this type of stress.[121] Taken together, these studies provide an indication that m^6A-methylation could be a vital mechanism to guarantee that translation of a subset of mRNAs during heat shock.

1.4.2 m^6A switch

Initial studies could show that m^6A does not perturb the Watson-Crick interface and, thus, does not alter classical base pairing.[126] Nevertheless, m^6A has been shown to influence RNA structure. A mechanism termed m^6A-switch regulates the binding of a nuclear protein termed heterogeneous nuclear

ribonucleoprotein C (HNRNPC).[127] Local hairpin foldings within mRNAs containing both a m^6A- and a HNRNPC binding site are normally not accessible for the RNA binding protein. Methylation of the hairpin reorganizes the structure and allows the binding of HNRNPC. This in return influences splicing of the transcript harboring the methylated hairpin. The m^6A status of the RNA can be reverted through specialized enzymes (see 1.5.1.1). The removal of the methylation from the RNA allows it to fold back to its default state and, again, prevents the binding of HNRNPC. This capability of the RNA to undergo either an accessible or inaccessible state dependent on the presence or absence of m^6A, defines the switching character of this phenomenon.

1.4.3 m^6A recognition by the YTH domain family - translating m^6A into function

Several ideas have been proposed on how a single methyl group at the N^6 position of an adenine can be translated into a molecular or cellular response. One concept postulates that upon methylation, the binding of different RNA binding proteins is prevented either directly or by modulating the surrounding RNA structure, as discussed in the previous section. Another interesting concept was proposed by Dominissini and colleagues. They hypothesized that certain proteins might exist with binding properties specific for m^6A.[41] Upon binding, these proteins could then induce a down-stream process that results in a molecular/cellular effect. These "reader" proteins would, therefore, function as translators of the modifications they bind. This concept resembles a similar mechanism found within proteins that efficiently bind DNA containing 5-methylcytosine (e.g. MeCP2).[128] RNA pull-down experiments using m^6A-methylated RNA were conducted, coupled with mass spectrometry, to find proteins with binding properties specific for this modification.[41] Within these experiments, the YTH domain family (YTHDF) members YTHDF2 and YTHDF3 were identified to bind the methylated RNA but not the unmethylated control.

As indicated by their name, both proteins harbor a domain that has been termed the YT521-B homology (YTH) domain. Early assumptions assigned the m^6A-binding ability to this protein domain, since both YTHDF2 and YTHDF3 only have this domain in common. Structural analysis of the founding member of this protein family YT521-B (also known as YTH domain containing protein 1 (YTHDC1)) and functional analysis of YTHDF2 could provide experimental evidence that the YTH domain indeed binds specifically to m^6A.[129–131] To date, the human YTH family consists of five members: YTHDF1-3, YTHDC1 and YTHDC2. Homologs of these proteins have been found throughout different eukarya, ranging from complex organisms such as humans, rodents and insects down to simple representatives such as *Hydra vulgaris* and yeast.[130] So far, only the human YTH proteins YTHDF1, YTHDF2 and YTHDC1 have been shown to

functionally associate with m^{6}A. The next sections briefly summarize the functional roles of these RNA binding proteins.

1.4.3.1 YTHDF2

As one of two YTH proteins identified in the initial RNA-pulldown experiment conducted by Dominissini *et al.*, this protein has provided the first insight on which biological functions m^{6}A can promote.[41] YTHDF2 is mostly localized within the cytoplasm where it encounters and binds methylated mRNAs. After binding, YTHDF2 destabilizes the transcript by localizing the RNA into a sub-cytoplasmic structure termed processing-bodies (P-bodies).[129] P-bodies are cytoplasmic foci in which mRNAs can either be stored or degraded.[132,133] The overall protein organization of YTHDF2 can be divided into two functional parts. The N-terminal region of this protein is proline-, glutamine- and asparagine-rich (P/Q/N-rich) and is most likely responsible for P-body localization.[129] The C-terminal half of YTHDF2 bears the YTH domain and was shown to efficiently enrich m^{6}A-methylated mRNA. This study provided first direct evidence for a YTH domain-m^{6}A interaction. Taken together, in the cytoplasm m^{6}A can function as a mRNA destabilization signal that is promoted by YTHDF2. This interaction can directly regulate the half-life of the mRNA and the population size of the translatable transcripts. By influencing the translatable pool, this in return has an influence on the number of mRNAs that can be associated with polysomes (Fig. 1.3).

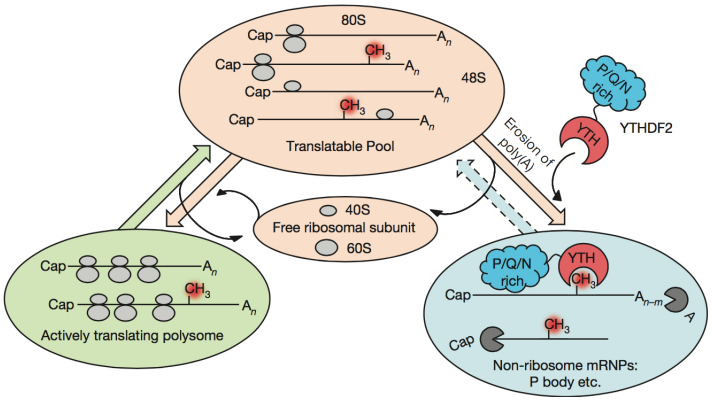

Figure 1.3 YTHDF2 destabilizes m^{6}A-methylated mRNAs and influences their half-life After transcription, m^{6}A methylation and mRNA-processing/transport, mRNAs can either engage in translation or can be bound by YTHDF2. This YTH protein interacts with methylated mRNA via its YTH-domain and localizes the bound transcript into P-bodies. This transport is facilitated by the P/Q/N-rich domain of the protein. Within these foci, cytoplasmic RNAs can be either stored or degraded. The latter effect results in a shorter half-life of mRNAs targeted by YTHDF2. Figure adapted from Wang2014a[129]

Additionally to this finding, some evidence has been collected that YTHDF2 can help promote cap-independent translation upon heat shock. A recent study showed that YTHDF2 can shuttle into the nucleus under stress conditions.[121] Within this compartment, it is assumed that YTHDF2 binds to m^6A present in the 5'-UTR of (pre-)mRNAs. This interaction protects these methylated sites from demethylation that would otherwise occur within unstressed cells, as YTHDF2 is normally not present in the nucleus. After export into the cytoplasm, the methylated 5'-UTR can engage in cap-independent translation that is promoted through the interaction of eIF3 with the methylated adenosine that was (presumably) protected by nuclear YTHDF2 (see 1.4.1).

1.4.3.2 YTHDF1

YTHDF1 is the second YTH domain containing protein whose function within the cell was investigated in more detail. Like YTHDF2, YTHDF1 is localized within the cytoplasm and interacts with mRNAs harboring m^6A-methylated 3'-UTRs. This binding is carried-out with the YTH domain that resides within the C-terminal half of the protein.[134] In contrast to YTHDF2, the N-terminal portion of YTHDF1 does not destabilize the bound transcripts, but rather promotes their translation (Fig. 1.4).[134] This molecular effect is facilitated by YTHDF1 through the interaction with eukaryotic initiation factors and in particular with eIF3. However, this 3'-UTR dependent induction of translation seems to be a different mechanism than the one promoted solely by eIF3 binding to the 5'-UTR during heat shock. The process of the former is not completely investigated, whereas the latter case relies on the direct interaction between m^6A and eIF3 (see 1.4.1). Another vital requirement for the YTHDF1-dependent mechanism seems to be the formation of a closed looped mRNA structure prior to translation, which is promoted by eIF4G.[134,135] This conclusion was made by Wang *et al.* through experiments using internal ribosome entry site (IRES) reporters that either omitted or required eIF4G for efficient enhancement of translation promoted by YTHDF1.[134] Translation is a multi-stage process involving several steps such as assembly of the 43S complex on the mRNA, AUG scanning and initiation and elongation of translation.[135] The current model for YTHDF1-promoted translation is that this protein interacts with initiation factors to increase translation efficiency of target mRNAs. Translation efficiency is defined as the quotient of protein synthesis and mRNA abundance. Thus, YTHDF1 enhances the protein out-put of methylated transcripts compared to non-methylated ones without the necessity of increasing transcription.

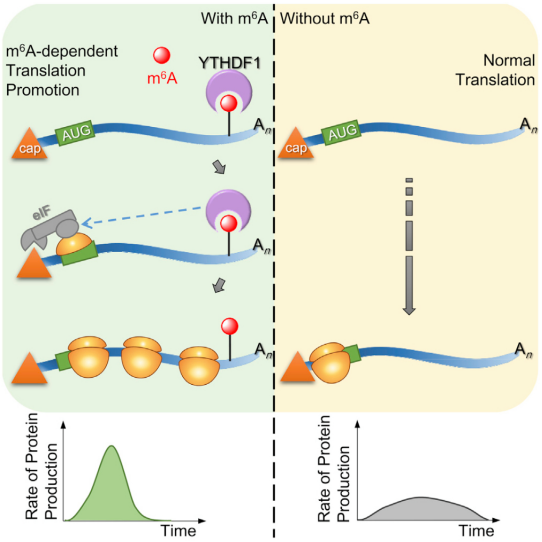

Figure 1.4 YTHDF1 promotes translation in a m^{6}A-dependent manner Messenger transcripts that have experienced m^{6}A methylation can undergo YTHDF1-promoted translation. For this process, YTHDF1 binds to the methylated 3'-UTR of mRNAs and interacts with translation initiation factors such as the eIF3 complex. This protein-protein interaction is vital to enhance translation efficiency resulting in an increase of protein synthesis while the abundance of target mRNAs remains the same. Figure adapted from the graphical abstract of Wang *et al.*2015[134]

A central question that can be asked is: can the mechanisms promoted by YTHDF1 and YTHDF2 both coexist within the cell? If they are both spatiotemporally present within a cell, which one is more dominant or how are theses two processes regulated? Wang and colleagues demonstrated that targets shared by both proteins can experience enhanced translation (YTHDF1) and display shorter half-lifes (YTHDF2).[134] Shared target mRNAs of both YTH proteins are bound at different time points during their life cycle. These transcripts are preferably first bound by YTHDF1, resulting in higher protein synthesis, before they are bound by YTHDF2, targeting them for storage or degradation in P-bodies. This temporal separation of both m^{6}A-promoted mechanisms allow a complex regulation of both translation and mRNA stability. With such a regulation network, one could imagine that such processes enable a quick response to different cellular or molecular stimuli that occur during various events such as stem cell differentiation, gametogenesis and embryonic development.

1.4.3.3 YTHDC1

YTHDC1 (also known as YT521-B) was the founding member of the YTH-domain protein family. Before the association of the YTH-domain with m^{6}A-binding, studies indicated an involvement of this protein in alternative splicing.[136] This protein was found in subnuclear foci termed YT-bodies.[136–138] These foci are claimed to represent so-called transcription centers and are in close proximity to other nuclear structures such as coiled bodies and nuclear speckles.[137] Through structural analysis it has been demonstrated that the YTH-domain that resides in the C-terminus of YTHDC1 can efficiently bind m^{6}A facilitated by the highly conserved tryptophan residues at the amino acid positions 380 and 431.[130,131]

Recently, a mechanism was reported in which YTHDC1 can regulate alternative splicing in a m^{6}A- dependent fashion (Fig. 1.5).[139] With its N-terminal half, YTHDC1 can bind to the serine/arginine-rich splicing factors (SRSF) SRSF3 and SRSF10. The binding sites of all three proteins have been demonstrated to reside within the boundaries of 5'- and 3'-splice sites. In addition to this, m^{6}A methylation peaks can also be found within these regions, indicating a possible interconnection between mRNA methylation and splicing. The formation of a SRSF3/YTHDC1 complex promotes exon inclusion. This is facilitated through the binding of YTHDC1 to a methylated splice site which in return allows SRSF3 to enforce the inclusion of the targeted exon.

Interestingly, binding of YTHDC1 to SRSF10 results in an antagonistic effect. The formation of this heterodimeric complex results in the suppression of the splicing reaction promoted by SRSF10 alone (exon skipping). Not only does YTHDC1 influence the function of both SRSFs, but also their localization. While the import of SRSF3 into nuclear speckles is stimulated by YTHDC1, the opposite is observed for SRSF10. This import into nuclear speckles is another indication that YTHDC1 is involved in splicing, as many splicing factors (e.g. various SRSFs) are enriched in these subnuclear structures.[140–143] The underlining mechanism on how this selective import is facilitated remains enigmatic. This YTH-protein is the third representative that clearly underlines that "reader"-proteins are essential to translate the m^{6}A-methylation into a specific function but are not the only mechanism on how this modification can influence cellular physiology. Further challenges within the field will be to identify more proteins with maybe novel m^{6}A-binding domains and to functionally validate these.

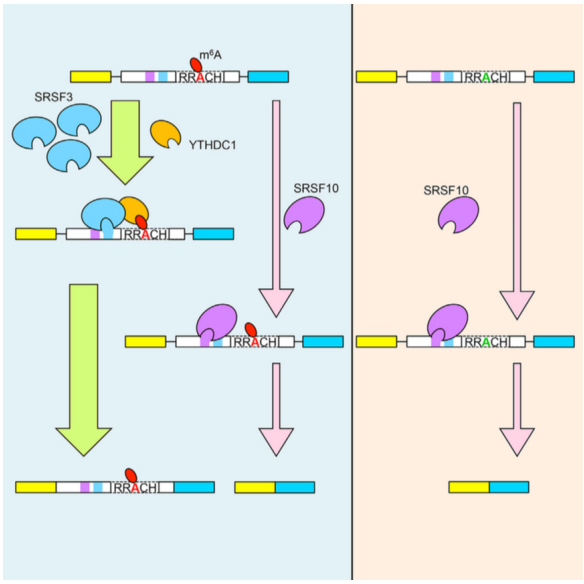

Figure 1.5 YTHDC1's involvement in alternative splicing m^6A methylation sites in close proximity of a potential splice site can be bound by the nuclear YTH protein YTHDC1 that forms a complex with SRSF3. The splicing factor binds its own sequence located near a methylated m^6A-site. Binding of this complex to both sites (m^6A methylation and SRSF3-binding) facilitates the inclusion of the methylated exon in the spliced transcript. This process is antagonized by a different splicing factor termed SRSF10. This protein leads to exon-skipping upon binding to its sequence of an unmethylated transcript and/or blocking the binding of the YTHDC1/SRSF3 complex. Figure adapted from the graphical abstract of Xiao *et al.*2016[139]

1.5 Proteins shaping the m^6A methylome

1.5.1 m^6A-demethylases - modulators of the m^6A landscape

Even though m^6A has been known to be present within mRNA since the sixties, the field recently has attracted great attention through the discovery of specialized enzymes that can revert the methylation at the N6-position of adenine. Investigations conducted on these "erasers" were, together with advances in mapping of m^6A in different RNAs, the driving force for the renaissance of the m^6A field. So far, two proteins have been identified that can demethylate RNAs containing m^6A. This finding suggests that m^6A in addition to other RNA modifications is reversible. This resembles several processes found within the field of epigenetics, for instance DNA-methylation or histone modifications.[144]

1.5.1.1 Fat Mass and Obesity-Associated Protein (FTO)

The fat mass and obesity-associated protein (FTO) was the first enzyme identified with m^6A-demethylase activity.[106] It was, however, first presumed that this protein is a DNA/RNA repair enzyme, since FTO has been shown to be related to the AlkB protein family and is able to oxidize 3-methylthymine in single-stranded DNA and 3-methyluracil in ssRNA.[145–148] As suggested by its name, certain human variants of FTO have been associated with an increased body-mass-index (BMI).[149,150] Strikingly, genetic studies carried out in Fto knock-out ($Fto^{-/-}$) mice have demonstrated that the inactivation of the Fto-gene leads to a reverse phenotype, the reduction of total body mass.[151] A proposed hypothesis is that the lack of Fto in the mice leads to a higher energy expenditure. This in return is the cause for the observed reduction in body weight. Some evidence for this hypothesis has been provided by a study indicating that FTO might function as a nutrient sensor that influences amino acid levels within the cell.[152] The hypothesis of the involvement of the RNA demethylase in energy homeostasis is further supported by the observation that FTO is essential for adipogenesis via the regulation of mRNA splicing[153]

FTO is predominantly found within the nucleus as a putative nuclear localization signal (NLS) within its N-terminus has been predicted *in silico* but has not been functionally validated so far.[146,154] Different reports have, however, indicated that FTO can shuttle between the nucleus and the cytoplasm.[152,155] It has yet to be determined what the underlining mechanism is and what the biological relevance of this trafficking between compartments is. Within the nucleus, FTO localizes into nuclear speckles and thus is present in the same nuclear sub-compartment as YTHDC1 (see 1.4.3.3) and the methyltransferase that establishes m^6A within mRNAs (see 1.5.2).

FTO utilizes oxygen, α-ketoglutarate and non-haem bound Fe^{II} to catalyze the oxidation of m^6A. This reaction resembles that of Ten-eleven translocation (TET) proteins that convert m^5C in DNA into cytosine.[156–159] Another similarity between this RNA- and the DNA-demethylases is that the oxidation of the methylated base is a step-wise process.[160] FTO has been shown to convert m^6A first into N^6-hydroxy methyladenosine (hm^6A) and then N^6-formyladenosine (f^6A). The latter can then be hydrolyzed by the surrounding water in the cell to give rise to an unmethylated adenosine (Fig.1.6).[161]

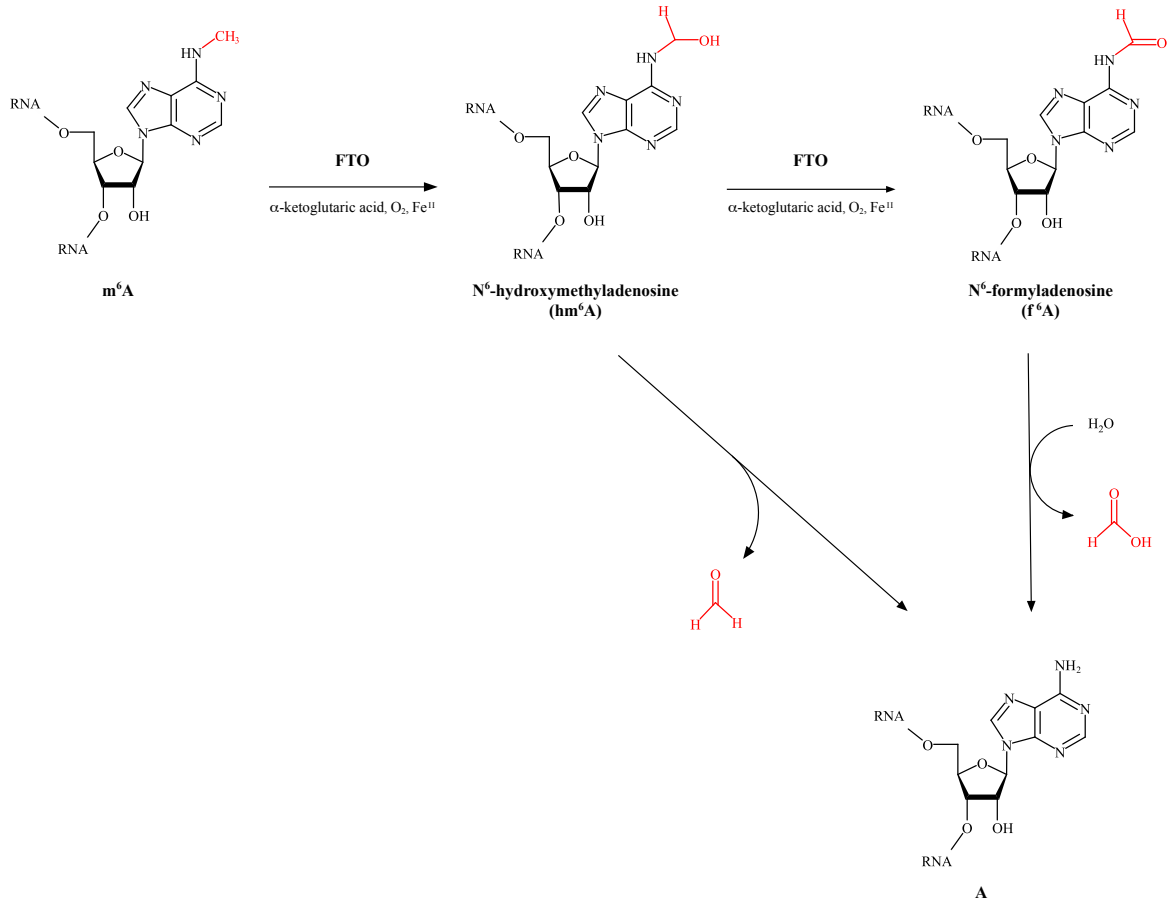

Figure 1.6 Purposed demethylation reaction of m^{6}A catalyzed by FTO The m^{6}A demethylase FTO removes the methyl-group on the N6 position of adenosine in a step-wise fashion. First, oxygen and α-ketoglutarate are utilized to convert m^{6}A into N^6-hydroxymethyl adenosine (hm^{6}A). This product can spontaneously react to adenosine by releasing a formyl group. Hm^{6}A can be further oxidized to N^6-formyladenosine (f^{6}A), during a second reaction round. This product can then be hydrolyzed, thereby releasing formic acid that in return gives rise to an unmethylated adenosine.

1.5.1.2 Alkylation repair homolog 5 (ALKBH5)

The Alkylation repair homolog 5 (ALKBH5) is the second representative of m^{6}A-demethylases that has been identified.[107] This protein has a similar catalytic activity as FTO on substrates containing m^{6}A. ALKBH5 requires for its oxidation reaction the cofactors α-ketoglutarate, oxygen and iron, which are identical to the ones utilized by FTO.[162,163] Even though both proteins are dependent on the same cofactors for their catalysis and generate the same end-product, so far it seems that ALKBH5 cannot generate the same intermediates as observed for FTO. This could indicate that both demethylases might pursue different routes for demethylation or the reaction efficiency between both proteins varies.[164,165]

Another difference between ALKBH5 and FTO are the phenotypes observed in knock-out mice. Primarily spermatogenesis was effected upon deletion of the first exon of Alkbh5, resulting in viable but sterile male mice. Alkbh5 does not only impact the morphology of the resulting spermatozoa, but also influences the architecture of the testis. ALKBH5 co-localizes to nuclear speckles and therefore can be found in the same sub-nuclear structure as FTO and other proteins that interact with m^6A. An observed cell physiological consequence of the absence of ALKBH5 is the accelerated export of mRNAs from the nucleus.[107] The underlying mechanism that interconnects the demethylation reaction catalyzed by ALKBH5 and mRNA export has not been investigated so far. However, an involvement of reader proteins such as members of the YTH protein family could be hypothesized.

Another aspect that needs to be addressed within the field is that it is not clear on how the demethylases choose their substrate. Are other protein factors necessary or certain RNA structures? Results from these investigations could then in return shed light on how deficiencies in demethylation are translated into so complex and diverse phenotypes.

1.5.2 METTL3-METTL14 complex - the m^6A-writer

First experimental approaches to identify and characterize the protein or proteins in humans that establish the methylation of adenine within mRNA were conducted by Bokar and colleagues in the mid-nineties.[166,167] The outcome of these experiments pointed out that the human m^6A-methyltransferase is a high molecular weight complex and is build-up by two distinct components. These subunits can be separated under non-denaturing conditions and were termed MT-A and MT-B that posses molecular weights of 200 kDa and 875 kDa respectively.[167] It was suggested that the MT-B portion of the complex possesses nucleic acid affinity, as it can be purified using single stranded DNA coupled to an agarose matrix. Beside this experiment, no further characterization of the complex was conducted. For the MT-A subunit it could be shown that this component of the methyltransferase contains a 70 kDa protein that can bind SAM. This protein was therefore named MT-A70, which would latter be renamed to METTL3 (methyltransferase-like protein 3).

Besides METTL3, additional components of the human m^6A-methyltransferase complex were described by independent groups. METTL14, another member of the METTL protein family, was found to interact directly with METTL3.[168,169] Both proteins together form a stable heterodimer with a calculated molecular weight of 120 kDa. In a two dimensional native/SDS-PAGE experiment a molecular weight of approximately 200 kDa could be determined. This finding suggests that the METTL3/METTL14 dimer

(METTL3/14) could be the MT-A component of the methyltransferase complex initially described by Bokar *et al.*[167]

The METTL3/14 complex is predominantly localized within nuclear speckles. Therefore, the m^{6}A-writer and both demethylases are present and carry out their function in the same sub-nuclear compartment. How the activities of the writer and erasers are modulated within the same space is still under investigation. Insight into the regulation mechanism could also shed light on how the selectivity of the methyltransferase is established or how certain sites are protected or abolished. For the localization into nuclear speckles, the METTL3/14 requires the interaction of the Wilms' tumor 1-associating protein (WTAP). This protein has been shown to interact directly with METTL3.[168,170] Depletion of the protein results in the improper import of the METTL3/14 into nuclear speckles and a diffuse distribution within the nucleoplasm. This mislocation is most likely also responsible for the observed reduction of endogenous m^{6}A-levels induced upon knock-down of WTAP. However, a modulating effect on the catalysis of METTL3/14 promoted by WTAP has not been extensively investigated *in vitro* and cannot be ruled out.

The vast majority of studies have concentrated on the biological impact of METTL3. It has been, for instance, demonstrated by several publications that METTL3 and its homologs are essential for survival of multicellular organisms such as mice, *Drosophila* and *Arabidopsis*.[171–173] Within all these species, embryos fail to develop to full maturity. Some insight to the molecular implications of METTL3 during embryonic development has been recently provided to some detail in mice.[169,171,174] The first two published studies conducted in mouse embryonic stem cells (mESC), presented rather contradictory results. Whereas Wang *et al.* demonstrated that upon knock-down of METTL3 and METTL14 lead to a reduced ability of self-renewal, Batista and colleagues provided results that suggested the opposite.[169,174] In their study, mESC METTL3$^{-/-}$ cells displayed a complete block of differentiation and display enhanced self-renewal capacity.

The study conducted by Geula *et al.* has to some extent resolved these at first glance controversy observations.[171] During early development, pluripotent mESCs can posses two molecular distinct states. The first one is the so-called "naïve" state in which the stem cells posses an unbiased developmental potential. Within the second "primed" state, the cells are poised to initiate lineage specific programs.[175,176] The Geula study could show that within naïve mESCs, mRNAs encoding for pluripotency factors are predominant and m^{6}A-methylated, which has a negative impact on mRNA half life. Depletion of METTL3 within this state leads to an upregulation of these factors, by increasing their stability. The higher abundance of pluripotency factors leads to a so-called hyper-naïve phenotype (Fig. 1.7). A hallmark of this state is a poor differentiation potential of the cells, which was demonstrated in the study by teratoma

formation assays. This incapability to initiate differentiation is the cause for the observed lethality of the embryo shortly after implantation.

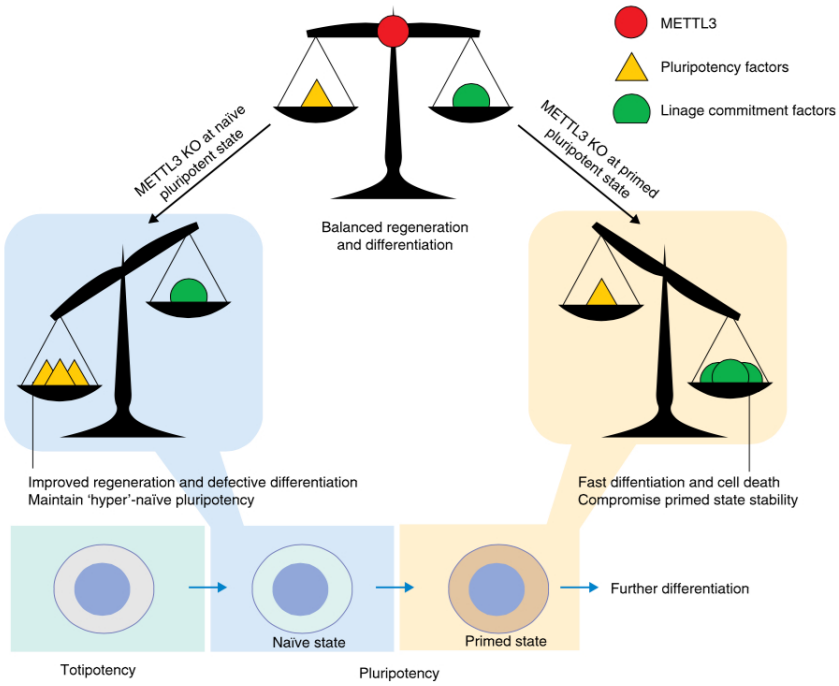

Figure 1.7 METTL3 is essential for the balancing of developmental factors during different pluripotent cell states Depending on the state in which METTL3 is depleted, cells can either enter a hyper-naïve or highly committed differentiation state. This is the result of reduced m^6A-methylation, which in return stabilizes the highly abundant mRNAs encoding for pluripotency maintenance factors in the naïve or dominating differentiation-factors in the primed state. Figure adapted from Zhao and He.[177]

A different phenotype is observed when METTL3 is depleted from pluripotent cells that posses a "primed" state. These mESCs normally display a high abundance of mRNAs encoding for lineage-commitment factors. These are as well methylated like the pluripotency factor mRNAs observed in the naïve phenotype. Abolishing m^6A by knocking-down METTL3 leads to an accelerated differentiation that destabilizes the primed state and ultimately leads to cell death (Fig. 1.7). From the Geula study, it seems evident that METTL3 plays a crucial role to maintain a transcriptional balance during different phases of embryonic development. By manipulating the abundance of METTL3 at certain stages leads to a disruption of this balance and can therefore lead to the different observed phenotypes.

Studies conducted in other organisms could link METTL3 to other developmental processes other than embryonic development. For example oogenesis in female *Drosophilas* is greatly impaired when these flies carry a hypomorphic mutation of IME4, the fly homolog of METTL3.[172] Multicellular organisms

are not the only ones that display defects in complex biological processes such as those previously described. For *S. cerevisiae*, it has been demonstrated that these microorganisms rely on m^6A-methylation for the proper execution of meiosis. Interestingly, this modification is completely absent during the vegetative life-cycle of the cell and accumulates during the transition into the sexual phase.[116,119,178,179] These findings clearly highlight the importance of both the methylation machinery and m^6A and their involvement in complex biological processes.

1.6 Aim of the thesis

Compelling evidence has been collected over the last five years that demonstrate the importance and impact of m^6A on different biological processes. At the heart of the various mechanisms influenced by this post-transcriptional modification lies the methyltransferase machinery. Even though the importance of the METTL3/14 complex has been studied to some detail, several unanswered questions still remain. For instance, why does the minimal m^6A-methyltransferase complex potentially carry two methyltransferases? Which portion(s) of the complex interacts with WTAP? Which protein domain(s) of METTL3 and METTL14 are essential for the formation and stability of the heterodimer? These questions should be addressed biochemically using recombinant proteins and by recapitulating the methylation process *in vitro*. Another aspect investigated in this thesis is how the three known interactors of the m^6A-machinery (METTL3/14 and WTAP) are imported into the nucleus. For this, potential nuclear localization sequences are first predicted using the Eukaryotic Linear Motif resource tool.[180,181] Next, NLS mutants of the individual proteins should be generated and the impact on protein localization of these introduced mutations should be analyzed during immunofluorescence experiments.

2. Results

2.1 Structure prediction of the human METTL3/14 complex

Since little information on the architecture of the human N6-methyltransferase has been published, we sought out to characterize the protein complex using different biochemical methods. As a first step, the secondary structures of both METTL3 and METTL14 were predicted using the online tool Psipred (see section 5.2.6.2 and the sections 6.1 and 6.2 in the appendix). The bioinformatic data obtained using this approach allowed the definition of structured domains within both METTL proteins (Fig. 2.1). METTL3 possesses three distinct protein regions that are separated by unstructured segments. The first two regions have to date unknown function. The third domain of METTL3, that resides within the C-terminus, is the so-called MT-A70 domain. This domain has been reported to be associated with SAM-binding and catalysis.[178,182] METTL3 posses within the first amino acids of this domain a DPPW motif that is found in other methyltransferases as well and is responsible for the catalytic activity of these proteins.[178,182]

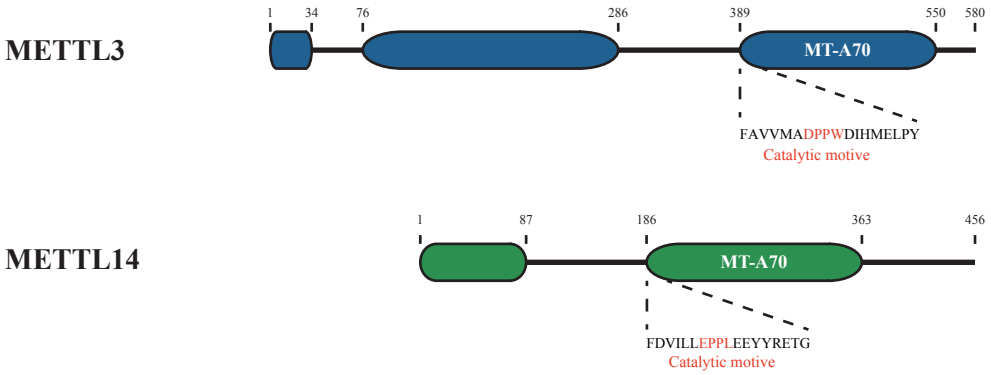

Figure 2.1 Schematic representation of METTL3 and METTL14 Structural domains of METTL3 and METTL4 have been defined using the secondary structure prediction algorithm Psipred (see Fig.6.1 and 6.2 in the appendix). METTL3 is divided into three distinct domains. The first two domains have not been associated with a specific function, whereas the last structured region represents the annotated MT-A70 domain. METTL14 also contains this MT-A70 domain that is similar to the one found in METTL3. The predicted catalytic residues within the MT-A70 domains of both proteins have been highlighted in red. In addition to the MT-A70 domain, METTL14 possesses a second structured region at its N-terminus with unknown function. Numbers indicated above each protein display the amino acid position of the domain boundaries.

METTL14 also possesses a MT-A70 domain, which is located within the center of the protein. However, distinct from METTL3, this methyltransferase-like protein harbors a slightly different catalytic motif. The domain harbors an EPPL- and not a DPPW-tetrad. It has not been determined yet, if the substitutions at the first and fourth position of this catalytic motif has any functional impact on the assembled complex or not. Besides the MT-A70, METTL14 has a structured N-terminus with unknown function. These structure predictions were essential in order to design full-length and truncation constructs that have the aim to provide structural and functional information of the METTL3/14 dimer.

2.2 Purification and functional analysis of the human METTL3/14 complex

The group that first purified the METTL3/14 complex could demonstrate that this minimal complex is sufficient for the formation of m^6A *in vitro*.[168] Subsequent experiments conducted with each subunit alone demonstrated that of the two METTL proteins present in the complex, METTL14 possesses a higher activity than METTL3. So far, however, it has not yet been tested if METTL14 is the catalytic subunit within the reconstituted complex. In addition to this, the structural prediction conducted in the previous section could show differences in the catalytic motif of both METTL proteins. METTL14 possesses an EPPL-motif that diverges from the catalytic active DPPW-motif seen in other methyltransferases.[178,182] To address if the EPPL-motif is still functional and to test if METTL14 is the catalytic subunit within the dimer, a SAM-binding experiment, using the assembled METTL3/14 complex, and a mutational study were performed. Besides cofactor-binding and methylation activity, RNA-binding of the binary complex was also investigated *in vitro*.

For all these experiments an expression and purification system needed to be established in order to obtain different METTL3/14 complexes. In addition to this, a read-out system also had to be set-up that can efficiently monitor the catalytic activity of the different methyltransferase complexes during the mutational analysis.

2.2.1 Expression and purification of human METTL3/14

Full length METTL3 and METTL14 were cloned into a single vector (pFastBac Dual, designed and cloned by Dr. Nora Treiber, University Regensburg) to guarantee the expression of both proteins in a single cell. Within this plasmid, only METTL3 was tagged with the Glutathione S-transferase protein (GST). This construct was utilized to generate a high-titer baculovirus suspension that in return was used to promote the expression of both METTL proteins in SF21 cells. A GST-pulldown was performed from the lysates of these infected cells. As displayed by Fig.2.2 A, not only was the GST-tagged METTL3 purified with this approach but also the untagged METTL14 protein. This result indicates that both constructs are capable to form a dimer within insect cells and that a native complex can be isolated from these cells.

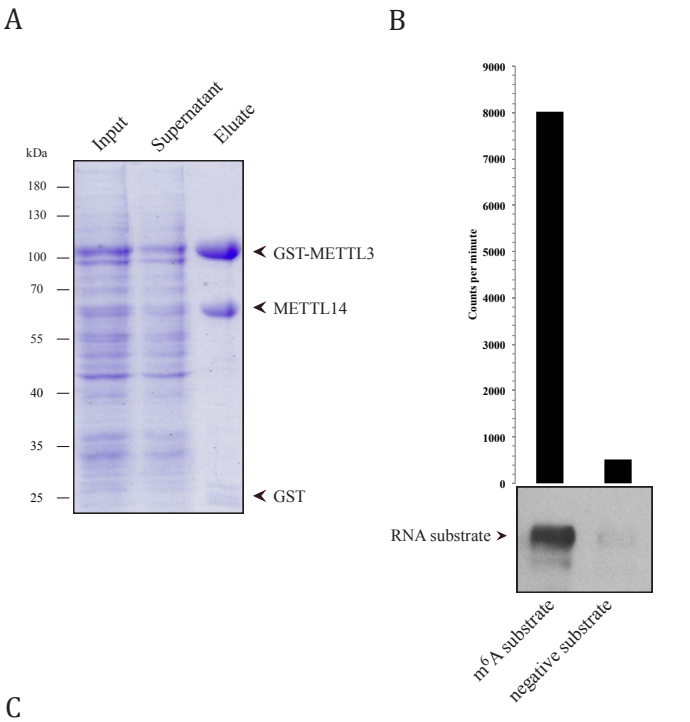

Figure 2.2 Purification of an active GST-METTL3/14 complex from Sf21 cells A) GST-tagged human METTL3 and untagged human METTL14 were purified from Sf21 cells infected with a baculovirus construct encoding for both proteins. B) Catalytic activity of the purified GST-METTL3/14 complex shown in A) was demonstrated using a m^6A *in vitro* methylation assay, which utilizes ^3H-marked SAM. To demonstrate methylation specificity, an RNA that either harbored the methylation consensus sequence GGACU or a variant missing the methylatable adenine was used in the assay. After the methylation reaction, the RNA was retrieved for activity measurements in a scintillation counter or for a radiographic analysis. C) Shown are the RNA sequences of the substrates used for the *in vitro* methylation assay.

The retrieved protein complex from this small-scale purification was split into to two separate setups to perform a m^6A *in vitro* methylation assay (Fig. 2.2 B). During this assay, the purified complex was either incubated with an RNA substrate containing a single m^6A-methylation site (GGACU) or with an RNA that possesses a uracil instead of an adenine within the predicted methylation sequence (GGUCU). The latter substrate, therefore, functioned as a negative control during the assay (Fig. 2.2 C).

^3H-labeled SAM was used as a cosubstrate in this methylation assay and, thus, made it possible to assess the methylation activity of the protein complex in a scintillation counter, after removing non-utillized SAM and retrieving the RNA. The reaction containing the m^6A-RNA substrate displayed a robust signal of several thousand counts per minute (c.p.m.). The negative substrate, on the other hand, only displayed background levels of radioactivity. To validate the scintillation measurement, the RNA from both methylation reactions was isolated and loaded onto a denaturing gel. After separation, the RNA was blotted onto a membrane that was afterwards exposed to an X-ray film (Fig. 2.2 B, in cooperation with Dr. Thomas Treiber, University Regensburg). Similarly to the scintillation measurement, only the RNA containing the RRACH motif displayed a robust signal compared to the negative substrate. These two experiments indicate that the recombinant METTL-complex purified from Sf21 cells is active and can distinguish between a methylatable and non-methylatable substrate. This, therefore, suggests that a native and active GST-METTL3/METTL14 complex was efficiently purified.

2.2.2 METTL3 can efficiently bind SAM within the METTL3/14 dimer

One of the key questions that should be addressed with the purified protein complex is: why does the METTL3/14 complex posses two methyltransferases that could be potentially active? As a first experiment it should be tested if both proteins in the complex are capable to bind the methyl donor SAM. For this experiment the GST-tagged METTL3/14 complex was purified in a similar fashion as described in the previous section (Fig.2.3 A and see section 2.2.1).

The recombinant complex was then pre-incubated with ^3H-marked SAM before conducting a time course experiment, in which the METTL3/14 complex was irradiated with UV light to cross-link the methyl donor to one or both METTL proteins. After cross-linking, the proteins from each sample were loaded onto a SDS-PA gel, in order to separate METTL3 and METTL14 from one another. The gel was then subsequently fixated and incubated in scintillation solution. The treated gel was then dried and exposed to a X-ray film to visualize any cross-link events that have occurred during UV-irradiation (Fig. 2.3 B). Interestingly, during the time-course of $30\,\mathrm{min}$, only a single band can be identified that gradually intensifies dur-

ing the experiment. This band possesses a molecular weight of approximately 100 kDa and correlates to the calculated size of GST-METTL3 (90.8 kDa). This experiment indicates that SAM can be more efficiently cross-linked to METTL3 than to METTL14. This in return allows to hypothesize that METTL3 could probably be the only methyl donor-binding subunit within the dimeric complex.

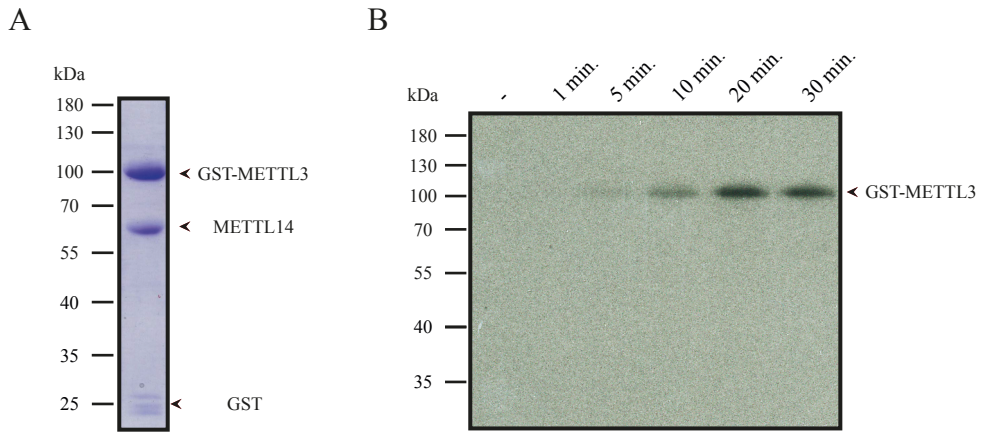

Figure 2.3 METTL3 can efficiently bind SAM within the METTL3/14 complex A) Coomassie gel of batch-purified GST-METTL3/14 used for the SAM cross-linking experiment. B) Recombinant GST-METTL3/14 complex was incubated with ^{3}H-marked SAM and cross-linking of the complex with the cofactor was induced by UV light (254 nm). Irradiation time for the different setups is indicated above the displayed radiogram.

2.2.3 Large-scale purification and refinement of the METTL3/14 complex

To further investigate if both or only one of the two METTL proteins is catalytically active, mutant constructs should be designed and expressed which should then be tested in an *in vitro* methylation assay. Beside this experiment, other experiments such as electrophoretic mobility shift assays (EMSAs; see 2.2.6) or chemical cross-linking and mass spectrometry analysis (CX-MS; see 2.3.3) of the complex required larger quantities of the dimer, which cannot be achieved by GST-batch purification. Not only a higher yield of recombinant protein should be achieved, but a strategy should also be developed that allows the removal of contaminants, such as free GST-protein, from the preparation of the complex. Acquiring a homogeneous and highly purified sample of the complex minimizes artifacts and also allows to accurately determine the concentration of the dimer. This in return facilitates the possibility to make quantitative and qualitative comparisons between experiments.

Sf21 lysates generated from cells infected with baculoviruses encoding for the METTL3/14 complex were first purified using a GST-trap. Glutathione-eluted proteins were then treated with TEV protease, in order to cleave the GST-tag from METTL3 during dialysis (purification program written and HPLC operated by Dr. Thomas Treiber, University of Regensburg). A gel filtration was carried out as a final step to obtain the highly purified human METTL3/14 complex. As assessed in a PA gel (Fig. 2.4 A), the integrity of the complex is not compromised during the multiple purification steps. This indicates that the METTL3/14 complex is quite stable in solution over the time period of two days, in which the dimer is purified.

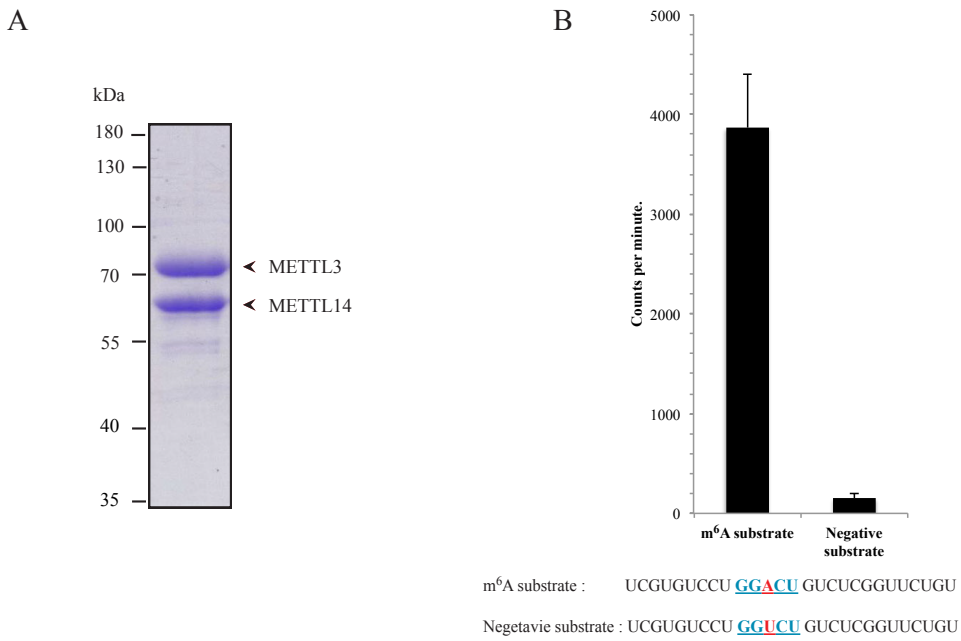

Figure 2.4 HPLC purification of the recombinant METTL3/14 complex A) Large-scale purification of human METTL3/14 from infected Sf21 cells. Recombinant protein was purified using a GST-trap column and by subsequently removing the tag via TEV-digestion and HPLC gelfiltration. B) Activity of the purified and polished METTL3/14 complex was examined in a m^6A *in vitro* methylation assay using modified RNA substrates (compare with Fig. 2.2 C).

As this purification strategy varies from the one previously used, we next assessed if the refined complex is still active using the same *in vitro* m^6A-methylation assay as described in section 2.2.1 (Fig. 2.4 B). The HPLC-purified and untagged METTL3/14 complex can efficiently methylate the adenosine present in a RRACH sequence context. The negative substrate on the other hand, only displays low activity that are close to background measurements (data not shown). This leads to the conclusion that the established purification strategy does not have a negative impact on catalysis of the METTL3/14 complex. Additionally, this strategy allows to purify constructs that more closely resemble a complex that is endogenously present in cells.

2.2.4 Construction of mutant variants of the METTL3/14 complex

It has been published that the formation of m^6A can be sufficiently catalyzed by METTL14 alone.[168] METTL3, on the other hand, did not demonstrate any activity by itself in the experiments conducted in the same report. However, the activity of each individual subunit has not been investigated within the context of the dimeric complex. In addition to this, the result obtained from the SAM cross-linking experiment also challenges the view of METTL14 being the catalytic subunit of the mRNA-methyltransferase complex. Therefore, variants of the METTL3/14 complex were constructed in which either the DPPW-motif in METTL3 or the EPPL-motif in METTL14 carry point-mutations (Fig. 2.5 A; plasmids designed and cloned by Dr. Nora Treiber, University Regensburg). Two of the four predicted catalytic residues (shown in red) that reside within the N-terminus of the MT-A70-domain of both proteins were exchanged for alanines (shown in blue). These manipulations should allow to test if both proteins are catalytically active or not. The resulting mutant constructs were termed METTL3 APPA or METTL14 APPA in order to clarify which of the two METTLs bear the described substitutions.

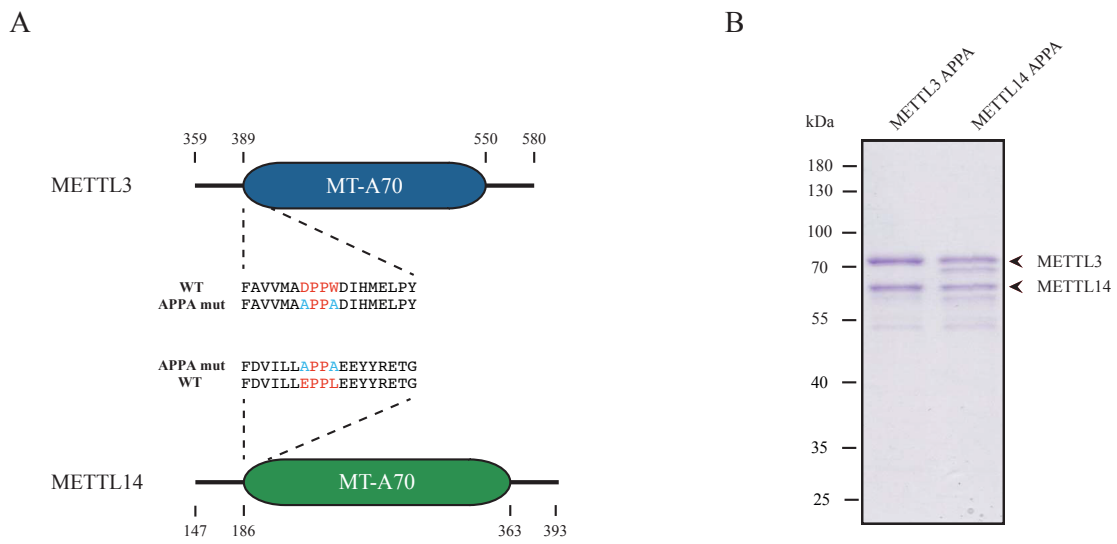

Figure 2.5 Generation of catalytic mutants of METTL3 and METTL14 A) Schematic representation of the MT-A70 domain of METTL3 and METTL14. The predicted catalytic residues (red) of both wild-type (WT) METTL proteins are located in the N-terminal region of the MT-A70 domain. The first and fourth amino acid of the catalytic motif have been exchanged for alanines (shown in blue) in order to generate APPA mutants of METTL3 and METTL14. B) Coomassie staining of the recombinant APPA mutants using the same purification strategy as explained in section 2.4. Indicated numbers illustrate the amnio acid position within the respective protein.

Both APPA mutants were expressed in Sf21 cells and purified in a similar fashion as described in section 2.2.3. The purified protein complexes were analyzed on a PA gel to investigate if the introduced alterations have any impact on the dimerization-capability of both METTL proteins (Fig. 2.5 B). Both the METTL3 APPA as well as the METTL14 APPA mutant can efficiently associate with their appropriate counterpart and both complex variants can be readily purified.

2.2.5 Methyltransferase activity relies solely on the MT-A70 domain of METTL3

After purifying the different mutant variants of the METTL3/14 complex, the catalytic activity of these constructs should be examined during an *in vitro* methylation assay (Fig. 2.6).

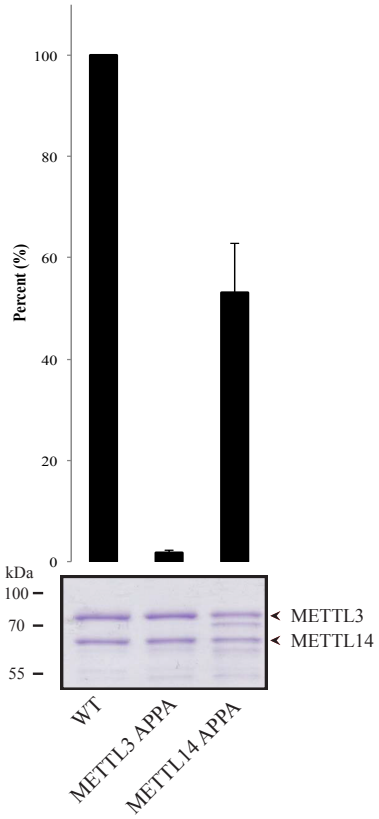

Figure 2.6 METTL3 is the catalytic subunit of the human METTL3/14 complex The catalytic activity of the three METTL3/14 complex variants (WT, METTL3 APPA and METTL14 APPA) were examined in an *in vitro* methylation assay. Activities were first normalized to the RNA amount isolated from each setup after the methylation reaction. Afterwards, the activities of the APPA mutants were normalized to the wild type signal.

Both the wild type and METTL14 APPA complex display a robust activity. The reduced activity observed for the METTL14 APPA construct, when compared to the wild type, is likely the result of utilizing unequal amounts of protein in the assay and not from the introduced mutation. The METTL3/14 complex bearing two point mutations within METTL3 shows no significant activity in comparison to the other two versions of the dimer. This results demonstrates that the DPPW-motif of METTL3 is essential for m^6A-formation in the context of the METTL3/14 dimer.

2.2.6 The METTL3/14 complex displays no clear substrate-binding specificity

Methylation activity of the METTL3/14 complex relies on the binding of the dimer to its RNA substrate. Electrophoretic mobility shift assays (EMSAs) were conducted to determine and calculate the dissociation constant of the methyltransferase (Fig. 2.7 A). Different concentrations of wild type METTL3/14 were incubated with a ^{32}P-labeled RNA substrate, harboring the same methylation sequence as used for the *in vitro* methylation assays, as described in the previous sections 2.2.3 and 2.2.5. Within the tested concentration range and under standard EMSA buffer conditions (including yeast tRNA and heparin), no shift of the protein complex can be observed. A prominent shift, on the other hand, is displayed by the setup that includes the methyltransferase but omits both EMSA buffer additives used in the other samples (lane 5).

These observations lead to experiments that should examine which of the two components blocks the binding of the METTL3/14 complex to its methylation substrate. First, setups containing the recombinant dimer and an increasing amount of yeast tRNA were analyzed in an EMSA (Fig. 2.7 B). The indicated shift observed in the reaction containing no tRNA (lane 2) is significantly reduced when including tRNA in the EMSA buffer (lane 3). Increasing the concentration of tRNA rapidly abolishes the shift (lanes 3 - 7) and above a tRNA-threshold of $250\,\mu g/ml$, no shift can be detected (lanes 8 - 9). Next, the impact of heparin on the observed RNA-binding of METTL3/14 was examined (Fig. 2.7 C). Similar to the experiment conducted with yeast tRNA, increasing amounts of heparin was added to each setup containing the EMSA incubation buffer and the METTL3/14 complex (lanes 3 - 8). In the setup omitting heparin (lane 2), a shift with three distinct bands can be observed. The upper two bands lose intensity that correlates with higher concentrations of the polyanion (lanes 6 - 8).

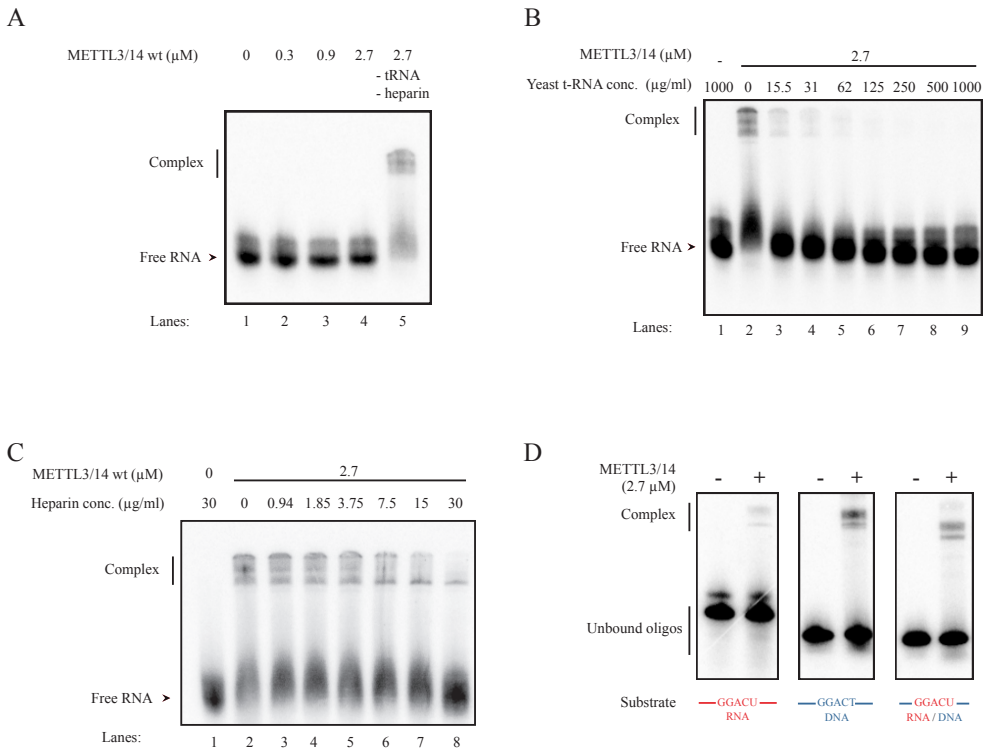

Figure 2.7 The METTL3/14 complex binds unspecifically to polyanions A) An electrophoretic mobility shift assay was performed with various concentrations of the METTL3/14 complex and under two different buffer conditions. B) RNA substrate-binding of the METTL3/14 complex was challenged using various concentrations of yeast t-RNAs in an EMSA. C) EMSA analyzing the RNA-binding of METTL3/14 when incubated with different concentrations of heparin. D) Recombinant METTL3/14 complex was incubated with different nucleic acid substrates and binding was assessed in an EMSA.

In a final experiment, different nucleic acid substrates containing a single RRACH motif were used. The recombinant METTL3/14 complex was either incubated with a RNA-, DNA-substrate or a hybrid that contained a RNA RRACH motif flanked by DNA sequences (Fig. 2.7 D, panels from left to right). For all three setups, a prominent shift can be observed induced by the association of the complex with its nucleic acid substrate. Taken together, these EMSA experiments point out that the METTL3/14 complex has an affinity towards polyanionic macromolecules and does not display any type of substrate specificity when confronted with different types of nucleic acids.

2.3 Mapping of protein-interacting regions of METTL3, METTL14 and WTAP

Within published reports and the previous sections of this work, it has been demonstrated that the METTL3/14 complex is sufficient to catalyze the methylation of adenines within a given RRACH motif *in vitro*.[168] Both proteins are also essential for maintaining the m^6A-methylome of mRNA molecules within the cell nucleus.[168] Besides METTL3 and METTL14, a third protein has been identified that is essential for the function of the methyltransferase complex within the cell by directly interacting with METTL3. This interactor is WTAP and has so far been described as an auxiliary protein of the dimeric complex.[168,170] This protein is crucial to transport METTL3/14 from the nucleoplasm into nuclear speckles. Interfering with the import into these sub-nuclear structures results in a reduction of global m^6A-methylation present on mRNA. The next experiments should further characterize the interaction of WTAP with METTL3. The interacting regions between both proteins should be mapped using truncation constructs of both WTAP and METTL3. In addition to this, the dimerization domain of METTL3 and METTL14 should be mapped in a similar fashion as well, since no structural information of the METTL3/14 complex has been published. The results obtained from these experiments should allow to gain a first insight into the architecture of the human N^6-methylatransferase and its interaction with WTAP.

2.3.1 A short helix at the N-terminus of METTL3 is sufficient to interact with WTAP

As a first approach to mapping the interaction between WTAP and METTL3, a global structure prediction of WTAP was made analogous to the one that was carried out for METTL3 and METTL14 (Fig. 2.8 A and see section 2.1). Psipred predicts that the C-terminus of the protein is not structured at all, whereas the N-terminal region consists of seven individual α-helices (Fig. 6.3 in the appendix). The primary sequence of WTAP was additionally scanned with the algorithm COILS that calculates the likelihood of proteins forming coiled-coil structures (Fig. 2.8 B).[183] This bioinformatic approach was selected due to the high abundance of helices in the N-terminus of WTAP, some of which span over more than forty amino acids.

The algorithm scans the primary sequence of a given protein in defined windows of 14 (in green), 21 (in blue) or 28 (in red) amino acids. COILS scans proteins for heptad-sequences that are characteristic for coiled-coils and assigns these regions a probability score between zero and one (Fig. 2.8 B). The higher the score the better these regions fulfill the criteria of forming these tertiary protein structures. By using this tool, three distinct regions could be detected that posses coiled-coil properties. The first coiled-coil of WTAP lies within its N-terminus and can only be detected within a sliding-window of 14 and 21 amino

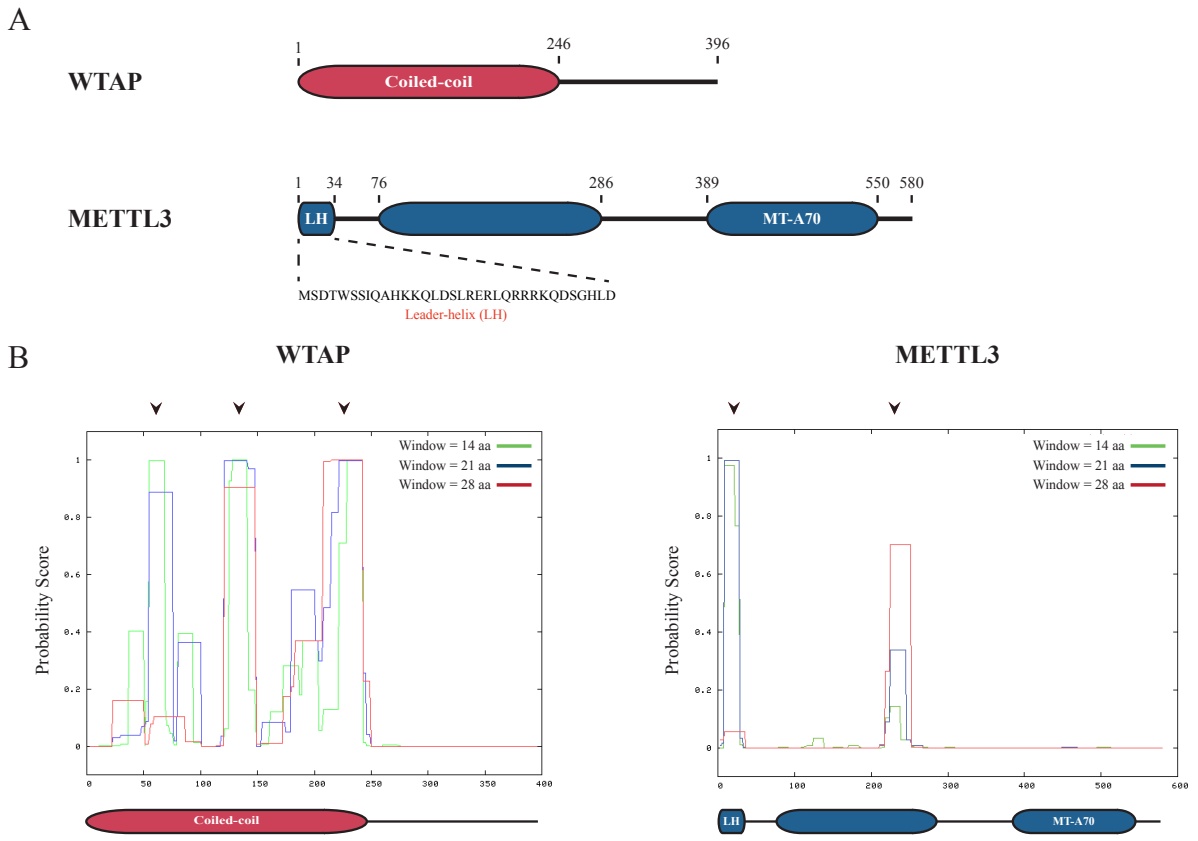

Figure 2.8 Prediction of a coiled-coil domain of WTAP and a potential interacting region within METTL3 A) Schematic representation of the predicted domains of WTAP and METTL3 using Psipred. The coiled-coil prediction algorithm COILS indicates that the N-terminal region of WTAP consists of a collection of three predicted coiled-coils. Within METTL3, two coiled-coil predictions were found within the first and second structured region of the protein. The first structured region of METTL3 has been termed the leader helix (LH) and was chosen as a candidate to test the interaction with WTAP. Predicted coiled-coils of WTAP and METTL3 are indicated with an arrow head above each plot.

acids with an observed probability score of more than 0.8 (or 80 %). The remaining two coiled regions can be detected for all three search-intervals with similar scores as observed for the first coil. Based on this data, a hypothesis could be formulated that the N-terminus of WTAP contains a coiled-coil domain and could be a possible interaction surface for METTL3.

As multimeric coiled-coils have been described to facilitate protein-protein binding, it is possible that the METTL3-WTAP interaction could be mediated by this mechanism.[184–186] Therefore, METTL3 was scanned using the same tool to investigate if this protein as well contains any regions that fulfill the requirements of forming a coiled-coil. *In silico* analysis reveals two probable coiled-coil regions (Fig. 2.8 B). Interestingly, one of the two regions has a score of over 90 % within two of the applied scanning-intervals. This predicted coiled-coil is located within the first 34 amino acids of the N-terminus of

METTL3, which has been termed the "leader helix", and was chosen as a first candidate for further biochemical investigations.

To test if this N-terminal segment of METTL3 possess the capability to bind to WTAP, a construct was designed in which the leader helix was fused to the C-terminus of GFP (GFP-LH). The plasmid encoding this fusion protein was coexpressed with a vector harboring a myc-tagged WTAP in HEK 293T cells. With these cells, a myc-IP was performed and binding of the GFP-LH construct was assessed in a anti-GFP immuno blot (Fig. 2.9 A). Interestingly, the short fragment from METTL3 fused to GFP is efficiently copurified with WTAP during the IP (lane 2), whereas in the absence of the myc-tagged protein no enrichment of the leader helix can be detected (lane 4). Within a control IP (lane 6), a band representing GFP can be detected in the IP although the leader helix is not present. However, this GFP band is likely to be the result of unspecific binding that is promoted by the high expression of the fluorescent protein, as seen in the input (lane 5; 3-4 fold higher as in lanes 1 and 3).

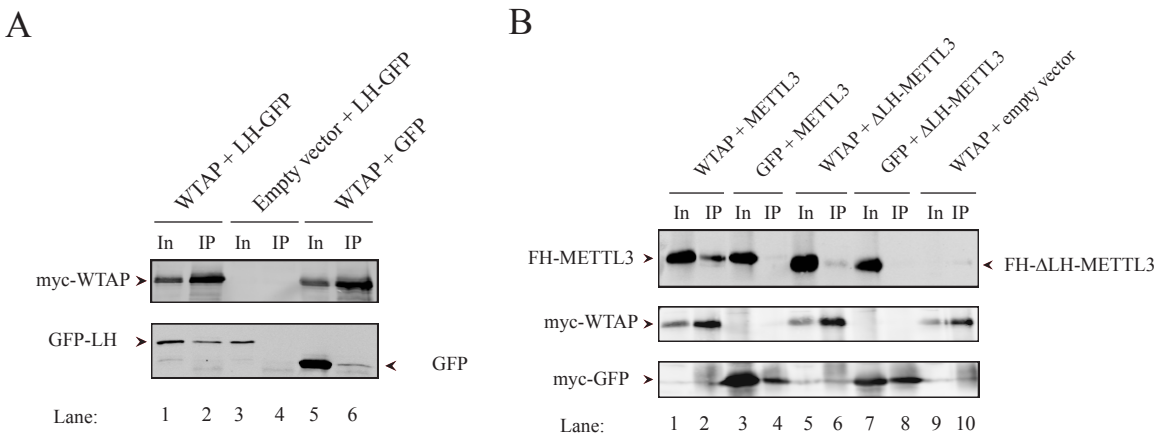

Figure 2.9 The METTL3 leader-helix is essential for the METTL3-WTAP interaction A) A GFP-LH fusion protein was tested if it can effectively bind to myc-tagged WTAP, which was immuno-purified from HEK 293T cells expressing both constructs. B) WTAP-binding was compared between wild type METTL3 and a construct missing the LH-region (△LH-METTL3). A myc-IP was performed to enrich for WTAP and the possible copurification of the two METTL3 constructs was examined in a Hemagglutinin (HA) immuno-blot. FH, FLAG/HA-tag

As a complementary experiment to test the observation made with the GFP fusion protein, the same IP experiments were performed using a mutant of METTL3, in which the leader helix was missing (ΔLH-METTL3; Fig. 2.9 B). When enriching for WTAP and performing a Hemagglutinin (HA) immuno-blot, the mutant is not efficiently copurified in comparison to the wild type construct of METTL3 (lanes 6 and 2, respectively). This indicates that the binding capability between METTL3 and WTAP is impaired when the first N-terminal helix from METTL3 is missing. Taken together, both experiments provide evidence for a role of the leader helix facilitating the interaction between WTAP and the METTL3/14 complex.

2.3.2 Mapping of the METTL3-interacting region of WTAP

Next, the protein region of WTAP should be determined that binds to METTL3. For this, C-terminal truncations of WTAP (CT) were designed by first removing the predicted unstructured portion of WTAP (C-terminus; see Fig.2.8 A) and then deleting step-wise Psipred-predicted α-helices (Fig. 2.10 A and see appendix Fig. 6.3; constructs cloned by Christian Rittinger, University Regensburg). These constructs all bear a myc-tag at their N-terminus and were cotransfected with FLAG/HA-tagged METTL3 (FH-METTL3) into HEK 293T cells. Lysates from these cells were then the starting material for FLAG-IPs (Fig. 2.10 B). The constructs CT1 to CT3 copurified with FH-METTL3 to a similar extent as the wild type WTAP (lanes 8, 10, 12 and 6 respectively). On the other hand, the shortest of the tested constructs (CT4) failed to copurify with METTL3 (lane 14).

In order to further test this observation, a second experiment was carried-out using the same WTAP truncations. This time, however, the constructs were coexpressed in HEK 293T cells with the GFP-LH fusion protein, which has been shown in the previous section to bind to full-length WTAP (Fig. 2.10 C). In this experiment, a myc-IP was conducted to enrich for the individual WTAP constructs. An anti-GFP immuno blot was then performed to investigate which of the CT-constructs can efficiently copurify the METTL3 leader helix. Interestingly, the same constructs (CT1-3) that bind to the full-length METTL3 also bind to the GFP fusion protein (lanes 8, 10 and 12). However, the interaction observed for the construct CT3 is not as intense as for the other two WTAP versions. This experiment also could display that the construct CT4, again, fails to associate with the presented METTL3 construct.

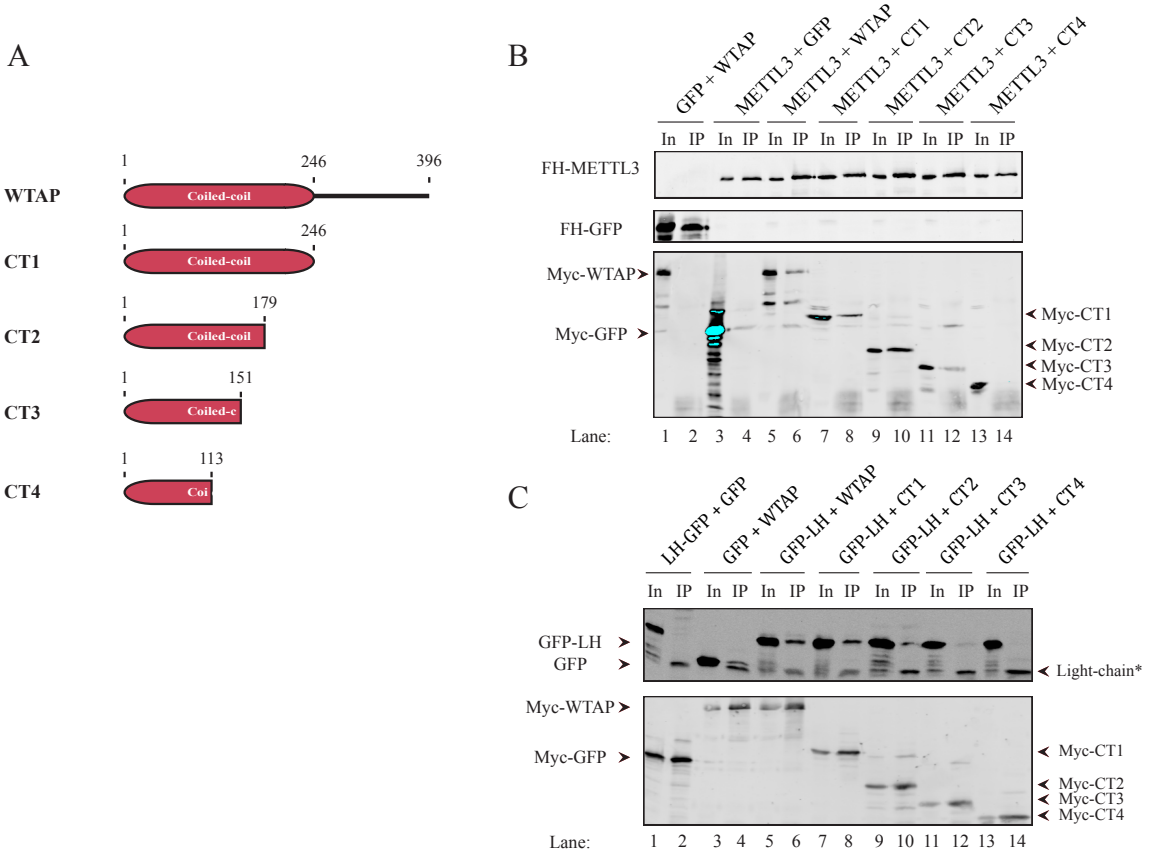

Figure 2.10 METTL3-binding capability of WTAP resides within its first 150 amino acids A) Schematic of the C-terminal truncations of WTAP (CT) generated to map the METTL3-binding region of this protein. B) Truncations shown in A) or the full length protein of WTAP were coexpressed with FLAG/HA-tagged METTL3 in HEK 293T cells. A FLAG-IP and afterwards an anti-myc immuno blot was performed to detect constructs that can still bind to METTL3. C) HEK 293T cells expressing one of the myc-tagged versions of WTAP and GFP-LH were subject to a myc-IP. Binding of the GFP fusion protein was then assessed in an anti-GFP immuno blot.

These experiments suggest that the METTL3-interacting region of WTAP resides within the predicted coiled-coil domain of the protein (aa 1-246). The truncation construct CT3, which can still bind to the methyltransferase subunit, narrows the binding region down to the first 151 amino acids of WTAP. In order to more accurately map the METTL3-interaction domain, N-terminal truncations of WTAP (NT) were constructed next and a complementary experiment was performed (Fig. 2.11 A). FLAG-IPs were conducted in a similar fashion as carried-out for the C-terminal truncation constructs (Fig. 2.11 B). This experiment revealed that the deletion of the first 47 amino acids reduces the binding of the NT1 construct to METTL3 (lane 8), but can still enrich it. The remaining two truncations showed no sign of METTL3-binding, as no detectable signal is observed in the anti-myc immuno blot.

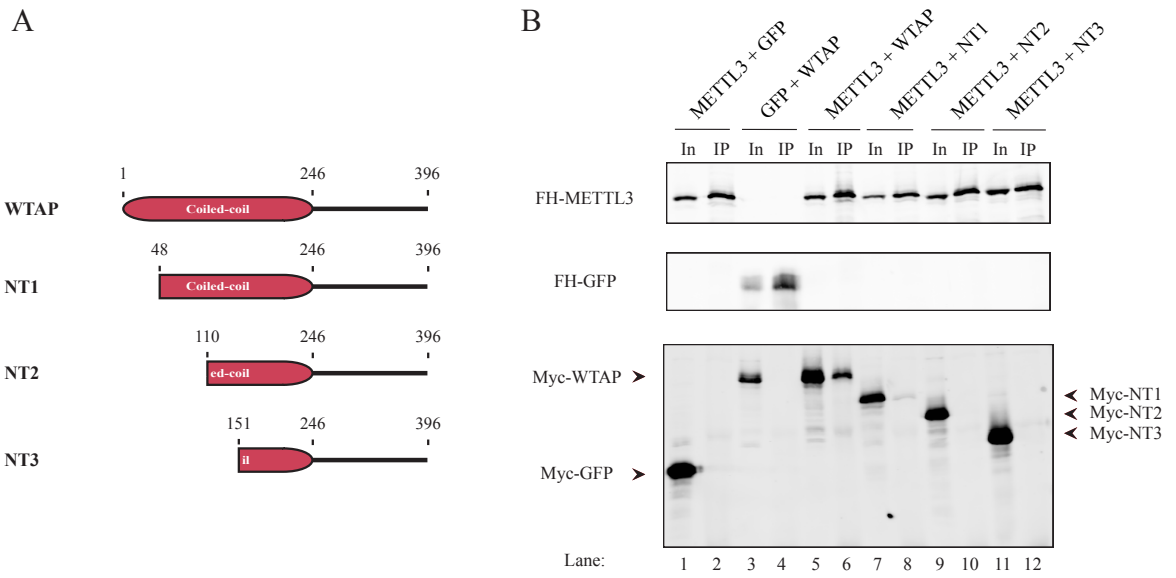

Figure 2.11 Narrowing down METTL3-binding with N-terminal truncations of WTAP A) Schematic of the N-terminal truncations of WTAP generated to map METTL3-binding. B) FLAG/HA-tagged METTL3 was purified from HEK 293T cells that additionally expressed one of the different myc-tagged WTAP constructs. Bound WTAP proteins within the IP sample were detected in a anti-myc immuno blot.

Both truncation experiments point out that the region essential for METTL3-binding lies within the amino acids 48 to 151. When comparing these findings with the coiled-coil prediction of WTAP, then it can be hypothesized that the two first predicted coils are involved in the binding of METTL3 (Fig. 2.12). Evidence for this is given by the fact that both constructs showing no binding to METTL3 (indicated in red) are missing one of the two predicted coil-regions, whereas the constructs showing reduced but detectable association (indicated in green) still harbor both structured segments of WTAP.

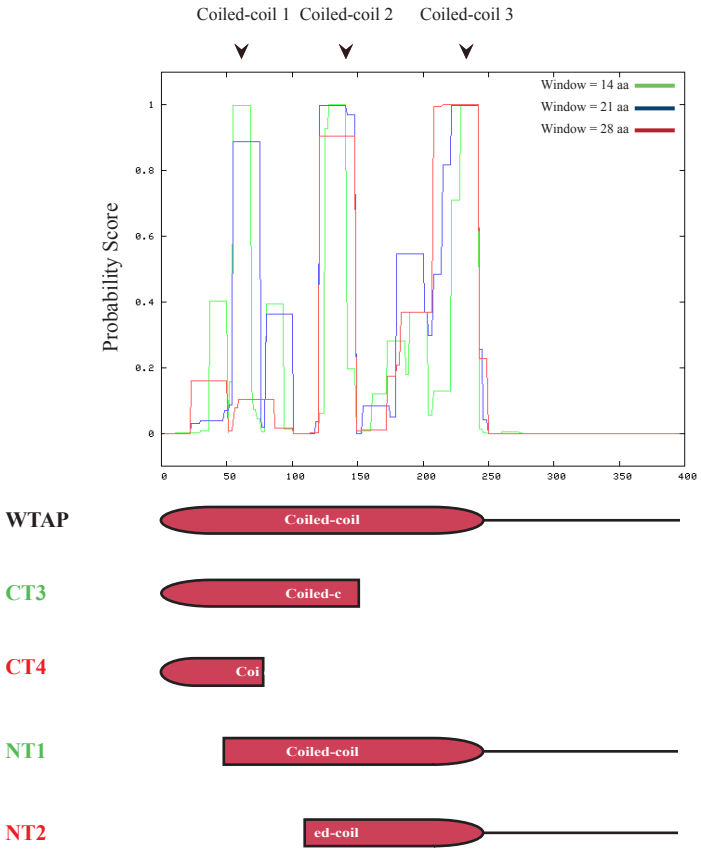

Figure 2.12 Summary of the WTAP truncation experiments WTAP truncation constructs showing significant METTL3-binding (in green) and those with no observable binding (in red) were compared with the coiled-coil prediction of WTAP. Predicted coiled-coils are indicated above the coil-plot diagram with arrow heads.

2.3.3 Investigating METTL3-METTL14 dimerization

METTL3 and METTL14 have been reported to form a stable dimer.[168] However, the exact interaction surface or protein domain that promotes this dimerization had not been determined when these experiments were planned. Since both METTL proteins share a common domain, namely the MT-A70 domain, this region was the first candidate to test its dimerization capability. For this, a similar approach was chosen as applied for the mapping of the WTAP-METTL3 interaction. Three untagged METTL14 truncation constructs (METTL14-F1 to F3) were designed, in which the N- and C-terminal portion around the MT-A70 domain were removed in different combinations (Fig. 2.13 A). Each construct was then cloned into an expression vector encoding for a GST-tagged ΔLH-METTL3 fusion protein (constructs were designed and cloned by Dr. Nora Treiber, University Regensburg).

These vectors were utilized to generate baculovirus stocks that were used to infect Sf21 cells for recombinant expression of the METTL protein variants. Lysates from these cells were then subjected to a GST-pulldown experiment that should enrich for the Δ-LH-METTL3 construct (Fig. 2.13 B). The retrieved eluates from this experiment were assessed in a coomassie gel to inspect which of the untagged METTL14s could be efficiently copurified with METTL3. Interestingly, all untagged versions of METTL14 could be detected (lanes 2-4), even the smallest construct that solely contains the MT-A70 domain (lane 4). This experiment also indicates that the leader helix of METTL3 is not necessary for the interaction between both METTL proteins (lane 1).

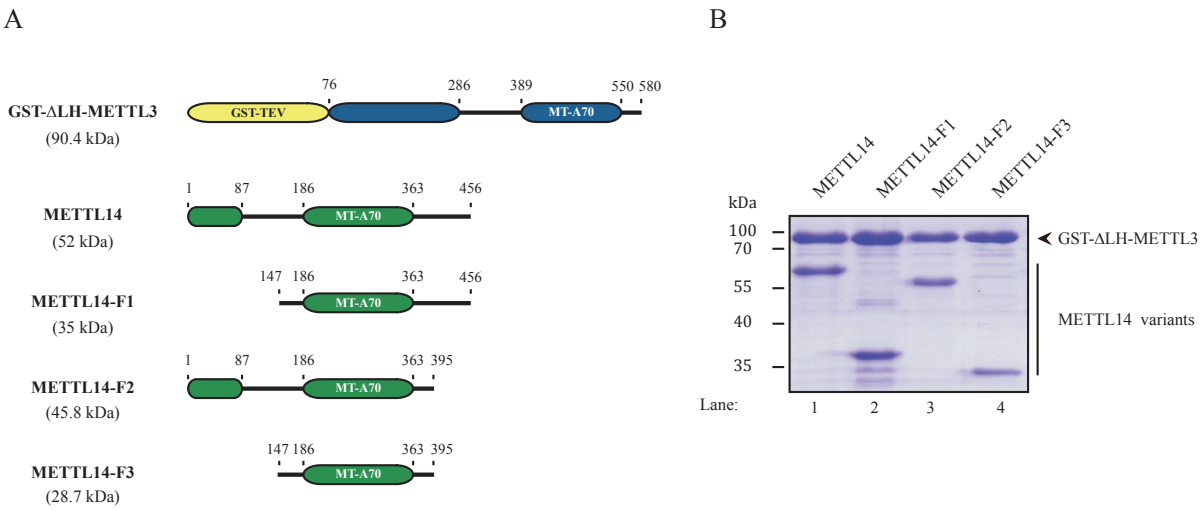

Figure 2.13 METTL14 dimerizes with METTL3 via its MT-A70 domain A) Schematic of the constructs used to determine the dimerization domain of METTL14. B) Sf21 cells were infected with baculoviruses that promote the co-overexpression of GST-tagged ΔLH-METTL3 and one of the different untagged METTL14 constructs shown in A). The GST-tagged METTL3 variant was enriched during a GST-pulldown experiment. METTL14 proteins that could be efficiently copurified with this approach were detected in a Coomassie gel.

This experiment indicates that the dimerization region of METTL14 resides within its MT-A70 domain. From this data, it was hypothesized that METTL3 interacts with its MT-A70 domain in a similar fashion. In order to validate the previous experiment and to gain evidence for the proposed working hypothesis, a cross-linking and mass spectrometry experiment (CX-MS) was conducted in close collaboration with the group of Franz Herzog (LMU, Munich). For this experiment, full-length METTL3 and METTL14 were expressed and purified as described within the first section of this work (see section 2.2.3). The native protein complex was then treated with a chemical cross-linker and subsequently digested with a protease. The resulting cross-linked protein fragments were afterwards analyzed via mass spectrometry.

The detected intermolecular (in blue) and intramolecular (in red) cross-links were then visualized with the online tool xVis Crosslink Analysis Webserver (Fig. 2.14; experiment preformed by Götz Hagemann, LMU).

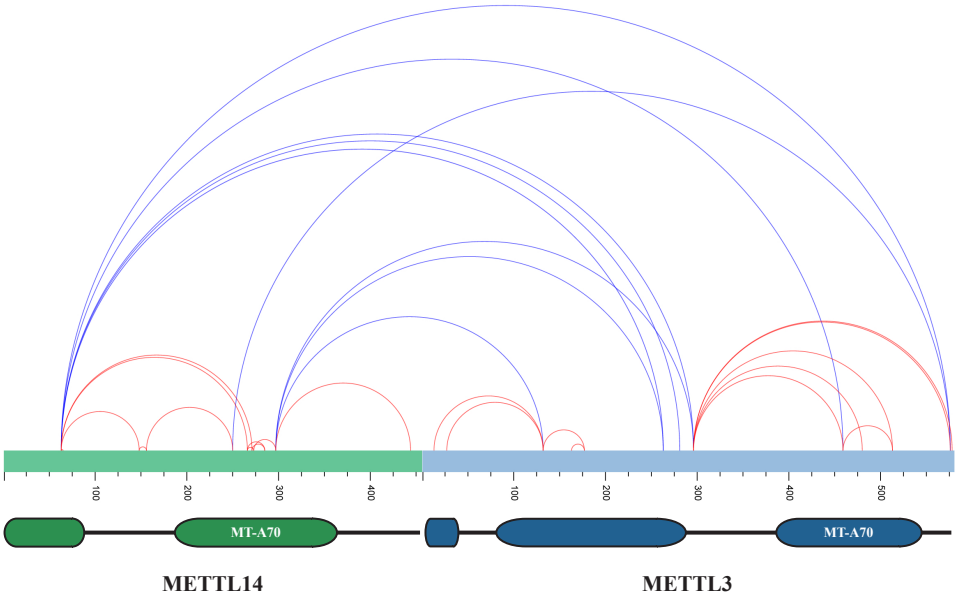

Figure 2.14 Investigating METTL3-METTL14 protein interaction via a chemical cross-linking combined with mass spectrometry Recombinant METTL3/14 complex was purified as described in a previous section of this work. The native complex was then chemically cross-linked and subsequently fragmented using a protease. The resulting cross-linked peptides were analyzed via mass spectrometry. Intermolecular and intramolecular cross-links are indicated in blue and red respectively.

Since the GST-pulldown experiment provided evidence for the interaction of the MT-A70 domain of METTL14 with METTL3, cross-links within this region were closely examined. Opposite to the findings of the pulldown experiment, no cross-links were found that would confirm the hypothesized interaction of the MT-A70 domains of both METTL proteins. The cross-linking events found within the MT-A70 region of METTL14 were either associated with the second structured domain of METTL3 or its C-terminus. When examining the MT-A70 domain of METTL3, then only a single intermolecular crosslink with the N-terminus of METTL14 can be detected.

Crosslinks detected in this approach are dependent on the chemical crosslinker utilized in the preparation of the samples as well as the distance of the functional groups that can form covalent bonds with the agent. It is therefore possible that the interaction observed in the GST-pulldown is not detected in this experiment, because the appropriate reagent was not used or the cross-linkable amino acids within both MT-A70 domains were to far apart from each other. In conclusion, the results obtained from this experiment do not provide a clear-cut view on the exact dimerization region of METTL3 and does not

support the proposed interaction of METTL14's MT-A70 domain with METTL3.

2.4 Investigating nuclear import of the METTL3/14 complex and WTAP

Both the METTL3/14 complex as well as the auxiliary protein WTAP reside in the nucleus.[168,170] In the literature it has been demonstrated that WTAP is not required to import the METTL3/14 complex into the nucleus, as the complex resides in the nucleoplasmn if WTAP is depleted from the cell.[170] However, it has not been determined on how these components are imported into the nucleus. The next experiments should investigate if all three known interacting proteins possess a functional nuclear localization signal (NLS). Additionally, experiments were conducted to explore if the METTL3/14 complex is assembled in the cytoplasm and imported as a whole or if the individual subunits are first imported into the nucleus before assembly.

2.4.1 Both WTAP and METTL3 possess a predicted and functional NLS

The primary sequences of WTAP, METTL3 and METTL14 were scanned using the Eukaryotic Linear Motif resource tool to identify sequences that resemble canonical NLSs (see 5.2.6.4).[180,181] For all three proteins, high confident predictions could be determined (Fig.2.15 A-C). A characteristic feature of NLSs are positively charged amino acids that are critical for the interaction with factors (such as importins) that facilitate the import of cargo proteins into the nucleus.[187–189] Point mutations (Fig.2.15 A-C; indicated in red; designed and cloned by Franziska Weichmann, University Regensburg) were introduced into the predicted NLS of all three proteins (NLS-mut). These mutant constructs were then transfected into HeLa cells. The localization of the resulting proteins was then assessed during immunofluorescence experiments (all IF experiments conducted by Franziska Weichmann, University Regensburg) and compared with the corresponding wild type construct. As expected, the wild type constructs of WTAP, METTL3 and METTL14 show a clear nuclear signal. Interestingly, the nuclear import of the two NLS mutants of WTAP and METTL3 seems to be impaired after introducing the indicated mutations. However, the METTL14 mutant still localized within the nucleus. This indicates that this protein either does not possess a canonical NLS or is imported via a different mechanism.

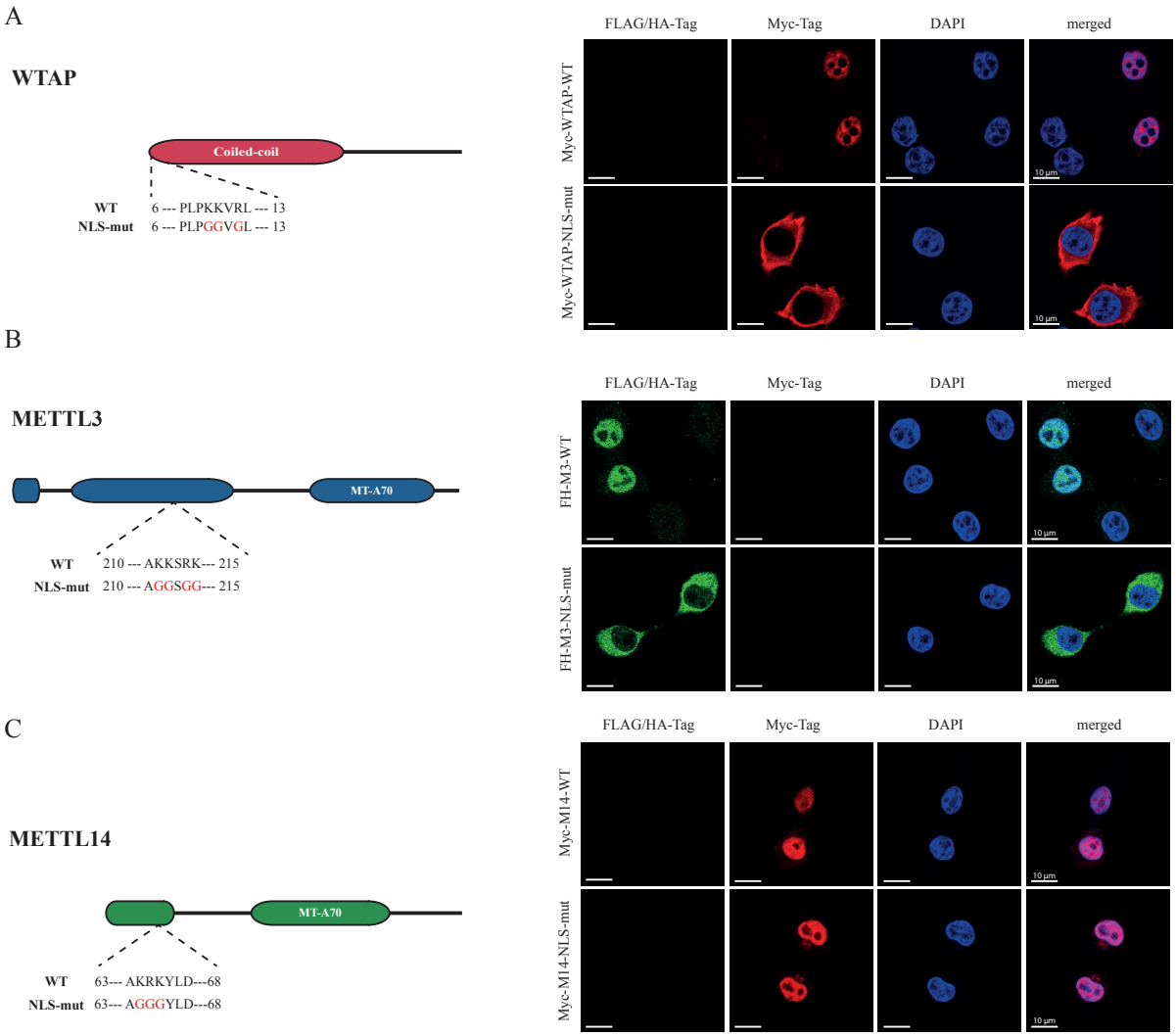

Figure 2.15 WTAP and METTL3 posses functional nuclear localization signals A) The potential NLS of WTAP was predicted *in silico* and positively charged residues were exchanged for glycine (indicated in red). The import of wild type and NLS mutante WTAP was assessed in an immune fluorescence experiment conducted in HeLa cells. The approach described for WTAP was also applied for METTL3 (M3; B) and METTL14 (M14; C). Numbers indicate the amino acid position of the predicted NLS for each protein. FH, FLAG/HA-tag; WT, wild type

2.4.2 The interaction with METTL3 is essential for the nuclear import of METTL14

After this mutational experiment, a hypothesis was formulated. This proposes that the translocation of METTL14 across the nuclear envelope could rely on the interaction with METTL3. This in return requires the cytoplasmic formation of the minimal methyltransferase complex before it is imported into the nucleus. In this model, the nuclear transport of the protein complex would only need a single functional NLS and not one for each individual subunit. To test this working-hypothesis, the myc-tagged "NLS mutant" of METTL14 (M14-NLS-mut) was coexpressed in HeLa cells with either the wild type construct or NLS mutant of METTL3 (M3 and M3-NLS-mut respectively, both FLAG/HA-tagged). The localization of the METTL proteins was then investigated via an immunofluorescence experiment (Fig. 2.16 A).

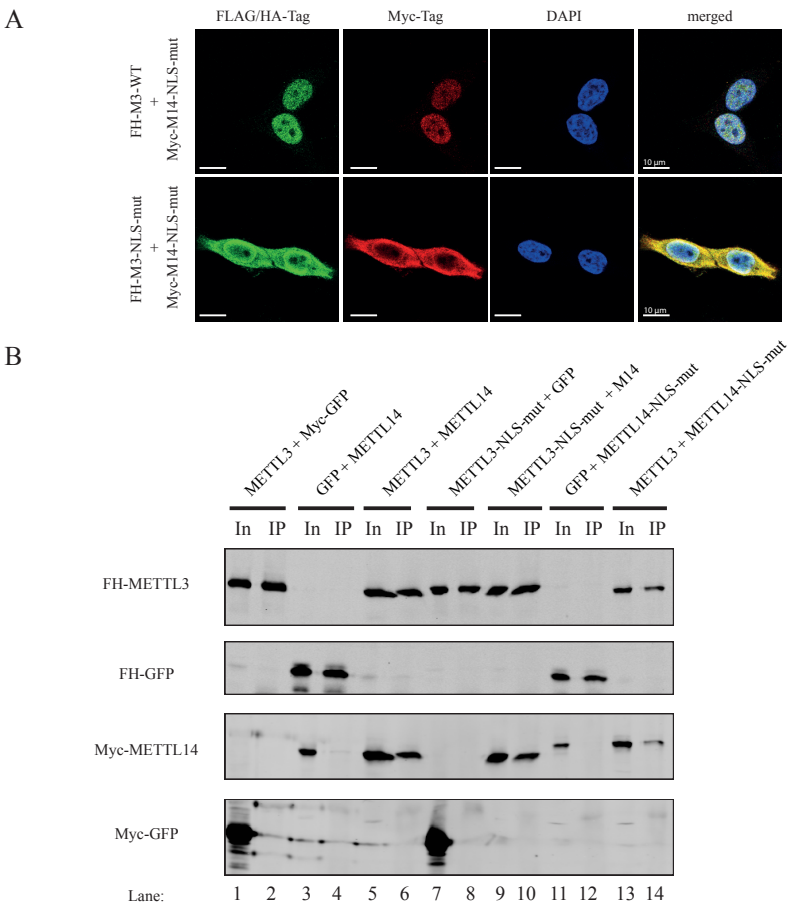

Figure 2.16 The import of METTL14 into the nucleus relays on an intact NLS of METTL3 A) Wild type or NLS mutant METTL3 (M3 and M3-NLS-mut respectively) was cotransfected in HeLa cells with the predicted NLS mutant of METTL14 (M14-NLS-mut). The localization of the METTL proteins was then assessed via immunofluorescence. B) Both wild type and NLS mutants of METTL3 (FLAG/HA tagged) and METTL14 (myc-tagged) were transfected in different combinations into HEK 293T cells. FLAG-IPs were performed to examine the binding capability of the different METTL3 and METTL14 variants.

Transfection of the predicted NLS mutant of METTL14 together with wild type METTL3 show a nuclear abundance of both proteins within HeLa cells (upper panels). Interestingly, when the NLS mutant of METTL3 is coexpressed, then the same METTL14 construct is retained in the cytoplasm (lower panels). In order to test if this relocalization of METTL14 relies on a direct interaction with the NLS mutant of METTL3, co-immunoprecipitation experiments were conducted (Fig. 2.16 B). Within these experiments, different combinations of wild type and NLS-mutant constructs were tested. Wild type METTL3 can still efficiently copurify the predicted NLS mutant METTL14 in anti-FLAG-IPs (lane 14), indicating that the introduced mutation has no effect on the dimerization of both METTL proteins. Interestingly, a stable interaction of METTL14 is also detectable when precipitating the mutant variant of METTL3 (lane 10), suggesting that the cytoplasm localization of METTL14 could be the result of the binding to the METTL3 NLS-mutant.

The results from these experiments provide evidence that the nuclear import of METTL3 and METTL14 relies on the identified NLS present in METTL3. This observation also favors the hypothesis that the dimeric methyltransferase complex is most likely formed in the cytoplasm and translocated as a whole across the nuclear envelope. The data gathered within this work provides a first insight into the import of core components of the m^6A methyltransferase as well as the interaction regions between the three known interactors. Finally, biochemical analysis of the METTL3/14 complex clearly show that METTL14 is not necessarily the catalytic subunit within the dimer, thus changing the currently established model on m^6A-formation.

3. Discussion

3.1 A revised view on METTL3/14 catalysis

The current view on the formation of m^6A was mainly provided by a report published by Liu and colleagues.[168] The group identified METTL14 as an additional component of the N6-adensosine methyltransferase complex and analyzed the catalytic activity of the two METTL proteins separately. During this experiment it was observed that METTL14 alone possesses a higher methyltransferase activity than METTL3. This led to the assumption that METTL14 is the catalytic subunit of the METTL3/14 complex. However, since this publication, another report has indicated some controversy. Experiments conducted by another group suggest that METTL3 and METTL14 by themselves are not stable. This is not only true *in vitro*, but has been demonstrated as well *in vivo*.[169] These findings, therefore, challenged the conclusion made during the initial report of the METTL3/14 complex concerning the activity of each subunit outside the context of the assembled dimer. During this thesis this controversy should be further biochemically investigated.

The results obtained from the SAM cross-linking (see Fig. 2.3) experiment and the mutational analysis using the recombinant APPA mutants (see Fig. 2.6) suggest that the activity of the binary complex is solely dictated by METTL3 . Different publications provide further evidence for this hypothesis. Early fractionation experiments conducted to enrich for the m^6A-methyltrasferase from nuclear extracts, led to the initial identification of METTL3.[167] In a SAM-binding experiment similar to the one conducted here, the group could only identify MT-A70 (METTL3) as the SAM-binding subunit of the complex.[167] The authors further demonstrated that their isolated MT-A70 containing complex is active and can methylate substrates within a RRACH motif. These characteristics point-out that the authors examined the same methyltransferase complex as the one investigated in this thesis. To that time, however, it was not known that METTL14 is a crucial component of the methyltransferase. Nevertheless, it can be assumed that METTL14 was also present in the complex studied by Bokar and colleagues, since their complex displays the same biochemical properties as observed for the purified METTL3/14 dimer.[169]

Another report that underlines the proposed importance of METTL3 in the formation of m^6A was presented by Fustin and colleagues.[190] This group investigated the cellular circadian clock and the impact METTL3 has on it. A METTL3 construct was designed in which the DPPW-motif was mutated. Upon the expression of this construct, the length of the circadian periods within the cell were extended in

comparison to the wild type control. However, the group did not investigate if these mutations have an effect on global m^6A-levels present on mRNA and was only assumed. Nevertheless, this study could show that an intact DPPW-motif within METTL3 is crucial for the cell and it has been demonstrated that this motif is key for the catalytic function of other methyltransferases.[178,182] Therefore these studies further favor a catalytic involvement of METTL3 within the dimeric methyltransferase complex.

The most convincing evidence confirming the findings of this work that METTL3 is truly the active subunit within the METTL3/14 dimer, has been provide by two independent groups. During the preparation of this thesis, two crystal structures of the methyltransferase domains (MTDs) from METTL3 and METTL14 have been published.[191,192] Additional structures were obtained in which the protein complex was co-crystallized with the methyldonor SAM (Fig. 3.1 A-C). Both structures reveal that SAM is only associated within a binding pocket of METTL3, and therefore confirming the finding of the SAM cross-linking experiment. When examining the SAM-bound METTL3 structure, it can be seen that the methyldonor is not only in close proximity of the DPPW-motif, but is also coordinated by the aspartate of the tetrad (Fig. 3.1 B and C).

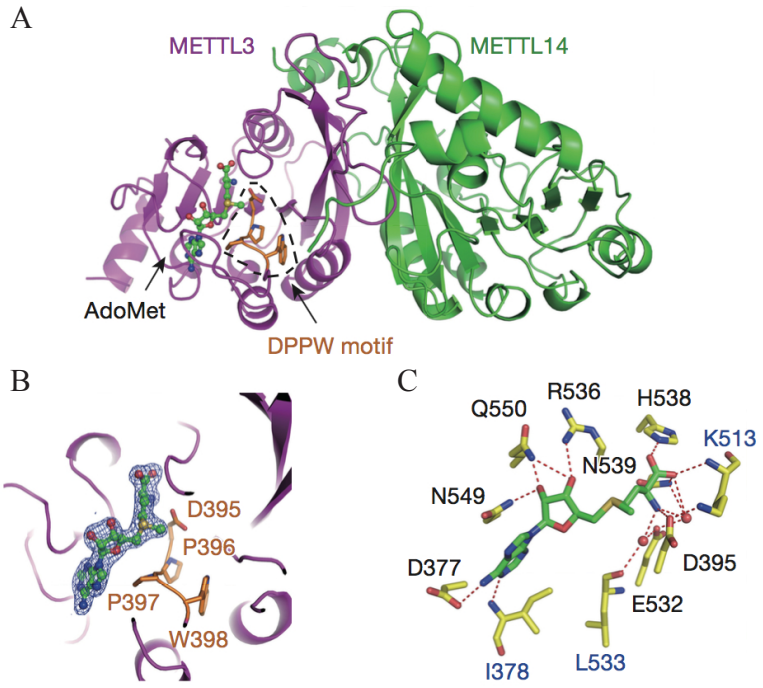

Figure 3.1 Crystal structure of the MT-A70 domain of METTL3 and METTL14 A) Overall structure of the MT-A70 domains of METTL3 (purple) and METTL14 (green). B) Close-up of the SAM-binding pocket within METTL3. Indicated in orange are the residues that form the DPPW-motif, which are essential for METTL3 activity. C) Shown are the amino acids involved in the coordination of SAM within the binding pocket of METTL3. Figure adapted from Wang *et al.*[192]

These structures offer direct evidence and an explanation for the observed loss of activity in the METTL3 APPA mutant during the *in vitro* methylation assays. Upon mutation of D395, SAM-binding might be greatly impaired or even obliterated and would result in the loss of methyltransferase activity. Indeed, Wang *et al.*conducted isothermal titration calorimetry experiments that compared the wild type METTL3/14 complex with a mutant variant of METTL3 (D395A) and could demonstrate that no significant SAM-binding was present in the mutant variant of the binary complex.[192] Besides METTL3, METTL14 was also in the scope of the mutational analysis of this thesis. The experimental results suggest that this subunit is not directly involved in the formation of m^6A , since mutation of the EPPL-motif showed that methylation activity was still present. The observed reduction in activity of the METTL14 APPA mutant was likely the result of the smaller quantities of the complex used during the assay. Similar to the experiment conducted with the APPA mutants, the group that published the second structure also examined METTL14 by introducing a single point mutation, the glutamate of the EPPL-tetrad was exchanged for an alanine (E192A).[191] In agreement with the findings of this thesis, no significant reduction could be observed when the predicted catalytic sequence of METTL14 is altered.

Both published crystal structures as well as the results gathered from the SAM cross-linking experiment and the mutational study provide evidence that METTL3 alone is essential for catalytic activity of the complex and that the EPPL-motif from METTL14 is not directly involved mechanistically. This, therefore, revises the view in the field that METTL14 is the catalytic subunit of the complex. Nevertheless, important roles for METTL14 have been proposed by the two structure papers concerning complex stability and substrate recognition, which are further discussed in the following sections.[191,192]

3.2 Dimerization of METTL3 and METTL14

The GST-pulldown experiment suggests a role of the MT-A70 domain from METTL14 to directly be involved in the dimerization with METTL3. However, the intended confirmatory cross-link MS analysis provided controversial results. When comparing both experimental approaches, then the results from the batch purification of the individual METTL14 truncations provide more convincing evidence than the MS analysis. This is due to the fact that all untagged METTL14 variants were copurified with GST-ΔLH-METTL3. Since it is unlikely that all three different METTL14 constructs were unspecifically copurified, the obtained results imply that the dimerization region of METTL14 resides within the structured MT-A70 domain.

By emphasizing the GST-pulldown results, how should the results of the CX-MS experiment then be in-

terpreted? In order to detect protein-protein interactions within both the GST-pulldown as well as the CX-MS method, a native, correctly folded and assembled protein complex is needed. While the GST-pulldown experiment generates simple results (binding vs. no-binding) the CX-MS can provide more detailed information of protein regions that are in close-proximity to each other.[193] However, the detection of the interactions between protein regions rely on several elements: the chemical agent used during the experiment, the distance and presence of cross-linkable functional groups.[194]

The CX-MS experiment performed in this work used bis-sulfosuccinimidyl suberate (BS3) as a chemical cross-linker to generate the detected cross-linked peptides. This reagent is used to cross-link the primary amine of lysines and the N-terminus.[194] BS3 also possesses a linker that spans eight carbon atoms. Since the CX-MS experiment of the METTL3/14 complex only utilized this single cross-linking agent, it is possible that the interaction between the MT-A70 domains of both METTL proteins could not be detected using this approach. In order to obtain a more accurate overview of the complex, different cross-linkers should have been tested. This might have identified high confident cross-links that would agree with the results of the GST-pulldown experiment.

As mentioned in the last section, two crystal structures have been published that provide a detailed view on the architecture of the MT-A70 domains of both METTL proteins (referred as MTD in both publications).[191,192] Close examination of both METTL3/14 structures show that both proteins dimerize via their MT-A70 domains (Fig. 3.2 A and B). Both domains establish an extensive network of hydrogen bonds between each other, resulting in a stable complex formation. A majority of the mapped residues involved in the protein-protein interaction of METTL14 with METTL3 are also present in the smallest METTL14 fragment (M14-F3) analyzed during the GST-pulldown experiment. The amino acids R135, D136 and Y146 of METTL14 were, however, missing in this METTL14 truncation construct and are shown in the crystal to also interact with METTL3 (Fig. 3.2 B (orange framed panel)).[192] Since a efficient copurification of METTL14 was observed, it can be assumed that these residues are not essential for the overall complex assembly of both METTL proteins, but might further stabilize the complex.

Taken together, the obtained CX-MS results could not determine the dimerization domain of METTL3 and METTL14. However, the GST-pulldown experiments demonstrated that the MT-A70 domain of METTL14 was likely to be involved in the complex formation and has been confirmed through the recently published structural studies. These structural reports additionally verified the assumption that METTL3, as well, promotes the dimerization with METTL14 via its MT-A70 domain.

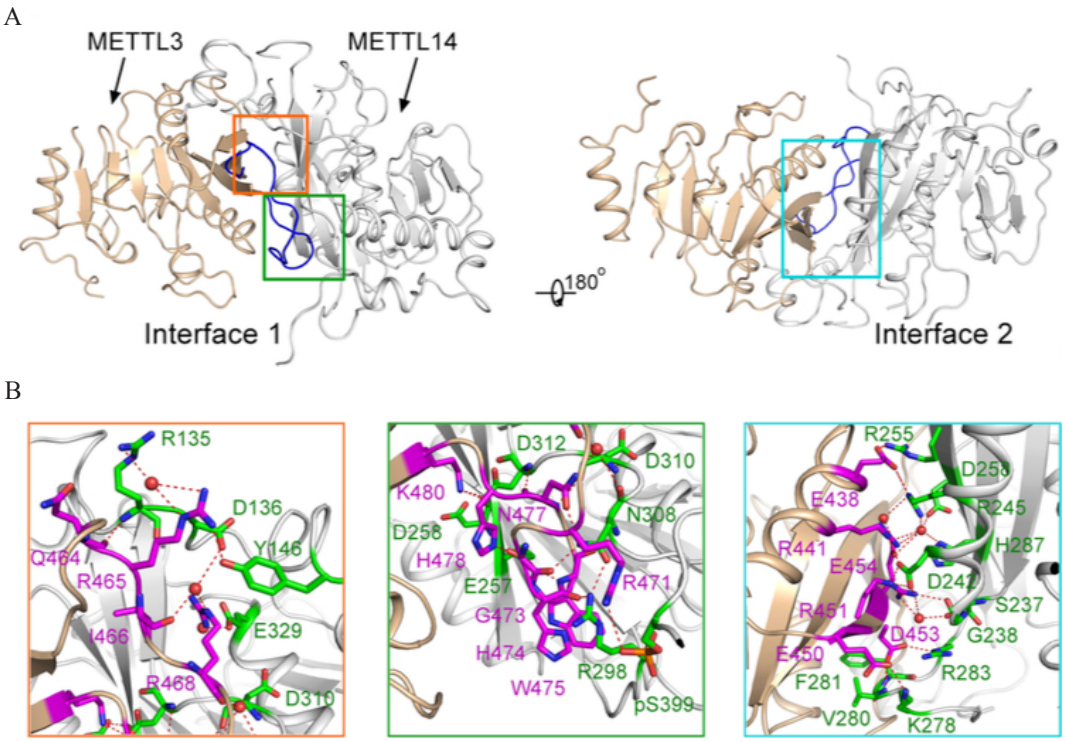

Figure 3.2 Detailed view of the METTL3-METTL14 dimerization via their MT-A70 domains A) The dimerization interface of METTL3 (colored wheat) and METTL14 (colored silver) are composed of the regions termed interface 1 and interface 2. Interface 1 is highlighted by a orange and green box, whereas interface 2 is framed by a cyan rectangle. B) Detailed view of the interface regions 1 and 2 showing the amino acids involved in the dimerization of both METTL proteins. The color of each frame corresponds to the highlighted region in A). Figure adapted from the extended data section of Wang *et al.*[192]

3.3 Substrate-binding of the METTL3/14 complex

Methylation of adenine within a RRACH motif requires a direct interaction between the RNA substrate and the METTL3/14 complex. Therefore, it has been proposed that the methyltransferase might also contain a protein domain(s) that introduces specificity. Substrate specificity has been observed *in vivo*, since not all RRACH motifs that are dispersed throughout mRNA become methylated.[40,41] Another topology aspect that underlines the need for specificity is demonstrated by the enrichment of m^6A within the 3' end of mRNAs.[40,41]

EMSAs of full length METTL3 and METTL14 could demonstrate that the complex is capable of binding an RNA substrate that has also been utilized during the *in vitro* methylation assays. However, closer examination of the observed shifts has shown that the protein complex seems to bind to polyanions in an unspecific fashion. This conclusion has been drawn as the binding of the methylatable RNA sub-

strate can be effectively abolished through the titration of yeast tRNA. In addition, different nucleic acid species (RNA, DNA or hybrid) containing an RRACH motif could all interact with the METTL protein complex, since a detectable shift within the EMSAs was observed. A third aspect that further indicates that the observed RNA-binding is unspecific is the fact that heparin can also interfere with the binding of the substrate RNA.

Experiments conducted by Wang *et al.*support the observations made during this work, as the authors have carried-out EMSAs using similar conditions.[192] However, the authors did not evaluate the specificity of the RNA binding by using different substrates, polyanion additives or varying the concentration of yeast tRNA. Within the structure of the same publication, a positive patch could be identified that is likely to be responsible for the binding to polyanions, since their observed RNA substrate-binding is greatly impaired upon the mutation of arginine and lysine residues residing within this patch. Careful examination of the crystal structure also revealed that the METTL3/14 complex seems to lack a canonical target recognition domain (TRD). TRDs are protein domains essential for introducing target specificity of nucleic acid modifying proteins.[195,196] The authors of the first published structure of METTL3/14 propose that METTL14 could contain protein regions that might compensate the lack of a traditional TRD.[192]

When testing this hypothesis with the EMSA data provided by this work, then it can be argued that target specificity of the protein complex might be achieved through another mechanism. The fact that methylation occurs within a degenerated RRACH motif supports the idea that the METTL3/14 complex might only posses a minimal specificity towards distinct RNA sequences and that the non-stochastic distribution of m^6A is facilitated by another factor or factors. A recent publication by Patil *et al.* provides experimental evidence that proteins other than METTL3 or METTL14 might provide target specificity for the m^6A-methylation machinery.[197]

In this report, two RNA-binding proteins were identified, namely RBM15 and RBM15B, that interact with the METTL3/14 complex via WTAP. In addition to the physical interaction of both RBM proteins, binding sites of RBM15 and RBM15B were found in close proximity of m^6A-sites within various mRNAs. Depletion of either RBM protein or both have a direct impact on cellular m^6A-levels, further supporting the idea that these proteins introduce target specificity. Both RBM15 and RBM15B belong to the split end (SPEN) protein family. All members of this family posses a similar protein architecture harboring three RNA recognition motifs in their N-terminus and a SPEN-Paralog-Ortholog-Conserved domain in the C-terminus.[198] Interestingly, in *Drosophila* a protein termed Nito has been identified to interact with the fly homologs of WTAP and METTL3 (Fl(2)d and Ime4, respectively).[199] Like RBM15 and RBM15B,

Nito as well belongs to the SPEN family and depletion of the protein has also a direct consequence on m^6A-levels. Therefore, it can be assumed that the association of RNA-binding proteins with the m^6A-methyltransferase and guiding the complex to specific RNA targets could be a common theme that is conserved between species.

These findings allow to hypothesize that the methylation of specific RRACH motifs is dictated by RNA binding proteins that interact with the METTL3/14 complex and function as modular TRDs. These proteins would tether the methyltransferase to certain regions within target RNAs. The anchored METTL3/14 complex can then scan the surrounding RNA region for RRACH motifs and modify these once the substrate is properly oriented within the dimeric methyltransferase. This model could elegantly explain the lack of a TRD within the methyltransferase complex and why METTL3 and METTL14 do not have to display a high degree of substrate specificity. Further studies will have to concentrate on the identification of further RNA binding proteins that interact with METTL3 and METTL14, or their homologs, in order to further support the model proposed here, since not all methylation sites are influenced by the RNA-binding proteins so far identified.

3.4 WTAP-METTL3 interaction

METTL3-WTAP interaction has been reported to be essential for the import of the methyltransferase complex from the nucleoplasm into nuclear speckles.[170] However, besides the localization of the complex into these sub-nuclear structures, it is not exactly known what other molecular roles WTAP fulfills. In this work, investigating the interacting region between WTAP an METTL3 was first carried out using an *in silico* approach. Examination of the protein sequence of both proteins revealed that predicted coiled-coils could be the underlining protein structures involved in their interaction. Protein-protein interactions promoted by multiple coiled-coils forming homo- or heteromeric complexes have been reported.[184–186] Therefore, this was a valid working hypothesis that was further investigated.

Experiments were performed using N- and C-terminal truncations of WTAP and different variants of METTL3 to investigate this predicted interaction mechanism. These experiments provided evidence that structures within the amino acids 48 to 151 of WTAP are essential for the direct interaction with the methyltransferase subunit. The work conducted by Ping and colleagues could show that indeed the WTAP region involved for the protein-protein interaction with METTL3 resides within the first 200 amino acids of its N-terminus.[170] However, no further mapping efforts were made to narrow this region down. Ultimately, structural information provided by cyro-electron microscopy or crystallization of a

WTAP/METTL3/METTL14 complex could provide further evidence for the working model derived from this work. However, both structural biology approaches rely on a robust heterologous expression of all components of the WTAP-m^{6}A-methyltransferase complex. Full length WTAP has been shown to easily form large protein aggregates when expressed in *E. coli* (Master Thesis David Wunderlich conducted within the Biochemistry I department) and insect cells.[168] Therefore, it may be beneficial to test a spectrum of soluble truncations of WTAP and try to co-crystallize these constructs with the METTL3 leader helix.

An alternative approach to validate the coiled-coil promoted interaction could be the construction and expression of refined WTAP mutants and repeating the performed Co-IP experiments. Coiled-coils are generally composed of so-called heptad repeats and the amino acids within these repeats are denoted with the letters a, b, c, d, e, and f (Fig. 3.3 A).[200] In many coiled-coils, hydrophobic amino acids are found within the positions a and d of the repeats. Amino acids at these positions are known to form a hydrophobic interface between coil-forming α-helices and enable their association with one another (Fig. 3.3 B).[201,202] Using this information, one strategy to provide further evidence on the coiled-coil-mediated interaction between WTAP and METTL3 would be to mutate amino acids within the positions a and d of the heptad repeats found in both proteins. An exchange of these hydrophobic amino acids for more hydrophilic ones could result in the loss of the observed interaction. Publications have shown that an exchange of amino acids at these positions can indeed promote the destabilization of coiled-coils.[184,203] WTAP or METTL3 leader helix constructs bearing these mutations could be tested within the system used in this work and add further information on the exact interaction mechanism of both proteins.

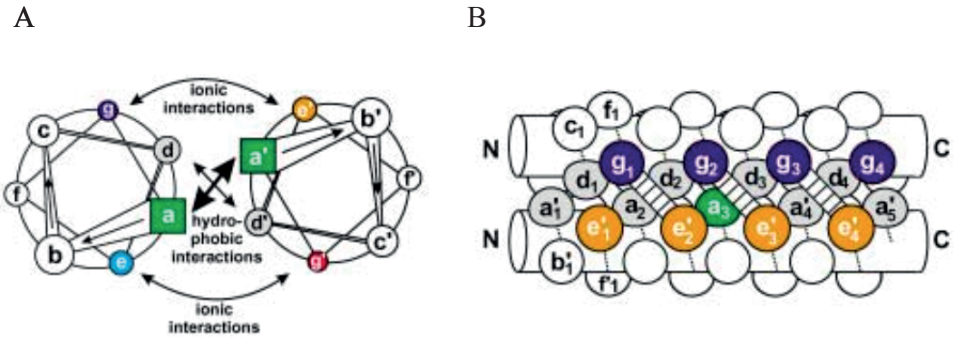

Figure 3.3 General structure of a coiled-coil A) Shown in a wheel diagram are two α-helices that form a coiled-coil. The amino acids of the heptad repeat of each helix are denoted from N- to C-terminus as a-f or a'-f'. Amino acids within the a/a' and d/d' position interact with its corresponding interaction partner via hydrophobic forces, whereas residues in position g/g' and e/e' interact through hydrophilic forces with each other. B) Amino acids within the a/a' and d/d' position of several heptad repeats form a hydrophobic surface that is essential for the formation of a coiled coil. Figure adapted from Mason and Arndt[200]

3.5 Cellular localization of the core methylation machinery components

All factors of the core methyltransferase machinery, namely WTAP, METTL3 and METTL14, are localized within nuclear speckles.[168,170] For the proper import into the nucleus, many nuclear proteins rely on an NLS embedded within their primary sequence.[187] Results from the IF experiments conducted within this work suggest that both WTAP and METTL3 posses a functional NLS that is required for their proper localization. Both signals can be categorized as classical monopartite NLS. These NLS are characterized to posses a signal stretch of basic amino acids that resembles the monopartite NLS of the simian virus 40 large T-antigen, which is considered a strong NLS due to its extensive characterization.[204–206] Using the NLS-scanning algorithm of the Eukaryotic Linear Motif resource tool, a classical monopartite NLS was also predicted for METTL14. Mutational analysis could, however, not provide evidence that this proposed NLS is actually functional. As a consequence it can be argued that METTL14 is imported into the nucleus via a different mechanism or utilizes an "exotic" NLS. This model would suggest that either the METTL proteins are imported separately or that the METTL3/14 complex as a whole is transported into the nucleus, which can be mediated by two different NLS. This, in return, would also suggest that the assembly of the METTL3/14 complex could occur both in the nucleus and the cytoplasm.

Besides this hypothesis another one was suggested that takes into account that each METTL protein by themselves are quite unstable.[169] With this stability issue, it seems more favorable for both proteins to dimerize upon completion of translation followed by the import of the whole METTL3/14 complex into the nucleus. Within this working model, a single NLS would be sufficient to localize the m^6A-methyltransferase into the nucleoplasm, since the transport into nuclear speckles relies on the interaction with WTAP.[170] Evidence for this model could be provided through the IF experiments. However, further experiments should be preformed to further back-up the formulated hypothesis. For instance, a complementary experiment could be to conduct the same experiments in a METTL3 knock-out cell line (generated using the CRISPR/Cas9 technology[207]). Within this defined genetic background, it should be possible to convincingly show the import of METTL14 via METTL3 during a rescue experiment. METTL14 should reside in the cytoplasm in the absence of ectopic METTL3. The proper localization of METTL14 should be displayed by the knock-out cell line after METTL3 has been reintroduced into the cells.

Within the field, it has been accepted that all core methyltransferase components are imported into the nucleus and carry-out their function within this compartment of the cell. A recent report from Lin *et al.* demonstrated that METTL3 seems to also fulfill a certain biological function within the cytoplasm.[208] The authors provide evidence for the existence of two distinct METTL3 pools. The first pool

associates with METTL14 and localizes to the nucleus to carry out the methylation of mRNA transcripts. The proposed second METTL3 population resides within the cytoplasm and stimulates translation, without METTL14 being present. Up-regulation of protein synthesis promoted by METTL3 was shown to be independent of the catalytic activity of the m^6A-methylatransferase subunit. When comparing these findings with the body of literature that has been published during the last five years and also taking the data generated during this work, several major questions arise that seem to contradict the proposed role of METTL3 in the cytoplasm.

One matter concerns again the stability of a monomeric METTL3. It has been convincingly demonstrated that this protein mostly relies on METTL14 binding to prevent its degradation when present alone in the cell.[169] This fact implies that METTL3 has to be stabilized through a protein other than METTL14 or that it is stabilized through a completely different mechanism. A proposed alternative stabilizing mechanism could be through the auto-assembly of METTL3. However, there is to date no experimental evidence that METTL3 can indeed form homo-dimers or a higher complex structures by itself that might have a similar stabilizing effect as seen for the interaction with METTL14.

Another question concerning the cytoplasmic role of METTL3 is how does this protein interact with cytoplasmic target mRNAs? Lin *et al*.demonstrate that the observed enhancement of translation does not depend on the MT-A70 domain of METTL3 but on the first 200 amino acids of the protein. The two published crystal structures clearly display the need of both MT-A70 domains of METTL3 and METTL14 for the binding of RNAs or negatively charged molecules in the nucleus. This would lead to the assumption that METTL3 could posses an additional RNA binding region distinct from its catalytic domain or that another protein that interacts with METTL3 facilitates the binding to the target mRNAs in the cytoplasm. This issue needs to be addressed to provide further evidence for the role of METTL3 in different compartments of the cell. Finally, a last aspect that deserves further investigation is how METTL3 can evade its import into the nucleus or how the protein can shuttle between the nucleus and the cytoplasm. The IF experiments conducted in this thesis clearly demonstrate that METTL3 posses a functional classical NLS. This leads to the hypothesis that the import signal of METTL3 has to be somehow repressed in order to stay in the cytoplasm or that the protein possesses an additional nuclear export signal (NES) that allows the shuttling of the protein between both cellular compartments.[209–212]

The suppression of an NLS can occur through different mechanisms. One possibility would be that the NLS is masked by another protein and thus prevents the binding of importins.[188,189] An alternative mode of action to prevent the import of proteins into the nucleus is through the modification (e.g. phosphorylation) of sites adjacent to the NLS.[213,214] These possibilities need to be investigated biochemically

and would provide a plausible answer on how METTL3 can be localized in the cytoplasm even with a functional NLS.

This discussion demonstrates that the import of the core methyltransferase components is barley understood. It is also not clear if the association of WTAP with the METTL3/14 complex occurs first in the nucleus or can already take place in the cytoplasm. The presence of a functional NLS in both METTL3 and WTAP could argue for the assembly of the trimeric complex (WTAP/METTL3/METTL14) in the nucleus, since the import of METTL3 and METTL14 most likely relies on a single NLS in METTL3. Another interesting matter would be to investigate which importin or importins facilitate the transport of the core methyltransferase components across the nuclear envelope.[215,216] Dissecting this is, however, far from trivial, since the nuclear transport of some cargo proteins can be facilitated by more than one importin.[217,218] Dissection of this cell biological aspect could also reveal a potential mechanism on how m^6A-levels can be regulated through alternative sub-cellular localization or how components of the methyltransferase (e.g. METTL3) can fulfill other physiological roles within the cell.

4. Outlook

The field of post-transcriptional RNA modifications has quickly expanded over the last 5 years. This area of research has provided some insight on a new regulatory layer present on RNA that has a significant impact on gene expression and RNA function (see section 1). Within this field, m^6A has been the most intensively studied mRNA modification. Even though the core methyltransferase has been identified and several m^6A-based mechanisms have been described, many biological aspects of this nucleic acid modification still remain elusive.

This work could provide evidence that the catalytic activity of the METTL3/14 complex is solely METTL3-dependent and does not rely on METTL14, which was previously reported.[168] A direct consequence of this observation is to ask the question: what is then the exact role of METTL14 in the complex? So far it seems that METTL14 only functions as a stabilizing factor of the dimeric methyltransferase. However, potential functions for METTL14, such as promoting the interaction with additional proteins associated with the binary complex, cannot be ruled out. Protein domains that lie outside of the MT-A70 domain of METTL14 could harbor the protein-protein interactions sites needed for this task. A question that arises from an evolutionary standpoint is why a second non-functional but highly conserved methyltransferase-like protein is incorporated in the METTL3/14 complex? Further investigations focusing on the catalysis of the methyltransferase complex might provide an explanation.

Another aspect of the m^6A-methyltransferase that needs to be further studied is the composition of the fully assembled complex *in vivo*. The initial characterization from Bokar and colleagues described the human m^6A-methyltransferase as a large protein complex with a predicted molecular weight of greater than 1 MDa.[166,167,219] This observation suggests that a complex exists that possesses more factors than the ones to date identified and validated, namely WTAP, METTL3 and METTL14. The identification of these novel interactions partners and investigating their role within the complex is currently one of the most investigated areas within the field. The RNA-binding proteins RBM15 and RBM15B are the newest factors to be considered an integral part of the m^6A- machinery.[197] The discovery of these proteins might provide a molecular explanation on how METTL3 only methylates a certain pool of RRACH-associated adenosines located in the 3'-UTR of mRNAs. However, not all m^6A-methylation sites that have been mapped so far possess a binding motif for one or both RBM proteins.[197] This leads to the assumption that additional RNA-binding proteins might associate with the methyltransferase in order to target the remaining methylation sites.

Identification and characterization of these additional components of the m^6A-methyltransferase complex could in return also help draw a clearer picture on when exactly this post-transcriptional modification is established. So far, hypotheses have been formulated that link m^6A-formation with splicing.[41,168,169] However, no direct biochemical evidence has been provided to confirm this assumption. These last sections clearly highlight that even though several aspects of methyltransferase complex are now becoming clearer, many other facets still remain elusive. This is not only true for the METTL3/14 complex, but also for other proteins associated with m^6A , such as the "readers" and "erasers". One challenge for the future will be to investigate the potential cross-talk between the "writer", "readers" and "erasers" and how this interaction manifests into a biological response. The findings from these studies will eventually help to understand this additional layer of gene regulation and how the epitranscriptome contributes to development and disease within different organisms.

5. Material and Methods

5.1 Material

5.1.1 Chemicals and Consumables

All chemicals (analytical grade) were purchased from AppliChem GmbH (Darmstadt, Germany), Sigma-Aldrich (St. Louis, USA), Merck (Darmstadt, Germany), Roth (Karlsruhe, Germany) and Thermo Fisher Scientific (Waltham, USA) unless otherwise stated.

Commercially available kits for the isolation of nucleic acids from different sources were purchased from Macherey-Nagel (Duüren, Germany), GE Healthcare (Little Chalfont, UK) or Thermo Fisher Scientific (Waltham, USA). Cell culture media and supplements were obtained from Sigma-Aldrich (St. Louis, USA). Radioisotopes were purchased from Hartmann Analytic GmbH (Braunschweig, Germany). Enzymes, nucleotides and RNA / DNA / protein standards were purchased from Thermo Fisher Scientific (Waltham, USA). DNA and RNA Oligonucleotides used in this work were purchased and synthesized by Metabion GmbH (Planegg, Germany) or Biomers (Ulm, Germany).

5.1.2 Oligonucleotides

Listed in the following tables (Tab.5.1 - 5.3) are the DNA, RNA and hybrid (RNA+DNA) oligonucleotides that were used in this thesis.

Table 5.1 DNA oligonucleotides used for cloning

Name	Orientation	Sequence (5' - 3')	Cloning into	Restriction site	Comment
METTL3-F	Forward	CGCTGCGGCCGCATGTCGGACACGTGGAGC	VP5	NotI	-
METTL3-R	Reverse	CGCTCCTAGGCTATAAATTCTTAGGTTTAGAGATGATACC	VP5	AvrII	-
METTL14 F	Forward	CGCTGCGGCCGCATGGATAGCCGCTTGCAGGAGATCC	pCS2-FAME	NotI	-
METTL14 R	Reverse	CGCTGAATTCTTATCGAGGTGGAAAGCCACCTCTGTG	pCS2-FAME	EcoRI	-
WTAP-F	Forward	CGCTGAATTCAATGACCAACGAAGAACCTC	pCS2-FAME	EcoRI	-
WTAP-R	Reverse	CGCTCTCGAGTTACAAAACTGAACCCTGTAC	pCS2-FAME	XhoI	-
WTAP CT1 R	Reverse	CGCTCTCGAGAGAGGCCTGAGACTGCTG	pCS2-FAME	XhoI	(designed and cloned by Christian Rittinger)
WTAP CT2 R	Reverse	CGCTCTCGAGACGTCCCTGGGACAGCT	pCS2-FAME	XhoI	(designed and cloned by Christian Rittinger)
WTAP CT3 R	Reverse	CGCTCTCGAGGCTATCAGGCGTAAACTTCC	pCS2-FAME	XhoI	(designed and cloned by Christian Rittinger)
WTAP CT4 R	Reverse	CGCTCTCGAGTACCATTGTTGATCTCAGTTGG	pCS2-FAME	XhoI	(designed and cloned by Christian Rittinger)
WTAP NT1 F	Forward	CGCTGAATTCAAACTCTAATGATGTAACTGGCCT	pCS2-FAME	EcoRI	-
WTAP NT2 F	Forward	CGCTGAATTCATCAACAATGGTAGACCCAGC	pCS2-FAME	EcoRI	-
WTAP NT3 F	Forward	CGCTGAATTCAACGCCTGATAGCCAAACAGG	pCS2-FAME	EcoRI	-
ΔLH-METTL3 F	Forward	CTACGGAATCCAGAGGCAGC	VP5 (plasmid amplification)	-	Deletion of LH from VP5-METTL3
ΔLH-METTL3 R	Reverse	GCGGCCGCTAGCGTAATCG	VP5 (plasmid amplification)	-	Deletion of LH from VP5-METTL3
LH-METTL3 F	Forward	GACTGGTACCAGCATGTCGGACACGTGGAGC	pcDNA5-FRT/TO N-GFP	KpnI	Cloning of METTL3 LH (designed by David Wunderlich)
LH-METTL3 R	Reverse	GACTCTCGAGATCCAAGTGCCCCGAGTC	pcDNA5-FRT/TO N-GFP	XhoI	Cloning of METTL3 LH (designed by David Wunderlich)
Mettl3_NLS_F	Forward	AACCAGCAAAGGAGCCAGCCGGGGGATCAGGGGGACATGCTGCCTCAGATGTTGA	VP5 (plasmid amplification)	-	(designed and cloned by Franziska Weichmann)
Mettl3_NLS_R	Reverse	TCAACATCTGAGGCAGCATGTCCCCCTGATCCCCCGGCTGGCTCCTTTGCTGGTT	VP5 (plasmid amplification)	-	(designed and cloned by Franziska Weichmann)
WTAP_NLS_F	Forward	AATGACCAACGAAGAACCTCTTCCCGGGGGGGTTGGATTGAGTGAAACAGACTTCAA	pCS2-FAME (plasmid amplification)	-	(designed and cloned by Franziska Weichmann)
WTAP_NLS_R	Reverse	TTGAAGTCTGTTTCACTCAATCCAACCCCCCCGGGAAGAGGTTCTTCGTTGGTCATT	pCS2-FAME (plasmid amplification)	-	(designed and cloned by Franziska Weichmann)
Mettl14_NLS_F	Forward	ATACCTCTGCTCCAAATGCAGGAGGTGGGTATCTGGATGAAGGAGAGACAGATG	pCS2-FAME (plasmid amplification)	-	(designed and cloned by Franziska Weichmann)
Mettl14_NLS_R	Reverse	CATCTGTCTCTCCTTCATCCAGATACCCACCTCCTGCATTTGGAGCAGAGGTAT	pCS2-FAME (plasmid amplification)	-	(designed and cloned by Franziska Weichmann)

Table 5.2 DNA oligonucleotides used as templates for T7 *in vitro* transcription reactions

Name	Orientation	Sequence (5' - 3')	Comment
loop RSV 2 + m6A substrate	sense	TAATACGACTCACTATAGGGACGAGTCCTGGACTGAAACGGATTTGTCCC	synthesis of methylation assay substrates
loop RSV 2 - m6A substrate	anti-sense	GGGACAAATCCGTTTCAGTCCAGGACTCGTCCCTATAGTGAGTCGTATTA	
loop RSV 2 + negative substrate	sense	TAATACGACTCACTATAGGGACGAGTCCTGGTCTGAAACGGTCTTGTCCC	synthesis of methylation assay substrates
loop RSV 2 - negative substrate	anti-sense	GGGACAAGACCGTTTCAGACCAGGACTCGTCCCTATAGTGAGTCGTATTA	
loop RSV 2 + m6A substrate (mod)	sense	TAATACGACTCACTATAGGGTCGTGTCCTGGACTGTCTCGGTTCTGT	synthesis of methylation assay substrates
loop RSV 2 - m6A substrate (mod)	anti-sense	ACAGAACCGAGACAGTCCAGGACACGACCCTATAGTGAGTCGTATTA	
loop RSV 2 + negative substrate (mod)	sense	TAATACGACTCACTATAGGGTCGTGTCCTGGTCTGTCTCGGTTCTGT	synthesis of methylation assay substrates
loop RSV 2 - negative substrate (mod)	anti-sense	ACAGAACCGAGACAGACCAGGACACGACCCTATAGTGAGTCGTATTA	

Table 5.3 Nucleic acid substrates for EMSAs

Substrate name	Sequence
EMSA RNA	UCGUGUCCUGGACUGUCUCGGUUCUGU
EMSA DNA	TCGTGTCCTGGACTGTCTCGGTTCTGT
EMSA RNA/DNA	UCGUGUCCUGGACTGUCUCGGUUCUGU

5.1.3 Vectors

The Vectors that are listed in the following table (Tab.5.4) represent: (1) plasmid backbones for the construction of mammalian expression plasmids, used in combination with the DNA oligonucleotides listed in Tab.5.1, (2) mammalian expression plasmids encoding for control proteins (e.g. VP5-GFP) or (3) plasmids designed and cloned by Dr. Nora Treiber (Regensburg University, Biochemistry I) that were used for the recombinant expression of proteins in Sf21 cells.

Table 5.4 Vectors used for cloning and already cloned constructs used in this work

Name	Tag	Comment
VP5	FLAG/HA	Plasmid collection Biochemistry I
pCS2-FAME	6x myc	Plasmid collection Biochemistry I
pcDNA5 FRT/TO	-	Plasmid collection Biochemistry I
pcDNA5 FRT/TO N-GFP	GFP	Cloned by Sam Ringle
VP5-GFP	FLAG/HA (GFP)	Plasmid collection Biochemistry I
pCS2-GFP	6x myc (GFP)	Plasmid collection Biochemistry I
pFastBac-FL-METTL3 + FL-METTL14	GST	Cloned by Dr. Nora Treiber
pFastBac-FL-METTL3 APPA + FL-METTL14	GST	Cloned by Dr. Nora Treiber
pFastBac-FL-METTL3 + FL-METTL14 APPA	GST	Cloned by Dr. Nora Treiber
pFastBac-ΔLH-METTL3 + FL- METTL14	GST	Cloned by Dr. Nora Treiber
pFastBac-ΔLH-METTL3 + METTL14-F1	GST	Cloned by Dr. Nora Treiber
pFastBac-ΔLH-METTL3 + METTL14-F2	GST	Cloned by Dr. Nora Treiber
pFastBac-ΔLH-METTL3 + METTL14-F3	GST	Cloned by Dr. Nora Treiber

5.1.4 Antibodies

In the following table (Tab.5.5) are the antibodies utilized for western blots (WB), immunoprecipitation experiments (IP) and immunofluorescence experiments (IF).

Table 5.5 Antibodies used for western blots (WB), immunofluorescence (IF) and immunoprecipitation (IP) experiments

Antibody	Raised in	Application	Dilution (WB/IF)	Supplier
α-HA clone 16B12	mouse	WB	1:1000	Covance Research Products
α-FLAG clone M2	mouse	WB/IF	1:1000/1:500	Sigma-Aldrich
α-FLAG clone 6F7	rat	WB/IP	1:1000	AG Kremmer (Helmholtz Center, Munich)
a-Myc clone 9E10	rabbit	WB/IF/IP	1:1000/1:500	Sigma-Aldrich
α-GFP clone 7.1 and 13.1 mix	mouse	WB/IP	1:1000	Roche
α-rat IRDye® 680RD	goat	WB	1:10000	LI-COR Biosciences
α-mouse IRDye® 680RD	goat	WB	1:10000	LI-COR Biosciences
α-rabbit IRDye® 680RD	goat	WB	1:10000	LI-COR Biosciences
α-rat IRDye® 800CW	goat	WB	1:10000	LI-COR Biosciences
α-mouse IRDye® 800CW	goat	WB	1:10000	LI-COR Biosciences
α-rabbit IRDye® 800CW	goat	WB	1:10000	LI-COR Biosciences
α-mouse Alexa Fluor® 488	goat	WB	1:10001	Thermo Fisher Scientific
α-rabbit Alexa Fluor® 555	goat	WB	1:10002	Thermo Fisher Scientific

5.1.5 Buffers and media

Composition of the different buffers and media used in this work will be specified under each individual method.

5.1.6 Cell lines and bacteria

5.1.6.1 Cell lines

Cell line	Description
HEK 293T	Human embryonic kidney cell line expressing the SV40 large T-antigen
HeLa	Cell line derived from a human cervix carcinoma
Sf21	Cell line derived from the ovaries of *Spodoptera frugiperda*

5.1.6.2 Bacteria

Strain	Genotype
XL1-Blue	endA1 gyrA96(nal^{R}) thi-1 recA1 relA1 lac glnV44 F'[::Tn10 proAB^{+} lacI^{q} Δ(lacZ)M15] hsdR17(rK^{-} mK^{+})
DH10Bac^{TM}	F^{-}*mcr*A Δ(*mrr-hsd*RMS-*mcr*BC) Φ80*lac*ZΔM15 ΔlacX74 *rec*A1 *end*A1 *ara*D139 Δ(*ara*,*leu*)7697 *gal*U *gal*K λ^{-} *rps*L *nup*G/bMON14272/pMON7124

5.2 Methods

5.2.1 Cloning of DNA constructs

5.2.1.1 Polymerase chain reaction (PCR), restriction digestion and ligation

Standard PCR reactions were carried out using a 2-step Phusion Polymerase protocol from Thermo Fisher Scientific. The composition of a standard reaction and the appropriate cycling conditions are listed in Tab.5.6 and Tab.5.7 respectively. Either plasmid DNA or cDNA that was synthesized using the First Strand cDNA Synthesis Kit (Thermo Fisher Scientific) was used as template for the amplification reaction.

Table 5.6 Composition of a standard 50 µl **PCR reaction**

Component	End concentration
DNA	X
HF buffer	1 x
Forward primer	0.5 µM
Reverse primer	0.5 µM
dNTPs	200 µM
Phusion	2 U

Table 5.7 Thermocycler program

Temperature	Time	
98 °C	1 min	
98 °C	1 min	30 cycles
72°C	30 s/kb	
72 °C	2 min	
16 °C	∞	

X: 5 ng **Plasmid DNA or** 2 µl **of a reverse transcription reaction that used** 1 µg **of total RNA**

Amplified PCR products were separated on a 0.5 % to 1 % agorose gel (using 1 x TBE containing 0.01 % ethidium bromide (EtBr)) and the DNA products were isolated and purified using the NucleoSpin® Gel and PCR Clean-up kit (MACHEREY-NAGEL GmbH). Compatible DNA overhangs were generated by incubating both PCR product and target vector with the same FastDigest (Thermo Fisher Scientific) enzyme pair. Reactions were prepared as recommended by the manufacturer. In restriction reactions containing plasmid DNA, 2 U of FastAP thermosensitive Alkaline Phosphatase (Termo Fisher Scientitc) was added to a 20 µl setup.

After incubation with the appropriate enzymes, PCR products were purified directly with the NucleoSpin® kit. The linearized plasmid was first subject to an agarose gel and after separation the plasmid was retrieved from the gel and purified with the NucleoSpin® Gel and PCR Clean-up kit. Ligation reactions were carried out utilizing the purified vector and a 3-fold molar excess of the digested insert.

Composition and reaction conditions followed the T4 DNA Ligase protocol of the manufacturer (Termo Fisher Scientitc). After ligation, the complete reaction was utilized for the transfromation of *E. coli* cells.

1 x **TBE**	89 mM Tris, 89 mM boric acid, 2 mM EDTA

5.2.1.2 Site-directed mutagenesis

Mutagenesis primers were designed according to QuikChange® Site-Directed Mutagenesis Kit manual (Agilent Technologies). Reaction composition and cycler conditions used to amplify the modified plasmids are listed in Tab.5.8 and Tab.5.9 respectively.

Table 5.8 Composition of a site-directed mutagenesis reaction

Component	End concentration
DNA	1 ng/µl
HF buffer	1 x
Forward primer	0.5 µM
Reverse primer	0.5 µM
dNTPs	200 µM

Table 5.9 Thermocycler program for a site-directed mutagenesis reaction

Temperature	Time	
98 °C	1 min	
98 °C	1 min	18 cycles
55 °C	20 s	
72°C	45 s/kb	
72°C	10 s	
16 °C	∞	

DNA from the reaction was purified using the NucleoSpin® Gel and PCR Clean-up kit. Before the transformation of *E. coli* cells, template DNA was removed from the reaction through enzymatic digestion. For this, the FastDigest enzyme DpnI was applied to the reaction and incubated according to the manufacturer's protocol (Thermo Fisher Scientific).

5.2.1.3 Heat-shock trans formation of *E. coli*

Chemically competent *E. coli* cells of the strain XL1-Blue were used for transformations. Cells were thawed on ice and then incubated for $10\,\mathrm{min}$ with the plasmid DNA (obtained from the sections 5.2.1.1 and 5.2.1.2). Heat-shock was carried out at $42\,^{\circ}\mathrm{C}$ for $1\,\mathrm{min}$ in a thermoblock and the cells were afterwards directly transferred onto ice for another $10\,\mathrm{min}$. Cells transformed with plasmids harboring an ampicillin resistance were plated directly onto LB_{Amp}-plates and incubated at $37\,^{\circ}\mathrm{C}$1 until visible

colonies were formed. For plasmids encoding other resistance markers (see Bac-to-Bac manual referred in section 5.2.3.3), cells were first incubated for 1 h at 37 °C in LB medium that contain no antibiotics. Afterwards, cells were concentrated via centrifugation (1 min; 8000 xg) and resuspended in 70 µl of LB-medium (no antibiotics). This suspension was then plated onto LB-plates containing the appropriate antibiotic and cultivated at 37 °C.

LB	1 % NaCl, 0.5 % yeast extract, 1 % tryptone, adjust pH to 7.2 - 7.5
LB agar	LB medium, 1.5 % agar
LB/ LB agar with ampicillin	Ampicillin end concentration (100 µg/mL)

5.2.1.4 Isolation of plasmid DNA from *E. coli*

Plasmid DNA of different quantities and of high purity were isolated using the NucleoBond® Plasmid kit and NucleoBond® Xtra Midi kit from MACHEREY-NAGEL. The "Easyprep" method was used for the screening of clones and was carried-out as published by Berghammer and Auer.[220] Briefly, 2 ml of a overnight culture was centrifuged at 17 000 xg for 1 min to pellet the cells. Afterwards, the cells were resuspended in 40 µL of Easyprep buffer, boiled for 1 min at 99 °C and then transferred onto ice for an additional minute. Cell debris was afterwards centrifuged down at 17 000 xg for 10 min. 10 µL of the supernatant was then used for a standard test digestion in order to screen for appropriate DNA fragments during an agarose gel electrophoresis (see section 5.2.1.1).

Easyprep buffer	10 mM Tris/HCl pH 8.0, 1 mM EDTA, 15 % saccharose, 2 mg/mL lysozyme, 0.2 mg/mL RNase A, 0.1 mg/mL BSA

5.2.1.5 Sanger sequencing

DNA constructs were sequenced either by GATC Biotech AG (Konstanz, Germany) or Macrogen Europe (Amsterdam, The Netherlands). Sequencing reactions were prepared as recommended by the companies. DNA oligonucleotides for sequencing were designed according to the specifications listed on the GATC Biotech AG website (www.gatc-biotech.com).

5.2.2 Cell culture

5.2.2.1 Cultivation of human cell lines

Human cell lines were cultivated under standard conditions (37 °C, 95 % humidity and 5 % CO_2) in Dulbecco's modified Eagle medium (DMEM) supplemented with 10 % FBS and 1 % Penecillin-Streptomycin mix (all from Sigma-Aldrich).

Cells were passaged once they have reached a confluency of approximately 90 %. Cells were rinsed once with 1 x PBS and incubated for 5 min at 37 °C with an amount of a 1 x trypsin-EDTA solution that corresponded to 10 % of the initial culture volume. The trypsin reaction is then stop through the addition of fully supplemented DMEM (FBS and antibiotics). A desired amount of cells was then transferred into a new culture dish supplied with fresh medium.

1 x **PBS**	8 g/l NaCl, 0.2 g/l KCl, 1.78 g/l Na_2HPO_4 • (H_2O), 0.24 g/l KH_2PO_4 Adjust pH to 7.5 and autoclave

5.2.2.2 Cultivation of Sf21 cells

The insect cell line Sf21 derived from *Spodoptera frugiperda* was supplied with Sf-900™II SFM (Thermo Fisher Scientific) and cultivated at 27 °C with constant agitation (55 to 70 rpm). Cell density of the suspension culture was maintained between 1 to 4 $\times$ 10^6 cells/ml. At higher densities, the cells were subcultivated by diluting the cells down to 1 $\times$ 10^6 cells/ml with Sf-900 medium.

5.2.3 Protein based methods

5.2.3.1 Expression of recombinant proteins in HEK 293T using $Ca_3(PO_4)_2$

Large-scale recombinant protein production in HEK 293T cells was carried-out by transfecting the cells using the $Ca_3(PO_4)_2$-method. Prior to transfection, cells were seeded onto a 15 cm plate in order to achieve a confluency of approximately 25 %. Transfection setups were then prepared as shown in Tab.5.10 and directly added to the cells. Cells were afterwards further cultivated for 1 to 2 d under standard conditions (see section 5.2.2.1).

Table 5.10 Composition of a $2\,\mathrm{ml}$ setup for the transfection of HEK 293T cells with $Ca_3(PO_4)_2$

Component	Amount
H2O	860 µl
CaCl2	122 µl
DNA	1 - 10 µg
2x HEPES	1 ml (add dropwise)

2 x **HEPES-buffer**	274 mM NaCl, 1.5 mM Na_2HPO_4 , 54.6 mM HEPES pH 7.1

5.2.3.2 Expression of recombinant proteins in HeLa cells using Lipofectamine® 2000

For the transfection of HeLa cells using Lipofectamine® 2000 (Thermo Fisher Scientific), the cells were cultivated in antibiotic-free DMEM and were 90 to 95 $\%$ confluent prior to transfection. Lipid-DNA complexes were prepared in Opti-MEM® (Thermo Fisher Scientific) according to the protocol of the manufacturer. Cells were cultivated for 48 h after transfection before continuing any experiments. Transfections were carried-out by Franziska Weichmann (University Regensburg, Biochemistry I).

5.2.3.3 Expression of recombinant proteins in Sf21 cells

Baculovirus stocks were essentially generated as described in the Bac-to-Bac manual (Thermo Fisher Scientific). For the expression of recombinant proteins, 0.5 to 1 L cultures of Sf21 cells, with a cell concentration of 1×10^6 cells$/$ml, were prepared. Cells were infected with 10 ml of a P2 viral stock and incubated at 27 $^\circ\mathrm{C}$ for 72 h while constantly shaking. Cells were afterwards harvested via centrifugation (700 xg, $10\,\mathrm{min}$, room temperature) and, after removal of the supernatant, utilized for lysate preparation (see section 5.2.3.6). If protein isolation should be conducted at a later time point, then the pelleted cells are flash-frozen in liquid nitrogen and stored by $-80\,^\circ\mathrm{C}$.

5.2.3.4 Whole-cell lysate preparation from human cell lines

Cells transfected via the $Ca_3(PO_4)_2$-method were washed twice with 1 x PBS and then detached from the cultivation dishes using a cell scraper. The cell suspension was transferred into a 1.5 ml reaction tube and the cells were centrifuged for $10\,\mathrm{min}$ at 500 xg and 4 $^\circ\mathrm{C}$. The resulting cell pellet was then resuspended in CoIP lysis buffer (1 ml per 15 cm plate) and incubated for 10 min on ice. The resulting

crude lysate was afterwards centrifuged at 17 000 xg for 10 min and 4 °C to remove the cell debris. The supernatant was then passed through a 0.45 um filter and transferred into a new reaction tube.

1 x **CoIP lysis buffer**	25 mM Tris HCl pH 7.4, 150 mM KCl , 0.5 % NP-40 alternative, 2 mM EDTA, 0.5 mM AEBSF, 1 mM DTT

5.2.3.5 Immunoprecipitation

For immunoprecipitation (IP) experiments, antibodies commercially purchased or provided by the workgroup of Elisabeth Kremmer were coupled to protein G sepharose beads (GE Healthcare). Both the amount of beads and antibody were adjusted to the amount of lysate used for an experiment. Normally, 5 to 10 µg of purified antibody was added to 30 µl of beads. Prior to coupling, the beads were washed three times with 1 x PBS (centrifugation: 1500 xg, 30 s, 4 °C). Antibody and beads were coupled overnight at 4 °C, while the setup was constantly rotating. Antibodies that were not bound by the beads were removed the next day by washing thrice with CoIP lysis buffer.

Input samples were taken before adding the coupled beads to the lysate. IP reactions were then incubated at 4 °C and under constant rotation for 3 to 4 h. The beads were afterwards washed four times with CoIP washing buffer. Proteins were eluted by adding 2 x Laemmli sample buffer to the beads and boiling the IP setup for 5 min at 95 °C. The beads are then centrifuged down (17 000 xg, 1 min) and the supernatant is loaded onto a sodium dodecyl sulfate polyacrylamide gel (SDS-PA, see section 5.2.3.10).

CoIP washing buffer	50 mM Tris HCl pH 7.4, 300 mM KCl , 0.1 % NP-40 alternative, 1.5 mM $MgCl_2$, 0.5 mM AEBSF, 1 mM DTT

5.2.3.6 Lysate preparation from Sf21 cells expressing GST-METTL3 and METTL14

Suspension cultures of Sf21 cells expressing GST-tagged METTL3 and untagged METTL14 were harvested by pelleting the cells at 700 xg for 10 min at room temperature. Afterwards, the cell pellet was then washed twice in 1 x PBS using the same centrifugation settings. The resulting pellet of the last washing step is then resuspended in GST-lysis buffer. Cells were lysed via sonication (output setting: 4-5; duty cycle: 50 %) and the cell debris was removed by centrifugating at 40 000 xg for 1 h at 4 °C. The resulting supernatant was then filtered using a 0.45 µm diameter filter.

GST lysis buffer	1.5 M NaCl in 1 x PBS pH 7.0

5.2.3.7 HPLC purfication of GST-METTL3/14

HPLC-purification program was written and the Äkta purification system (GE Healthcare) was operated by Dr. Thomas Treiber (University Regensburg). Filtered lysate cotaining GST-tagged METTL3 was loaded onto a 5 ml GST-column and the bound proteins were washed with at least four column volumes of GST lysis buffer. Elution of the column-bound proteins was achieved with 2 to 3 columnvolumes of GST elution buffer. The collected fractions were analyzed via SDS-PAGE (see 5.2.3.10) and fractions containing the recombinant proteins were pooled together. Tobacco Etch Virus (TEV) protease was added to the pooled sample that was then dialysed overnight in a cold room against 1 L of 1 x PBS (pH 7.0). The dialyzed sample was afterwards concentrated using a Vivaspin centrifuge concentrator (Sartorius, cut-off 50 kDa). As a final step, the concentrate was loaded onto a gel filtration column packed with Superdex 200 resin (GE Healthcare). The column was equilibrated with gel filtration buffer prior to loading of the sample. Fractions containing the recombinant protein were then again pooled and concentrated (Vivaspin). Glycerol was added to the concentrated protein (endconcentration: $8\,\%$) that was afterwards flash-frozen in liquid nitrogen and stored at $-80\,^{\circ}\mathrm{C}$.

GST elution buffer	50 mM Tris, 20 mM glutathione in 1 x PBS pH 7.0
Gel filtration buffer	80 mM KCl, 1.5 mM $MgCl_2$, 15 mM HEPES pH 7.9

5.2.3.8 GST-pulldown

Depending on the amount of lysate used in the experiment, 20 to 100 µl of Glutathione Sepharose™Fast Flow beads (GE Healthcare) were washed three times with GST lysis buffer (centrifugation: $1500\,\mathrm{xg}$, $4\,^{\circ}\mathrm{C}$). The equilibrated beads were then added to the filtered lysate and incubated in a cold room for 3 h while constantly rotating. Afterwards, the lysate was removed and the beads were washed five times with GST lysis buffer (centrifugation: $1500\,\mathrm{xg}$, $1\,\mathrm{min}$, $4\,^{\circ}\mathrm{C}$). Proteins were eluted by adding 50 to 200 µl of elution buffer to the beads and incubating the setup for $30\,\mathrm{min}$ at room temperature while constantly shaking. This elution step was repeated once and the eluates were pooled.

5.2.3.9 Methanol chloroform precipitation

Aqueous protein solutions were concentrated using the methanol chloroform precipitation method according to Friedman *et al.*[221] In brief, 400 µl of methanol and 100 µl of chloroform were added to 400 µl of a aqueous protein solution and mixed vigorously. The setup is then centrifuged at 17 000 xg for 10 min at room temperature to separate the phases. The upper methanol/H_2O-phase is discarded without disturbing the interphase. 400 µl of methanol is added ontop of the interphase and mixed vigorously again. Proteins are then pelleted at 17 000 xg for 10 min and the resulting pellet is air-dried for 3 min at room temperature. The pellet is then dissolved in 1 x Laemmli sample buffer.

5.2.3.10 Sodium dodecyl sulfate polyacrylamide gel electrophoresis (SDS-PAGE), Coomassie staining, western blotting and silver staining

For the electrophoretic separation of proteins, sodium dodecyl sulfate polyacrylamide (SDS-PA) gels were prepared according to Laemmli.[222] Protein samples supplemented with sample buffer were boiled for 10 min at 95 °C prior to loading. Gels were initially run at 170 V and raised to 250 V, after the samples have passed the stacking gel. Separation was stopped when the bromophenol blue dye ran out of the gel.

Separation gel	10 to 12 % Acrylamide/Bis solution (37.5:1), 380 mM Tris/HCl pH 8.8, 0.1 % SDS, 0.1 % TEMED, 0.1 % APS
Stacking gel	5 % Acrylamide/Bis solution (37.5:1), 125 mM Tris/HCl pH 6.8, 0.1 % SDS, 0.1 % TEMED, 0.1 % APS
1 x **SDS running buffer**	25 mM Tris/HCl pH 7.5, 192 mM glycine, 1 % SDS
1 x **Laemmli sample buffer**	60 mM Tris/HCl pH 6.8, 2 % SDS, 5 % β-mercaptoethanol, 0.01 % bromophenol blue, 10 % glycerol

Coomassie staining was performed by incubating the gel for 1 to 2 h at room temperature in staining solution. Gels were afterwards rinsed thrice with Milli-Q-grade H_2O and destained with the destaining solution at room temperature, until visible bands were detected.

Coomassie staining solution	10 % acetic acid, 30 % ethanol, 0.25 % Coomassie R250
Destaining solution	10 % acetic acid, 30 % ethanol

For western blots, proteins were transferred (semi dry) onto a Hybond ECL membrane (GE Healthcare) using Towbin blotting buffer and a constant current of 2 A/cm^2 for 80 min. Membranes were blocked in 1 x TBST containing 5 $\%$ skim milk for 1 h at 4 $^{\circ}\mathrm{C}$. Afterwards, the primary antibody, diluted in blocking buffer, was added to the membrane and incubated overnight at 4 $^{\circ}\mathrm{C}$. Unbound antibody was removed by washing the membrane three times with 1 x TBST. The membrane was then incubated with the secondary antibody, diluted in blocking buffer, for 1 h at 4 $^{\circ}\mathrm{C}$. The membrane is then washed again thrice before documenting the results using the Odyssey scanner system (LI-COR Biosciences).

1 x **Towbin blotting buffer**	192 mM glycine, 25 mM Tris/HCl pH 8.6, 20 $\%$ methanol
1 x **TBS**	150 mM NaCl, 10 mM Tris/HCl pH 8
1 x **TBST**	150 mM NaCl, 10 mM Tris/HCl pH 8, 0.1 $\%$ Tween 20
Blocking solution	5 $\%$ skim milk powder in 1 x TBST

Silver stainings were carried out using a modified protocol of the method published by Blum *et al.*[223] First a gel was incubated in fixation solution for 20 min at room temperature. Afterwards, the gel was washed sequentially with washing solutions 1, 2 and ddH_2O for 10 min at room temperature. The sensitizer solution is then added to the gel for precisely 60 s. Next, three washing steps are carried-out using ddH_2O and afterwards the silver staining solution was added to the gel for 20 min at room temperature. After this step, the gel was washed thrice with ddH_2O and afterwards incubated with developer until bands with the desired intensity appeared. The reaction was then stopped by incubating and later storing the gel in stop solution.

Fixation solution	50 $\%$ methanol, 5 $\%$ acetic acid
Washing solution 1	50 $\%$ ethanol
Washing solution 2	30 $\%$ ethanol
Sensitizer solution	0.02 $\%$ sodium thiosulfate
Silver staining solution	6 mM silver nitrate, 0.0185 $\%$ formaldehyde
Developer	2 $\%$ sodium carbonate, 0.0185 $\%$ formaldehyde, 0.0004 $\%$ sodium thiosulfate
Stop solution	5 $\%$ acetic acid

5.2.3.11 *In vitro* m^{6}A methylation assay

In vitro methylation reactions were prepared as shown in Tab.5.11. Reactions were incubated at 30 °C for 1 h followed by an inactivation step (5 min, 65 °C). After heat-inactivation, free ^{3}H was removed from the reaction using G25 spin columns (GE Healthcare) according to the manufacturer's protocol. 10 µl of the flow-through was then diluted in 1 ml of Unisafe 1 scintillation cocktail (Zinsser analytic) and the counts per minute (c.p.m.) were determined in a LS 6500 scintillation counter (Beckman).

Table 5.11 Composition of a 20 µl m^{6}A *in vitro* methylation reaction

Component	End concentration
RNA	25 µM
DTT	1 mM
m^{6}A reaction buffer	1 x
^{3}H-SAM (15 Ci/mmol)	0.05 µCi/µl
Protein	2.5 µM

10 x m^{6}A methylation buffer 0.8 M KCl, 15 mM $MgCl_2$, 40 % glycerol, 150 mM HEPES pH 7.9

5.2.3.12 SAM-binding assay

A 20 µl reaction containing 1 Ci of ^{3}H-SAM (15 Ci/mmol), 5 to 20 µg of the GST-tagged METTL3/14 complex and 1 x m^{6}A reaction buffer was prepared and incubated for 10 min at room temperature. The setup was then UV irradiated (254 nm) for up to 30 min. 30 µl of ddH_2O was then added to the reaction that was afterwards subject to a gel filtration clean-up using G25 spin columns. 1 x Laemmli sample buffer was added to the setup that was afterwards separated on a 10 % PA gel (see 5.2.3.10). The gel was then incubated first in fixation solution and then in Amersham Amplify Fluorographic Reagent (GE Healthcare), both for 30 min at room temperature and under agitation. The gel was then dried for an hour at 80 °C and then exposed to an BioMax X-ray film (Kodak) for 1 to 2 weeks while stored at −80 °C.

Fixation solution 30 % ethanol, 10 % acetic acid

5.2.3.13 Electrophoretic mobility shift assay (EMSA)

Various RNA substrates needed to be radiolabeled with γ-^{32}-P before these were incubated together with the recombinant protein complex. For the labeling of *in vitro* transcribed RNA, the nucleic acid was first dephosphorylated (see Tab. 5.12 for reaction composition) and subsequently phosphorylated using γ-^{32}-P ATP (see Tab.5.13 for reaction composition). Dephosphorylation reactions were incubated at 37 $^{\circ}\mathrm{C}$ for 30 min and the reactions were afterwards heat-inactivated for 20 min at 75 $^{\circ}\mathrm{C}$. The complete reaction was then used for the phosphorylation reaction that was carried-out at 37 $^{\circ}\mathrm{C}$ for 1 h. 10 µl of ddH_2O was added to the reaction and a G25-column (GE Healthcare) clean-up was performed according to the manufacturer's protocol.

RNAs used in EMSAs that were chemically synthesized could be directly phosphorylated with radiolabeled ATP using the T4-PNK protocol of the manufacturer (Thermo Fisher Scientific). After labeling, the reactions followed the same clean-up step as those reactions utilizing *in vitro* transcribed RNA.

Table 5.12 Composition of a 10 µl **dephosphorylation reaction for EMSAs**

Component	End concentration
RNA	3 µM
Fast AP	0.1 U/µl
PNK buffer A	1 x

Table 5.13 Composition of a 20 µl **phosphorylation reaction for EMSAs**

Component	Amount / end concentration
Dephosphorylation reaction	10µl
T4 Poly nucleotide kinase	0.5 U/µl
PNK buffer A	1 x
γ-^{32}P-ATP (6 mCi/mmol)	1 uCi/µl

Enzymes and buffer were purchased from Thermo Fisher Scientific

After labeling and the clean-up step, the radiolabeled substrate RNA was diluted to obtain a 1 nM working stock. Recombinant protein, RNA (5 fmol) and incubation buffer (1 x endconcentration) were mixed together and the reactions were incubated for 30 min on ice. 6 $\%$ native PA gels were pre-run in 1 x EMSA running buffer for 30 min at 230 V in a cold-room before loading the reactions. Samples were separated for 3 h at 230 V and the gel was afterwards disassembled and dried for 1 h at 80 $^{\circ}\mathrm{C}$. A blanked storage phosphor screen was exposed to the dried gel overnight. The results were later documented using the Personal Molecular Imager System (BioRad).

10 x **EMSA running buffer**	450 mM Tris/HCl pH 7, 450 mM borate
5 x **incubation buffer**	50 mM MOPS pH 7, 250 mM KCl, 25 mM $MgCl_2$, 25 % glycerol
6 % **native PA gel**	6 % acrylamide/ N,N'-methylene bis-acrylamide, (37.5 :1), 1 x EMSA running buffer, 5 % glycerol, 0.08 % APS, 0.08 % TEMED

5.2.3.14 Cross-linking-MS analysis of METTL3/14

Recombinant METTL3/14 was expressed in Sf21 cells and purified as described above (see sections 5.2.3.3 and 5.2.3.7). The protein concentration was adjusted to 1 mg/L and sent to the group of Dr. Franz Herzog (LMU, Munich). The following steps were then carried-out by Götz Hagemann (LMU, Munich).

Cross-linking of the 2-subunit METTL3/14complex was performed by mixing 50 µg of the complex with 650 µM of an equimolar mixture of isotopically light (d0) and heavy (d12) labeled BS3 (bis-sulfosuccinimidylsuberate) for 30 min at 37 °C. The reaction was quenched by adding a final concentration of 100 mM ammonium bicarbonate for 20 min at 37 °C.

Cross-linked proteins were enzymatically digested by trypsin and cross-linked peptides were identified by tandem mass-spectrometry.[224,225] Cross-linked proteins were denatured by adding 2 sample volumes of 8 M urea and reduced by incubating with 5 mM Tris(2-carboxyethyl)phosphin at 35 °C for 15 min. Proteins were alkylated with 10 mM iodoacetamide for 35 min at room temperature in the dark. Samples were proteolytically digested using trypsin. For the trypic digest, proteins were first incubated with lysyl endopeptidase (1/50, w/w) for 2 h at 35 °C followed by the addition of trypsin (1/50, w/w) in a setup that contained 1 M urea. The reaction was carried-out overnight. Proteolysis was stopped by the addition of 1 %(v/v) trifluoroacetic acid (TFA).

Acidified peptides were purified by reversed-phase chromatography on C18 columns (Sep-Pak). Eluates were dried, reconstituted in 20 µl of mobile phase (water/acetonitrile/TFA, 75:25:0.1) and cross-linked peptides were enriched on a Superdex Peptide PC 3.2/30 column. Fractions of the cross-linked peptides were analyzed by liquid chromatography coupled to tandem mass spectrometry using a LTQ Orbitrap Elite (Thermo Scientific) instrument. The cross-link fragment ion spectra were searched and peptides identified by the open-source software xQuest.[225] The results were filtered according to the following parameters: score < 0.85, MS1 tolerance window of -4 ppm to 4 ppm and score ≥ 22 and manually validated. The filtered results were then visualized using the online tool xVis Crosslink Analysis Webserver (https://xvis.genzentrum.lmu.de/CrossVisNoLogin.php).

5.2.4 RNA based methods

5.2.4.1 Denaturing urea PAGE and blotting of RNA

Denaturing PA gels containing urea were casted as recommended by the manufacturer (National diagnostics or Roth). The percentage of the gel depended on the size of the RNA that should be analyzed. The polymerized gel pre-ran for $30\,\mathrm{min}$ at 400 V before loading the samples. RNA samples were supplemented with $2\,\mathrm{x}$ RNA sample buffer and boiled for $3\,\mathrm{min}$ at $95\,^{\circ}\mathrm{C}$ and then loaded onto the gel. After separation, the gel was disassembled and transferred into a staining solution ($1\,\mathrm{x}$ TBE and $0.01\,\%$ EtBr) for $10\,\mathrm{min}$ under steady agitation. To visualize the RNA, the gel was then placed on a UV light table and the result were documented.

Blotting (semi dry) of radiolabeled RNA from *in vitro* methylation assays onto an Amersham Hybond-N membrane (GE Healthcare) was carried-out at 20 V for $30\,\mathrm{min}$ using ddH_2O as a buffer system. After transfer of the RNA, the membrane was air-dried and exposed to a BioMax X-ray film (Kodak) using a TranScreen intensifying screen (GE Healthcare) for 1 to 2 weeks while stored at $-80\,^{\circ}\mathrm{C}$ (experiments were conducted in cooperation with Dr. Thomas Treiber, University Regensburg).

$2\,\mathrm{x}$ **RNA sample buffer**	$0.05\,\%$ xylene cyanol, $0.05\,\%$ bromphenol blue in formaide

5.2.4.2 T7 *in vitro* transcription

Substrate RNA for *in vitro* methylation assays were synthesized using the T7 DNA-dependant RNA polymerase. The enzyme used for the transcription reaction was purified by Dr. Thomas Treiber and Dr. Nora Treiber (both University Regensburg, Biochemistry I). A typical composition of a $1\,\mathrm{ml}$ reaction is shown in Tab.5.14.

Table 5.14 Composition of a $1\,\mathrm{ml}$ **T7 *in vitro* transcription reaction**

Component	End concentration
NTPs	10 mM
Tris pH 8	30 mM
MgCl2	25 mM
Triton X-100	0.01%
Spermidine	2 mM
Pyrophophatase	0.1 U/ml
DTT	10 mM
T7 RNA polymerase	0.1 mg/ml

Reactions were incubated at 37 °C overnight and then stopped through the addition of 1 ml of 2 x RNA sample buffer. Samples were then electrophoretically separated on a urea PA gel (see 5.2.4.1) and the RNA was visualized by UV shadowing. Transcripts of the correct size were cut-out of the gel and the RNA was eluted overnight with H_2O. The eluted transcript was then concentrated and desalted using a Vivaspin concentrator (Sartorius) with an appropriate cut-off.

5.2.5 Immunfluorescence microscopy

Immunofluorescence experiments were conducted by Franziska Weichmann (University Regensburg, Biochemistry I) and followed the subsequent protocol. Transfected HeLa cells (see 5.2.3.2; also preformed by Franziska Weichmann) were seeded into 24-well plates that contained a cover slip (12 mm diameter; Roth) in each well. The cells were further cultivated for 24 h under standard conditions. Cells were then washed twice with pre-warmed (37 °C) 1 x PBS-A and afterwards fixated with fixation buffer (1 ml, 10 min, 37 °C). The cross-linking reaction was stopped by replacing the fixation solution with the same volume of PBS-G and incubating the cells for 10 min at 37 °C. The sequential steps were all carried-out at room temperature. Setups were washed twice with PBS-A and then 500 µl of permeabilization solution was added to the fixated cells for 30 min. Cells were rinsed once with blocking buffer and then incubated for 30 min in 500 µl of this buffer. The blocking buffer was then discarded and replace by 500 µl of blocking buffer in which the primary antibody was diluted. After incubtaing the cover slips for 1 h, the cells were washed four times with blocking solution and the secondary antibody was then incubated for an additional hour. Setups were afterwards washed once with blocking buffer and then three times with 1 x PBS-A. 10 µl of Prolong® Gold mounting medium supplemented with 4',6-diamidino-2-phenylindole (DAPI, Thermo Fisher Scientific) was then added on top of each cover slip that were afterwards placed on a microscope slide. Setups were then dried for at least 12 h in the dark.

10 x **PBS-A**	2 g/L KCl, 2 g/L H_2PO_4, 80 g/L NaCl, 22 g/L Na_2HPO_4 • 7 H_2O, adjust pH to 7.4
Fixation buffer	4 % paraformaldehyde in PBS-A
PBS-G	7.5 g/L glycine in PBS-A
Permeabilization buffer	0.2 % Triton X-100 in PBS-A
Blocking buffer	0.05 % Triton X-100, 50 g/L BSA (Cohn-Fraction V) in PBS-A

Slides were analyzed using a TCS SP8 (Leica Microsystems) confocal microscope. This instrument is equipped with a 405 nm laser (for DAPI), an argon-ion laser (488 nm, for Alexa 488) and a DPSS laser

(561 nm, for Alexa 555). All confocal images were recorded using a HC PL APO 63x/1,30 GLYC CORR CS2 objective.

5.2.6 Bioinformatic methods

5.2.6.1 Nucleotide and protein sequences of METTL3, METTL14 and WTAP used in this work

Nucleotide sequences used for the cloning of METTL3, METTL14 and WTAP expression vectors were acquired from the NCBI database. For the different proteins the following NCBI reference sequences were used:

- METTL3 (NM_ 019852.3)
- METTL14 (NM_ 020961.2)
- WTAP (NM_ 004906.4)

The protein sequences of these genes were obtained by *in silico* translation of the above mentioned reference sequences using the program Serial Cloner (version 2.6; http://serialbasics.free.fr/Serial_Cloner.html).

5.2.6.2 *In silico* secondary structure predication of proteins using Psipred

Secondary structures within the proteins METTL3, METTL14 and WTAP were predicted using the online algorithm Psipred (http://bioinf.cs.ucl.ac.uk/psipred/).[226] Strands are indicated by arrows, whereas α-helices are represented by cylinders (see appendix). The retrieved predictions were used for the prediction of the overall structure and the construction of truncations of the above mentioned proteins.

5.2.6.3 *In silico* predication of coiled-coil structures within proteins using COILS

For the prediction of coiled-coils within the proteins METTL3 and WTAP, the online tool COILS was used (http://embnet.vital-it.ch/software/COILS_form.html).[183] This algorithm scans the primary sequence of the protein for heptad sequences that have been found to form coiled-coils.[200] Sliding windows of 14, 21 or 28 amino acids were applied in order to detect 2, 3 or 4 heptad sequences respectively. Depending on the composition of the analyzed heptad sequence, each amino acid position is allocated

a score between 0 and 1. The higher the score, the more likely the analyzed amino acid position fulfills the requirements to form a coiled-coil.

While using COILS, the following settings were used:

- Window width: all
- Matrix: MTIDK
- 2.5 fold weighting of positions a,d: yes
- Input sequence format: plain text

5.2.6.4 *In silico* prediction of nuclear localization signals using Eukaryotic Linear Motif resource tool

Nuclear localization sequences (NLS) were predicted using the Eukaryotic Linear Motif resource tool (http://elm.eu.org/search/).[180,181] The default settings of this tool were used for the prediction of NLS within METTL3, METTL14 and WTAP.

5.2.6.5 Quantification of gel bands using ImageJ

Bands from gels were quantified using the tool ImageJ (https://imagej.nih.gov/ij/index.html). Quantification was carried out according to the protocol found on the website (https://imagej.nih.gov/ij/docs/menus/analyze.html#gels, Chapter: Gels Submenu).

6. Appendix

The following figures contain the structure predictions of the proteins METTL3, METTL14 and WTAP that were referred to in the sections 2.1 and 2.3. The figures were generated using the online tool Psipred (see section 5.2.6.2). These structure predictions were used for the construction of Sf21 expression constructs (designed and cloned by Dr. Nora Treiber, University Regensburg) and truncation variants of METTL3 and WTAP (see sections 2.2 and 2.3 respectively).

METTL3

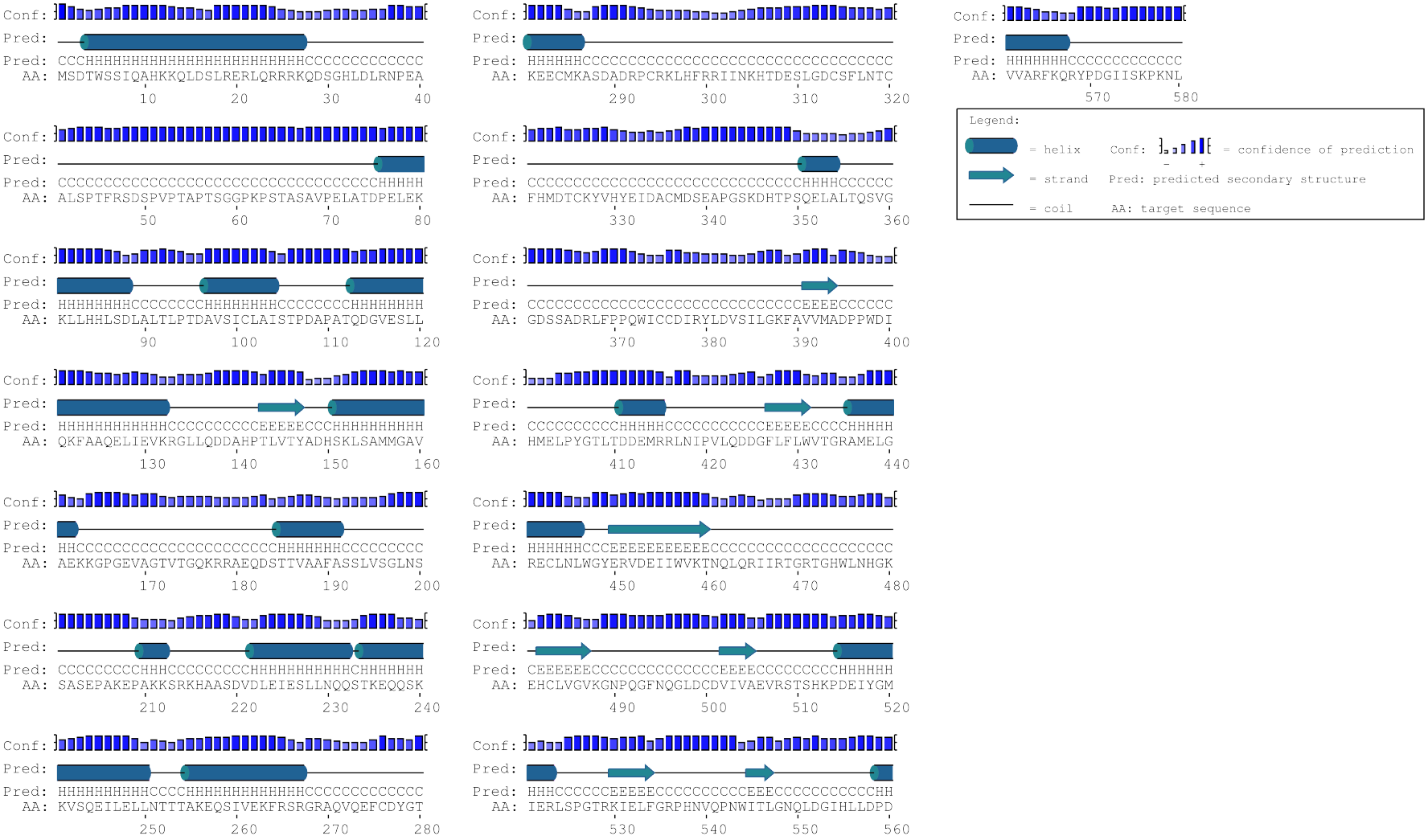

Figure 6.1 Secondary structure prediction of METTL3 using the online tool Psipred

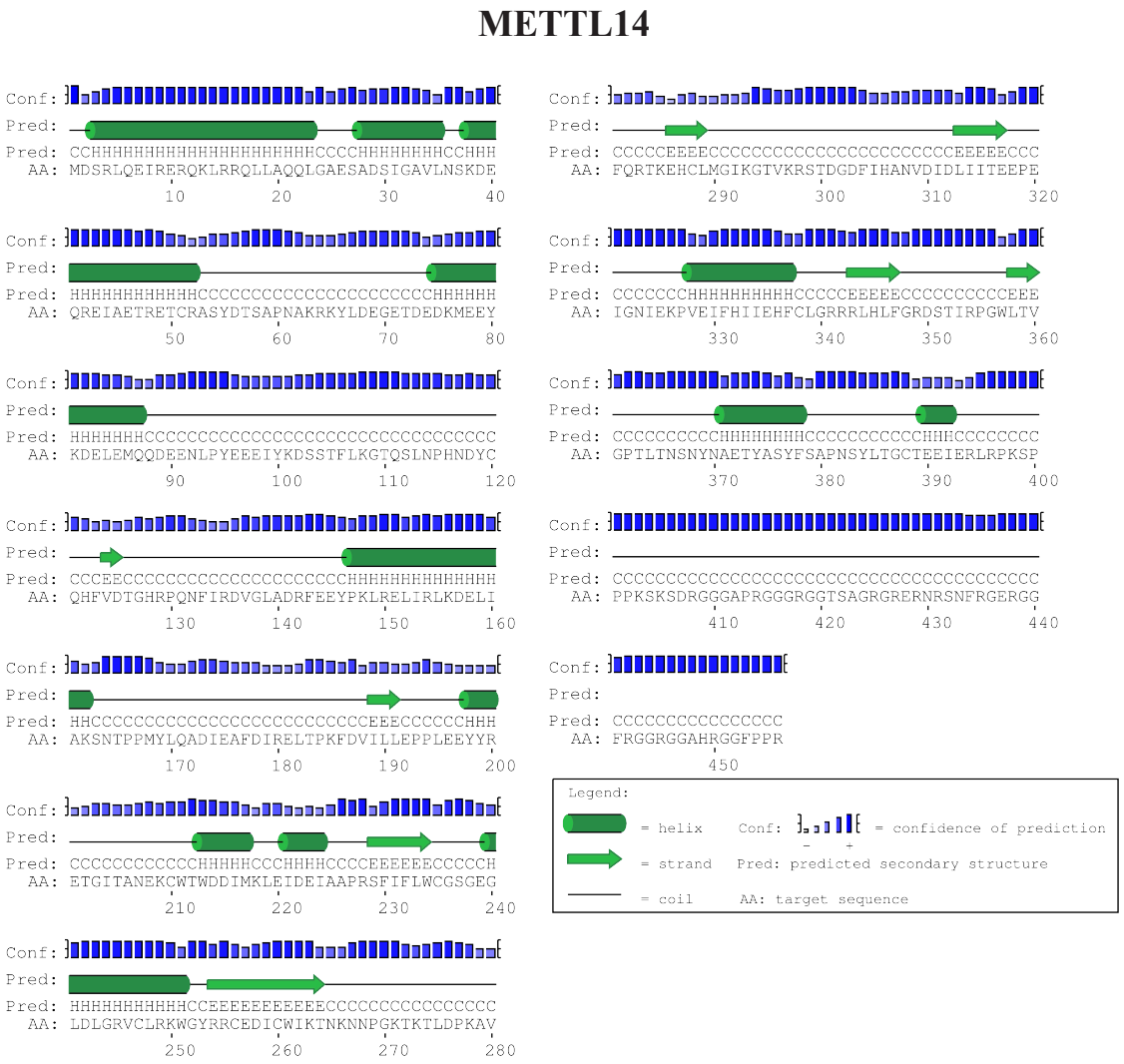

Figure 6.2 Secondary structure prediction of METTL14 using the online tool Psipred

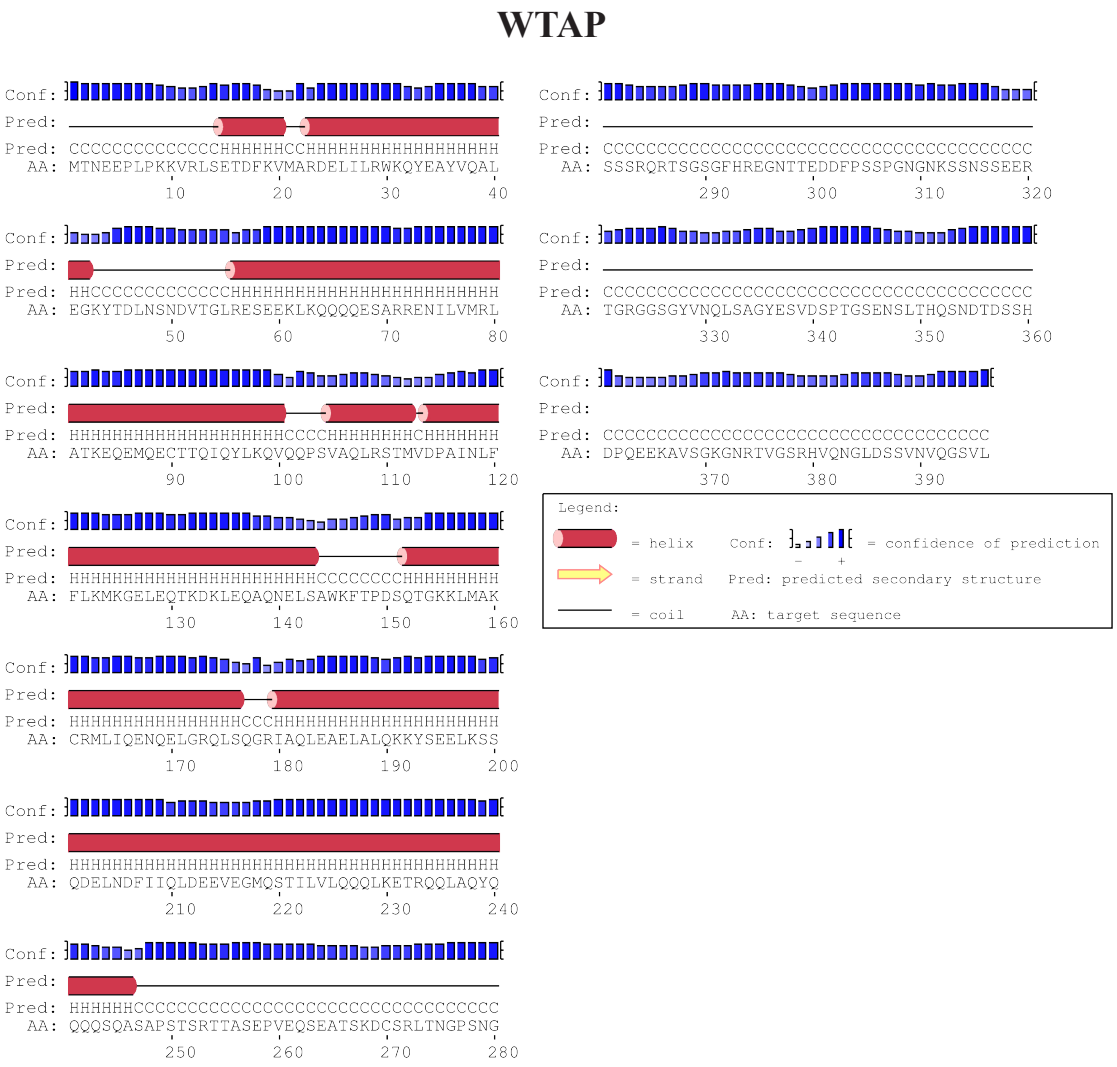

Figure 6.3 Secondary structure prediction of WTAP using the online tool Psipred

List of Tables

List of Figures

List of Abbreviations

A	adenine
A. thaliana	*Arabidopsis thaliana*
ADAR	adenosine deaminase acting on RNA
ALKBH5	Alkylation repair homolog 5
Amp	ampicillin
APS	ammonium persulfate
Asp^{GTC}	tRNA encoding for asparagine with the anticodon GTC (5'→3')
bp	base pair
BS3	bis-sulfosuccinimidyl suberate
BSA	bovine serum albumin
C	cytosine
c.p.m.	counts per minute
CMC	N-cyclohexyl-N'-(2-morpholinoethyl)carbodiimide metho-p-toluene sulfonate
CX-MS	chemical cross-linking combined with mass spectrometry analysis
DAPI	4',6-diamidino-2-phenylindole
ddH_2O	double distilled water
DMEM	Dulbecco's modified Eagle medium
DNA	desoxyribonuleic acid
DNMT2	DNA methytransferase 2
dsRNA	double-stranded RNA
E. coli	*Escherchia coli*
EDTA	2-(2-[Bis(carboxymethyl)amino]ethyl(carboxymethyl)amino)acetic acid
EMSA	electrophoretic mobility shift assay
EtBr	ethidium bromide
f^6A	N^6-formyladenosine
FBS	Fetal bovine serum
Fig.	figure
FTO	Fat mass and obesity-associated protein
G	guanine
Gly^{GCC}	tRNA encoding for glycine with the anticodon GCC (5'→3')
GST	Glutathione S-transferase protein
H	represents every base besides guanine (A,C,U)

^{3}H	radioactive hydrogen isotope tritium
$hm^{6}A$	N^{6}-hydroxymethyladenosine
HPLC	high performance liquid chromatography
Hsp70	Heat shock protein 70
IF	immunofluorescence
IP	immuno precipitation
IRES	internal ribosome entry site
kDa	kilodalton
LB	lysogeny broth
LB_{Amp}	LB containing ampicillin
$m^{5}C$	5-methylcytidin
$m^{6}A$	N^{6}-methyladenosine
mESC	mouse embryonic stem cell
METTL14	Methyltransferase-like protein 14
METTL3	Methyltransferase-like protein 3
miRNA	microRNA
mRNA	messenger RNA
MTD	methyltransferase domain
ncRNA	non-coding RNA
NES	nuclear export signal
NLS	nuclear localization signal
NSun2	NOP2/Sun RNA methyltransferase family member 2
ORF	open reading frame
^{32}P	phosphorus isotope 32
P-bodies	processing bodies
Ψ	pseudouridine
PA	polyacrylamide
PBS	phosphate-buffered saline
PCR	polymerase chain reaction
PUS	pseudouridine synthase
R	purine adenine or guanine (A or G)
RNA	ribonuleic acid
RNP	ribonucleoprotein
rRNA	ribosomal RNA
RT	reverse transcription
S. cerevisiae	*Saccharomyces cerevisiae*

S. frugiperda	*Spodoptera frugiperda*
S. pombe	*Schizosaccharomyces pombe*
SAM	S-adenosyl-methione
SDS	sodium dodecyl sulfate
SDS-PAGE	sodium dodecyl sulfate polyacrylamide gel electrophoresis
SFM	serum-free medium
snoRNA	small nucleolar RNA
snRNA	small nuclear RNA
SPEN	split end
Tab.	table
TBE	tris borate EDTA
TBS	tris-buffered saline
TBST	TBS with $0.1\,\%$ Tween 20
TEMED	N,N,N',N'-Tetramethylethane-1,2-diamine
TET	Ten-eleven translocation
TEV	Tobacco Etch Virus
TRD	target recognition domain
Tris	2-Amino-2-hydroxymethyl-propane-1,3-diol
tRNA	transfer RNA
TSS	transcription start site
U	uracil
UTR	untranslated region
Val^{AAC}	tRNA encoding for valine with the anticodon AAC (5'→3')
WTAP	Wilms' tumor 1-associating protein
YTH domain	YT521-B homology domain
YTHDF	YTH domain family

References

[1] Magdalena A. Machnicka, Kaja Milanowska, Okan Osman Oglou, Elzbieta Purta, Malgorzata Kurkowska, Anna Olchowik, Witold Januszewski, Sebastian Kalinowski, Stanislaw Dunin-Horkawicz, Kristian M. Rother, Mark Helm, Janusz M. Bujnicki, and Henri Grosjean. MODOMICS: A database of RNA modification pathways - 2013 update. *Nucleic Acids Research*, 41(D1), 2013.

[2] Toshiko Yamada-Okabe, Rikuo Doi, Osamu Shimmi, Mikio Arisawa, and Hisafumi Yamada-Okabe. Isolation and characterization of a human cDNA for mRNA 5'-capping enzyme. *Nucleic Acids Research*, 26(7):1700–1706, 1998.

[3] Walter E Kowtoniuk, Yinghua Shen, Jennifer M Heemstra, Isha Agarwal, and David R Liu. A chemical screen for biological small molecule-RNA conjugates reveals CoA-linked RNA. *Proceedings of the National Academy of Sciences of the United States of America*, 106(19):7768–7773, 2009.

[4] Chun Chu, Kalyan Das, James R Tyminski, Joseph D Bauman, Rongjin Guan, Weihua Qiu, Gaetano T Montelione, Eddy Arnold, and Aaron J Shatkin. Structure of the guanylyltransferase domain of human mRNA capping enzyme. *Proceedings of the National Academy of Sciences of the United States of America*, 108(25):10104–8, 2011.

[5] Robert Willem van Nues, Sander Granneman, Grzegorz Kudla, Katherine Elizabeth Sloan, Matthew Chicken, David Tollervey, and Nicholas James Watkins. Box C/D snoRNP catalysed methylation is aided by additional pre-rRNA base-pairing. *The EMBO journal*, 30(12):2420–30, 2011.

[6] Blerta Xhemalce, Samuel C Robson, and Tony Kouzarides. Human RNA methyltransferase BCDIN3D regulates microRNA processing. *Cell*, 151(2):278–88, oct 2012.

[7] C He. Grand challenge commentary: RNA epigenetics? *Nat Chem Biol*, 6(12):863–865, 2010.

[8] Yogesh Saletore, Kate Meyer, Jonas Korlach, Igor D Vilfan, Samie Jaffrey, and Christopher E Mason. The birth of the Epitranscriptome: deciphering the function of RNA modifications. *Genome biology*, 13(10):175, 2012.

[9] Michaela Frye, Samie R. Jaffrey, Tao Pan, Gideon Rechavi, and Tsutomu Suzuki. RNA modifications: what have we learned and where are we headed? *Nature Reviews Genetics*, 2016.

[10] Mary Grace Goll, Finn Kirpekar, Keith a Maggert, Jeffrey a Yoder, Chih-Lin Hsieh, Xiaoyu Zhang, Kent G Golic, Steven E Jacobsen, and Timothy H Bestor. Methylation of tRNAAsp by the DNA methyltransferase homolog Dnmt2. *Science*, 311(5759):395–8, 2006.

[11] Tomasz P Jurkowski, Madeleine Meusburger, Sameer Phalke, Mark Helm, Wolfgang Nellen, Gunter Reuter, and Albert Jeltsch. Human DNMT2 methylates tRNA(Asp) molecules using a DNA methyltransferase-like catalytic mechanism. *RNA (New York, N.Y.)*, 14(8):1663–70, 2008.

[12] Matthias Schaefer, Tim Pollex, Katharina Hanna, Francesca Tuorto, Madeleine Meusburger, Mark Helm, and Frank Lyko. RNA methylation by Dnmt2 protects transfer RNAs against stress-induced cleavage. *Genes and Development*, 24(15):1590–1595, 2010.

[13] Francesca Tuorto, Reinhard Liebers, Tanja Musch, Matthias Schaefer, Sarah Hofmann, Stefanie Kellner, Michaela Frye, Mark Helm, Georg Stoecklin, and Frank Lyko. RNA cytosine methylation by Dnmt2 and NSun2 promotes tRNA stability and protein synthesis. *Nature structural & molecular biology*, 19(9):900–5, sep 2012.

[14] D R Davis. Stabilization of RNA stacking by pseudouridine. *Nucleic acids research*, 23(24):5020–5026, 1995.

[15] Basma El Yacoubi, Marc Bailly, and Valérie de Crécy-Lagard. Biosynthesis and Function of Posttranscriptional Modifications of Transfer RNAs. *Annual Review of Genetics*, 46(1):120820103026000, 2011.

[16] Xue h. Liang, Qing Liu, and Maurille J. Fournier. rRNA Modifications in an Intersubunit Bridge of the Ribosome Strongly Affect Both Ribosome Biogenesis and Activity. *Molecular Cell*, 28(6):965–977, 2007.

[17] Dorota Piekna-Przybylska, Piotr Przybylski, Agnès Baudin-Baillieu, Jean Pierre Rousset, and Maurille J. Fournier. Ribosome performance is enhanced by a rich cluster of pseudouridines in the A-site finger region of the large subunit. *Journal of Biological Chemistry*, 283(38):26026–26036, 2008.

[18] Karen Jack, Cristian Bellodi, Dori M. Landry, Rachel O. Niederer, Arturas Meskauskas, Sharmishtha Musalgaonkar, Noam Kopmar, Olya Krasnykh, Alison M. Dean, Sunnie R. Thompson, Davide Ruggero, and Jonathan D. Dinman. RRNA Pseudouridylation Defects Affect Ribosomal Ligand Binding and Translational Fidelity from Yeast to Human Cells. *Molecular Cell*, 44(4):660–666, 2011.

[19] Douglas R. Drummond, John Armstrong, and Alan Colman. The effect of capping and polyadenylation on the stability, movement and translation of synthetic messenger RNAs in Xenopus oocytes. *Nucleic Acids Research*, 13(20):7375–7394, 1985.

[20] D L Gillian-Daniel, N K Gray, J Aström, a Barkoff, and M Wickens. Modifications of the 5' cap of mRNAs during Xenopus oocyte maturation: independence from changes in poly(A) length and impact on translation. *Molecular and cellular biology*, 18(10):6152–6163, 1998.

[21] Beate Schwer, Nayanendu Saha, Xiangdong Mao, Hsiao Wang Chen, and Stewart Shuman. Structure-function analysis of yeast mRNA cap methyltransferase and high-copy suppression of conditional mutants by AdoMet synthase and the ubiquitin cojugating enzyme Cdc34p. *Genetics*, 155(4):1561–1576, 2000.

[22] J Marcotrigiano, a C Gingras, N Sonenberg, and S K Burley. Cocrystal Structure of the Messenger RNA 5' Cap-Binding Protein (eIF4E) Bound to 7-methyl-GDP. *Cell*, 89(6):951 – 961, 1997.

[23] N Sonenberg, M a Morgan, W C Merrick, and a J Shatkin. A polypeptide in eukaryotic initiation factors that crosslinks specifically to the 5'-terminal cap in mRNA. *Proceedings of the National Academy of Sciences of the United States of America*, 75(10):4843–4847, 1978.

[24] N Sonenberg, K M Rupprecht, S M Hecht, and a J Shatkin. Eukaryotic mRNA cap binding protein: purification by affinity chromatography on sepharose-coupled m7GDP. *Proceedings of the National Academy of Sciences of the United States of America*, 76(9):4345–4349, 1979.

[25] B. J. Lamphear, R. Kirchweger, T. Skern, and R. E. Rhoads. Mapping of functional domains in eukaryotic protein synthesis initiation factor 4G (eIF4G) with picornaviral proteases. Implications for Cap-dependent and Cap-independent translational initiation. *Journal of Biological Chemistry*, 270(37):21975–21983, 1995.

[26] H Imataka and N Sonenberg. Human eukaryotic translation initiation factor 4G (eIF4G) possesses two separate and independent binding sites for eIF4A. *Molecular and cellular biology*, 17(12):6940–7, 1997.

[27] S Morino, H Imataka, Y V Svitkin, T V Pestova, and N Sonenberg. Eukaryotic translation initiation factor 4E (eIF4E) binding site and the middle one-third of eIF4GI constitute the core domain for cap-dependent translation, and the C-terminal one-third functions as a modulatory region. *Molecular and cellular biology*, 20(2):468–77, 2000.

[28] Aaron K. Lefebvre, Nadejda L. Korneeva, Marjan Trutschl, Urska Cvek, Roy D. Duzan, Christopher A. Bradley, J. W B Hershey, and Robert E. Rhoads. Translation initiation factor eIF4G-1 binds to eIF3 through the eIF3e subunit. *Journal of Biological Chemistry*, 281(32):22917–22932, 2006.

[29] Michael Rau, Theophile Ohlmann, Simon J. Morley, and Virginia M. Pain. A reevaluation of the Cap-binding protein, eIF4E, as a rate-limiting factor for initiation of translation in reticulocyte lysate. *Journal of Biological Chemistry*, 271(15):8983–8990, 1996.

[30] Neus Visa, Elisa Izaurralde, João Ferreira, Bertil Daneholt, and Iain W. Mattaj. A nuclear cap-binding complex binds Balbiani ring pre-mRNA cotranscriptionally and accompanies the ribonucleoprotein particle during nuclear export. *Journal of Cell Biology*, 133(1):5–14, 1996.

[31] Min Gao, David T. Fritz, Lance P. Ford, and Jeffrey Wilusz. Interaction between a Poly(A)-Specific Ribonuclease and the 5' Cap Influences mRNA Deadenylation Rates In Vitro. *Molecular Cell*, 5(3):479–488, 2000.

[32] Valentina Evdokimova, Peter Ruzanov, Hiroaki Imataka, Brian Raught, Yuri Svitkin, Lev P. Ovchinnikov, and Nahum Sonenberg. The major mRNA-associated protein YB-1 is a potent 5' cap-dependent mRNA stabilizer. *EMBO Journal*, 20(19):5491–5502, 2001.

[33] Michelle Steiger, Anne Carr-Schmid, David C Schwartz, Megerditch Kiledjian, and Roy Parker. Analysis of recombinant yeast decapping enzyme. *RNA*, 9(2):231–8, 2003.

[34] Elmar Wahle and Ursula Rüegsegger. 3'-End processing of pre-mRNA in eukaryotes, 1999.

[35] Stewart Shuman. What messenger RNA capping tells us about eukaryotic evolution. *Nature reviews. Molecular cell biology*, 3(8):619–625, 2002.

[36] Y Furuichi, M Morgan, a J Shatkin, W Jelinek, M Salditt-Georgieff, and J E Darnell. Methylated, blocked 5 termini in HeLa cell mRNA. *Proceedings of the National Academy of Sciences of the United States of America*, 72(5):1904–1908, 1975.

[37] François Bélanger, Janusz Stepinski, Edward Darzynkiewicz, and Jerry Pelletier. Characterization of hMTr1, a human Cap1 2âĂš-O-ribose methyltransferase. *Journal of Biological Chemistry*, 285(43):33037–33044, 2010.

[38] Maria Werner, Elzbieta Purta, Katarzyna H. Kaminska, Iwona A. Cymerman, David A. Campbell, Bidyottam Mittra, Jesse R. Zamudio, Nancy R. Sturm, Jacek Jaworski, and Janusz M. Bujnicki. 2'-O-ribose

methylation of cap2 in human: Function and evolution in a horizontally mobile family. *Nucleic Acids Research*, 39(11):4756–4768, 2011.

[39] Miroslaw Smietanski, Maria Werner, Elzbieta Purta, Katarzyna H Kaminska, Janusz Stepinski, Edward Darzynkiewicz, Marcin Nowotny, and Janusz M Bujnicki. Structural analysis of human 2'-O-ribose methyltransferases involved in mRNA cap structure formation. *Nature communications*, 5:3004, 2014.

[40] Kate D Meyer, Yogesh Saletore, Paul Zumbo, Olivier Elemento, Christopher E Mason, and Samie R Jaffrey. Comprehensive analysis of mRNA methylation reveals enrichment in 3' UTRs and near stop codons. *Cell*, 149(7):1635–46, jun 2012.

[41] Dan Dominissini, Sharon Moshitch-Moshkovitz, Schraga Schwartz, Mali Salmon-Divon, Lior Ungar, Sivan Osenberg, Karen Cesarkas, Jasmine Jacob-Hirsch, Ninette Amariglio, Martin Kupiec, Rotem Sorek, and Gideon Rechavi. Topology of the human and mouse m6A RNA methylomes revealed by m6A-seq. *Nature*, 485(7397):201–6, may 2012.

[42] Brenda L. Bass and Harold Weintraub. A developmentally regulated activity that unwinds RNA duplexes. *Cell*, 48(4):607–613, 1987.

[43] Brenda L. Bass and Harold Weintraub. An unwinding activity that covalently modifies its double-stranded RNA substrate. *Cell*, 55(6):1089–1098, 1988.

[44] Richard W Wagnert, Joseph E Smitht, Barry S Coopermant, and Kazuko Nishikurat. A double-stranded RNA unwinding activity introduces structural alterations by means of adenosine to inosine conversions in mammalian cells. *Proceedings of the National Academy of Sciences*, 86:2647–2651, 1989.

[45] T Melcher, S Maas, a Herb, R Sprengel, P H Seeburg, and M Higuchi. A mammalian RNA editing enzyme., 1996.

[46] J B Patterson and C E Samuel. Expression and regulation by interferon of a double-stranded-RNA-specific adenosine deaminase from human cells: evidence for two forms of the deaminase. *Mol Cell Biol*, 15(10):5376–5388, 1995.

[47] Michael S. Paul and Brenda L. Bass. Inosine exists in mRNA at tissue-specific levels and is most abundant in brain mRNA. *EMBO Journal*, 17(4):1120–1127, 1998.

[48] Erez Y. Levanon, Martina Hallegger, Yaron Kinar, Ronen Shemesh, Kristina Djinovic-Carugo, Gideon Rechavi, Michael F. Jantsch, and Eli Eisenberg. Evolutionarily conserved human targets of adenosine to inosine RNA editing. *Nucleic Acids Research*, 33(4):1162–1168, 2005.

[49] Federica Galeano, Anne Leroy, Claudia Rossetti, Irina Gromova, Philippe Gautier, Liam P. Keegan, Luca Massimi, Concezio Di Rocco, Mary A. O'Connell, and Angela Gallo. Human BLCAP transcript: New editing events in normal and cancerous tissues. *International Journal of Cancer*, 127(1):127–137, 2010.

[50] Tsutomu Suzuki, Hiroki Ueda, Shunpei Okada, and Masayuki Sakurai. Transcriptome-wide identification of adenosine-to-inosine editing using the ICE-seq method. *Nature Protocols*, 10(5):715–732, 2015.

[51] Joana M. P. Desterro, Liam P. Keegan, Miguel Lafarga, Maria Teresa Berciano, Mary O'Connell, and Maria Carmo-Fonseca. Dynamic association of RNA-editing enzymes with the nucleolus. *Journal of Cell Science*, 116(9):1805–1818, 2003.

[52] Christopher L Sansam, K Sam Wells, and Ronald B Emeson. Modulation of RNA editing by functional nucleolar sequestration of ADAR2. *Proceedings of the National Academy of Sciences of the United States of America*, 100(24):14018–23, 2003.

[53] Stefan Maas and Willemijn M. Gommans. Identification of a selective nuclear import signal in adenosine deaminases acting on RNA. *Nucleic Acids Research*, 37(17):5822–5829, 2009.

[54] A Strehblow, M Hallegger, and M F Jantsch. Nucleocytoplasmic distribution of human RNA-editing enzyme ADAR1 is modulated by double-stranded RNA-binding domains, a leucine-rich export signal, and a putative dimerization domain. *Mol Biol Cell*, 13(11):3822–3835, 2002.

[55] Jutta Fritz, Alexander Strehblow, Andreas Taschner, Sandy Schopoff, Pawel Pasierbek, Michael F Jantsch, H Poulsen, J Nilsson, C K Damgaard, J Egebjerg, and J Kjems. RNA-regulated interaction of transportin-1 and exportin-5 with the double-stranded RNA-binding domain regulates nucleocytoplasmic shuttling of ADAR1. *Molecular and cellular biology*, 29(22):7862–71, 2009.

[56] Swee Kee Wong, Shuji Sato, and David W Lazinski. Elevated activity of the large form of ADAR1 in vivo: very efficient RNA editing occurs in the cytoplasm. *RNA (New York, N.Y.)*, 9(5):586–598, 2003.

[57] K Nishikura, C Yoo, U Kim, J M Murray, P A Estes, F E Cash, and S A Liebhaber. Substrate specificity of the dsRNA unwinding/modifying activity. *The EMBO journal*, 10(11):3523–32, 1991.

[58] M Higuchi, S Maas, F N Single, J Hartner, a Rozov, N Burnashev, D Feldmeyer, R Sprengel, and P H Seeburg. Point mutation in an AMPA receptor gene rescues lethality in mice deficient in the RNA-editing enzyme ADAR2. *Nature*, 406(6791):78–81, 2000.

[59] K. A. Lehmann and B. L. Bass. Double-stranded RNA adenosine deaminases ADAR1 and ADAR2 have overlapping specificities. *Biochemistry*, 39(42):12875–12884, 2000.

[60] Qingde Wang, Mana Miyakoda, Weidong Yang, Jaspal Khillan, David L Stachura, Mitchell J Weiss, and Kazuko Nishikura. Stress-induced apoptosis associated with null mutation of ADAR1 RNA editing deaminase gene. *The Journal of biological chemistry*, 279(6):4952–61, 2004.

[61] Galit Lev-Maor, Rotem Sorek, Erez Y Levanon, Nurit Paz, Eli Eisenberg, and Gil Ast. RNA-editing-mediated exon evolution. *Genome biology*, 8(2):R29, 2007.

[62] Ling-ling Chen, Joshua N Decerbo, and Gordon G Carmichael. Alu element-mediated gene silencing. *The EMBO Journal*, 2794(12):1694–1705, 2008.

[63] B Sommer, M Kohler, R Sprengel, and P H Seeburg. RNA editing in brain controls a determinant of ion flow in glutamate-gated channels. *Cell*, 67(1):11–19, 1991.

[64] J Egebjerg and S F Heinemann. Ca2+ permeability of unedited and edited versions of the kainate selective glutamate receptor GluR6. *Proceedings of the National Academy of Sciences of the United States of America*, 90(2):755–9, 1993.

[65] Harryl D Martinez, Rohini J Jasavala, Izumi Hinkson, Latricia D Fitzgerald, James S Trimmer, Hsing-Jien Kung, and Michael E Wright. RNA editing of androgen receptor gene transcripts in prostate cancer cells. *The Journal of biological chemistry*, 283(44):29938–49, 2008.

[66] Martin Kohler, Nail Burnashev, Bert Sakmann, and Peter H. Seeburg. Determinants of ca2+ permeability in both TM1 and TM2 of high affinity kainate receptor channels: Diversity by RNA editing. *Neuron*, 10(3):491–500, 1993.

[67] H Lomeli, J Mosbacher, T Melcher, T Hoger, T Kuner, H Monyer, M Higuchi, A Bach, and P. Seeburg. Control of kinetic properties of AMPA receptor channels by nuclear RNA editing. *Science*, 266(5191):1709–1713, 1994.

[68] A. D J Scadden and C. W J Smith. Specific cleavage of hyper-edited dsRNAs. *EMBO Journal*, 20(15):4243–4252, 2001.

[69] Zuo Zhang and Gordon G. Carmichael. The fate of dsRNA in the Nucleus: A p54nrb-containing complex mediates the nuclear retention of promiscuously A-to-I edited RNAs. *Cell*, 106(4):465–475, 2001.

[70] Yoko Morita, Toshihiro Shibutani, Nozomi Nakanishi, Kazuko Nishikura, Shigenori Iwai, and Isao Kuraoka. Human endonuclease V is a ribonuclease specific for inosine-containing RNA. *Nature Communications*, 4:2273, 2013.

[71] Yukio Kawahara, Boris Zinshteyn, Praveen Sethupathy, Hisashi Iizasa, Artemis G Hatzigeorgiou, and Kazuko Nishikura. Redirection of silencing targets by adenosine-to-inosine editing of miRNAs. *Science (New York, N.Y.)*, 315(5815):1137–40, 2007.

[72] Niamh M. Mannion, Sam M. Greenwood, Robert Young, Sarah Cox, James Brindle, David Read, Christoffer Nellåker, Cornelia Vesely, Chris P. Ponting, Paul J. McLaughlin, Michael F. Jantsch, Julia Dorin, Ian R. Adams, A. D J Scadden, Marie Öhman, Liam P. Keegan, and Mary A. O'Connell. The RNA-Editing Enzyme ADAR1 Controls Innate Immune Responses to RNA. *Cell Reports*, 9(4):1482–1494, 2014.

[73] B. J. Liddicoat, R. Piskol, A. M. Chalk, G. Ramaswami, M. Higuchi, J. C. Hartner, J. B. Li, P. H. Seeburg, and C. R. Walkley. RNA editing by ADAR1 prevents MDA5 sensing of endogenous dsRNA as nonself. *Science*, 349(July 2015):1–9, 2015.

[74] Gillian I Rice, Paul R Kasher, Gabriella M A Forte, Niamh M Mannion, Sam M Greenwood, Marcin Szynkiewicz, Jonathan E Dickerson, Sanjeev S Bhaskar, Massimiliano Zampini, Tracy A Briggs, Emma M Jenkinson, Carlos A Bacino, Roberta Battini, Enrico Bertini, Paul A Brogan, Louise A Brueton, Marialuisa Carpanelli, Corinne De Laet, Pascale de Lonlay, Mireia del Toro, Isabelle Desguerre, Elisa Fazzi, Angels Garcia-Cazorla, Arvid Heiberg, Masakazu Kawaguchi, Ram Kumar, Jean-Pierre S-M Lin, Charles M Lourenco, Alison M Male, Wilson Marques, Cyril Mignot, Ivana Olivieri, Simona Orcesi, Prab Prabhakar, Magnhild Rasmussen, Robert A Robinson, Flore Rozenberg, Johanna L Schmidt, Katharina Steindl, Tiong Y Tan, William G van der Merwe, Adeline Vanderver, Grace Vassallo, Emma L Wakeling, Evangeline Wassmer, Elizabeth Whittaker, John H Livingston, Pierre Lebon, Tamio Suzuki, Paul J McLaughlin, Liam P Keegan, Mary A O'Connell, Simon C Lovell, and Yanick J Crow. Mutations in ADAR1 cause Aicardi-Goutières syndrome associated with a type I interferon signature. *Nature genetics*, 44(11):1243–8, 2012.

[75] N Suzuki, T Suzuki, K Inagaki, S Ito, M Kono, T Horikawa, S Fujiwara, A Ishiko, K Matsunaga, Y Aoyama, H Tosaki-Ichikawa, and Y Tomita. Ten novel mutations of the ADAR1 gene in Japanese patients with dyschromatosis symmetrica hereditaria. *J Invest Dermatol*, 127(2):309–311, 2007.

[76] Zachary D Smith and Alexander Meissner. DNA methylation: roles in mammalian development. *Nature reviews. Genetics*, 14(3):204–20, 2013.

[77] Déborah Bourc'his and Timothy H Bestor. Meiotic catastrophe and retrotransposon reactivation in male germ cells lacking Dnmt3L. *Nature*, 431(7004):96–99, 2004.

[78] Melany Jackson, Anna Krassowska, Nick Gilbert, Timothy Chevassut, Lesley Forrester, John Ansell, and Bernard Ramsahoye. Severe global DNA hypomethylation blocks differentiation and induces histone hyperacetylation in embryonic stem cells. *Molecular and cellular biology*, 24(20):8862–71, 2004.

[79] Dong Hoon Lee, Purnima Singh, Shirley Y. Tsai, Nathan Oates, Alexander Spalla, Claudio Spalla, Lucy Brown, Guillermo Rivas, Garrett Larson, Tibor A. Rauch, Gerd P. Pfeifer, and Piroska E. Szabó. CTCF-dependent chromatin bias constitutes transient epigenetic memory of the mother at the H19-igf2 imprinting control region in prospermatogonia. *PLoS Genetics*, 6(11), 2010.

[80] Christoph Bock, Isabel Beerman, Wen Hui Lien, Zachary D. Smith, Hongcang Gu, Patrick Boyle, Andreas Gnirke, Elaine Fuchs, Derrick J. Rossi, and Alexander Meissner. DNA Methylation Dynamics during In Vivo Differentiation of Blood and Skin Stem Cells. *Molecular Cell*, 47(4):633–647, 2012.

[81] Jeffrey E Squires, Hardip R Patel, Marco Nousch, Tennille Sibbritt, David T Humphreys, Brian J Parker, Catherine M Suter, and Thomas Preiss. Widespread occurrence of 5-methylcytosine in human coding and non-coding RNA. *Nucleic acids research*, pages 1–11, feb 2012.

[82] Vahid Khoddami and Bradley R Cairns. Identification of direct targets and modified bases of RNA cytosine methyltransferases. *Nature biotechnology*, 31(5):458–464, 2013.

[83] Xiaotian Zhang, Zhenyun Liu, Jie Yi, Hao Tang, Junyue Xing, Minqwei Yu, Tanjun Tong, Yongfeng Shang, Myriam Gorospe, and Wengong Wang. The tRNA methyltransferase NSun2 stabilizes p16INKâĄť mRNA by methylating the 3'-untranslated region of p16. TL - 3. *Nature communications*, 3 VN - re:712, 2012.

[84] Shobbir Hussain, Abdulrahim A. Sajini, Sandra Blanco, Sabine Dietmann, Patrick Lombard, Yoichiro Sugimoto, Maike Paramor, Joseph G. Gleeson, Duncan T. Odom, Jernej Ule, and Michaela Frye. NSun2-mediated cytosine-5 methylation of vault noncoding RNA determines its processing into regulatory small RNAs. *Cell Reports*, 4(2):255–261, 2013.

[85] Thomas M Carlile, Maria F Rojas-Duran, Boris Zinshteyn, Hakyung Shin, Kristen M Bartoli, and Wendy V Gilbert. Pseudouridine profiling reveals regulated mRNA pseudouridylation in yeast and human cells. *Nature*, 515(7525):143–6, 2014.

[86] Alexander F. Lovejoy, Daniel P. Riordan, and Patrick O. Brown. Transcriptome-wide mapping of pseudouridines: Pseudouridine synthases modify specific mRNAs in S. cerevisiae. *PLoS ONE*, 9(10), 2014.

[87] Schraga Schwartz, Douglas A. Bernstein, Maxwell R. Mumbach, Marko Jovanovic, Rebecca H. Herbst, Brian X. León-Ricardo, Jesse M. Engreitz, Mitchell Guttman, Rahul Satija, Eric S. Lander, Gerald Fink, and Aviv Regev. Transcriptome-wide mapping reveals widespread dynamic-regulated pseudouridylation of ncRNA and mRNA. *Cell*, 159(1):148–162, 2014.

[88] A Bakin and J Ofengand. Four newly located pseudouridylate residues in Escherichia coli 23S ribosomal RNA are all at the peptidyltransferase center: analysis by the application of a new sequencing technique. *Biochemistry*, 32(37):9754–9762, 1993.

[89] Philippe Ganot, Marie-Line Bortolin, and Tamás Kiss. Site-Specific Pseudouridine Formation in Preribosomal RNA Is Guided by Small Nucleolar RNAs. *Cell*, 89(5):799–809, 1997.

[90] Jingwei Ni, Amy L Tien, and Maurille J Fournier. Small Nucleolar RNAs Direct Site-Specific Synthesis of Pseudouridine in Ribosomal RNA. *Cell*, 89(4):565–573, 1997.

[91] N J Watkins, A Gottschalk, G Neubauer, B Kastner, P Fabrizio, M Mann, and R Lührmann. Cbf5p, a potential pseudouridine synthase, and Nhp2p, a putative RNA-binding protein, are present together with Gar1p in all H BOX/ACA-motif snoRNPs and constitute a common bipartite structure. *RNA (New York, N.Y.)*, 4(12):1549–68, 1998.

[92] Yeganeh Zebarjadian, Tom King, Maurille J. Fournier, Louise Clarke, and John Carbon. Point Mutations in Yeast CBF5 Can Abolish In Vivo Pseudouridylation of rRNA. *Molecular and Cellular Biology*, 19(11):7461–7472, 1999.

[93] Chen Wang, Charles C Query, and U Thomas Meier. Immunopurified small nucleolar ribonucleoprotein particles pseudouridylate rRNA independently of their association with phosphorylated Nopp140. *Molecular and cellular biology*, 22(24):8457–66, 2002.

[94] S Massenet, Y Motorin, D L Lafontaine, E C Hurt, H Grosjean, and C Branlant. Pseudouridine mapping in the Saccharomyces cerevisiae spliceosomal U small nuclear RNAs (snRNAs) reveals that pseudouridine synthase Pus1p exhibits a dual substrate specificity for U2 snRNA and tRNA. *Molecular and cellular biology*, 19(3):2142–2154, 1999.

[95] Xiaoju Ma, Xinliang Zhao, and Yi-Tao Yu. Pseudouridylation (Psi) of U2 snRNA in S. cerevisiae is catalyzed by an RNA-independent mechanism. *The EMBO journal*, 22(8):1889–1897, 2003.

[96] Isabelle Behm-Ansmant, Alan Urban, Xiaoju Ma, Yi-Tao Yu, Yuri Motorin, and Christiane Branlant. The Saccharomyces cerevisiae U2 snRNA:pseudouridine-synthase Pus7p is a novel multisite-multisubstrate RNA:Psi-synthase also acting on tRNAs. *RNA (New York, N.Y.)*, 9(11):1371–82, 2003.

[97] Xiaoju Ma, Chunxing Yang, Andrei Alexandrov, Elizabeth J Grayhack, Isabelle Behm-Ansmant, and Yi-Tao Yu. Pseudouridylation of yeast U2 snRNA is catalyzed by either an RNA-guided or RNA-independent mechanism. *The EMBO journal*, 24(13):2403–2413, 2005.

[98] John Karijolich and Yi-Tao Yu. Modifying the genetic code: Converting nonsense codons into sense codons by targeted pseudouridylation. *Nature*, 474(7351):395–398, 2012.

[99] Dan Dominissini, Sigrid Nachtergaele, Sharon Moshitch-moshkovitz, Eyal Peer, Nitzan Kol, Moshe Shay Ben-haim, Qing Dai, Ayelet Di Segni, Wesley C Clark, Guanqun Zheng, Tao Pan, Oz Solomon, Eran Eyal, Vera Hershkovitz, Dali Han, Louis C Doré, Ninette Amariglio, Gideon Rechavi, and Chuan He. The dynamic N 1 -methyladenosine methylome in eukaryotic messenger RNA. *Nature*, 530(7591):441–446, 2016.

[100] Xiaoyu Li, Xushen Xiong, Kun Wang, Lixia Wang, Xiaoting Shu, Shiqing Ma, and Chengqi Yi. Transcriptome-wide mapping reveals reversible and dynamic N(1)-methyladenosine methylome. *Nature chemical biology*, 12(5):311–316, 2016.

[101] Sarah Ozanick, Annette Krecic, Joshua Andersland, and James T Anderson. The bipartite structure of the tRNA m1A58 methyltransferase from S. cerevisiae is conserved in humans. *RNA (New York, N.Y.)*, 11(8):1281–1290, 2005.

[102] Christian Peifer, Sunny Sharma, Peter Watzinger, Stefanie Lamberth, Peter K??tter, and Karl Dieter Entian. Yeast Rrp8p, a novel methyltransferase responsible for m1A 645 base modification of 25S rRNA. *Nucleic Acids Research*, 41(2):1151–1163, 2013.

[103] Mark Helm, Richard Giegé, and Catherine Florentz. A WatsonâĹŠCrick Base-Pair-Disrupting Methyl Group (m 1 A9) Is Sufficient for Cloverleaf Folding of Human Mitochondrial tRNA Lys âĂă. *Biochemistry*, 38(40):13338–13346, 1999.

[104] R Sengupta, S Vainauskas, C Yarian, E Sochacka, a Malkiewicz, R H Guenther, K M Koshlap, and P F Agris. Modified constructs of the tRNA TPsiC domain to probe substrate conformational require-

ments of m(1)A(58) and m(5)U(54) tRNA methyltransferases. *Nucleic acids research*, 28(6):1374–80, 2000.

[105] Huiqing Zhou, Isaac J Kimsey, Evgenia N Nikolova, Bharathwaj Sathyamoorthy, Gianmarc Grazioli, James McSally, Tianyu Bai, Christoph H Wunderlich, Christoph Kreutz, Ioan Andricioaei, and Hashim M Al-Hashimi. m1A and m1G disrupt A-RNA structure through the intrinsic instability of Hoogsteen base pairs. *Nature Structural & Molecular Biology*, 23(9), 2016.

[106] Guifang Jia, Ye Fu, Xu Zhao, Guanqun Zheng, Ying Yang, and Chengqi Yi. N6-Methyladenosine in nuclear rna is a major substrate of the obesity-associated FtO. 7(december):6–9, 2011.

[107] Guanqun Zheng, John Arne Dahl, Yamei Niu, Peter Fedorcsak, Chun-Min Huang, Charles J Li, Cathrine B Vågbø, Yue Shi, Wen-Ling Wang, Shu-Hui Song, Zhike Lu, Ralph P G Bosmans, Qing Dai, Ya-Juan Hao, Xin Yang, Wen-Ming Zhao, Wei-Min Tong, Xiu-Jie Wang, Florian Bogdan, Kari Furu, Ye Fu, Guifang Jia, Xu Zhao, Jun Liu, Hans E Krokan, Arne Klungland, Yun-Gui Yang, and Chuan He. ALKBH5 Is a Mammalian RNA Demethylase that Impacts RNA Metabolism and Mouse Fertility. *Molecular cell*, 49(1):18–29, jan 2013.

[108] J. W. LITTLEFIELD & D. B. DUNN. Natural Occurrence of Thymine and Three Methylated Adenine Bases in Several Ribonucleic Acids. *Nature*, 182:1638 – 1640, 1958.

[109] Yasuo Iwanami and Gene M. Brown. Methylated bases of transfer ribonucleic acid from hela and L cells. *Archives of Biochemistry and Biophysics*, 124:472–482, 1968.

[110] Kate D Meyer and Samie R Jaffrey. The dynamic epitranscriptome: N6-methyladenosine and gene expression control. *Nature reviews. Molecular cell biology*, 15(5):313–26, 2014.

[111] R Desrosiers, K Friderici, and F Rottman. Identification of methylated nucleosides in messenger RNA from Novikoff hepatoma cells. *Proceedings of the National Academy of Sciences of the United States of America*, 71(10):3971–5, 1974.

[112] Robert P. Perry, Dawn E. Kelley, Karen Friderici, and Fritz Rottman. The methylated constituents of L cell messenger RNA: Evidence for an unusual cluster at the 5' terminus. *Cell*, 4(4):387–394, 1975.

[113] S Lavi and A J Shatkin. Methylated simian virus 40-specific RNA from nuclei and cytoplasm of infected BSC-1 cells. *Proceedings of the National Academy of Sciences of the United States of America*, 72(6):2012–6, 1975.

[114] Ueli Schibler, Dawn E. Kelley, and Robert P. Perry. Comparison of methylated sequences in messenger RNA and heterogeneous nuclear RNA from mouse L cells. *Journal of Molecular Biology*, 115(4):695–714, 1977.

[115] Sarah Horowitz, Amikam Horowitz, Timothy W Nilsen, Theodore W Munnsf, and Fritz M Rottman. Mapping of N6-methyladenosine residues in bovine prolactin riRNA. 81(September):5667–5671, 1984.

[116] Schraga Schwartz, Sudeep D Agarwala, Maxwell R Mumbach, Marko Jovanovic, Philipp Mertins, Alexander Shishkin, Yuval Tabach, Tarjei S Mikkelsen, Rahul Satija, Gary Ruvkun, Steven a Carr, Eric S Lander, Gerald R Fink, and Aviv Regev. High-resolution mapping reveals a conserved, widespread, dynamic mRNA methylation program in yeast meiosis. *Cell*, 155(6):1409–21, dec 2013.

[117] Guan-Zheng Luo, Alice MacQueen, Guanqun Zheng, Hongchao Duan, Louis C Dore, Zhike Lu, Jun Liu, Kai Chen, Guifang Jia, Joy Bergelson, and Chuan He. Unique features of the m6A methylome in Arabidopsis thaliana. *Nature communications*, 5:5630, 2014.

[118] Bastian Linder, Anya V Grozhik, Anthony O Olarerin-George, Cem Meydan, Christopher E Mason, and Samie R Jaffrey. Single-nucleotide-resolution mapping of m6A and m6Am throughout the transcriptome. *Nat Methods*, 12(8):767–772, 2015.

[119] Sudeep D Agarwala, Hannah G Blitzblau, Andreas Hochwagen, and Gerald R Fink. RNA methylation by the MIS complex regulates a cell fate decision in yeast. *PLoS genetics*, 8(6):e1002732, jan 2012.

[120] J M Keith, M J Ensinger, and B Mose. HeLa cell RNA (2'-O-methyladenosine-N6-)-methyltransferase specific for the capped 5'-end of messenger RNA. *The Journal of biological chemistry*, 253(14):5033–9, 1978.

[121] Jun Zhou, Ji Wan, Xiangwei Gao, Xingqian Zhang, Samie R Jaffrey, and Shu-Bing Qian. Dynamic m(6)A mRNA methylation directs translational control of heat shock response. *Nature*, 526(7574):591–594, 2015.

[122] Kate D. Meyer, Deepak P. Patil, Jun Zhou, Alexandra Zinoviev, Maxim A. Skabkin, Olivier Elemento, Tatyana V. Pestova, Shu Bing Qian, and Samie R. Jaffrey. 5' UTR m6A Promotes Cap-Independent Translation. *Cell*, 163(4):999–1010, 2015.

[123] Martin Holcik and Nahum Sonenberg. Translational control in stress and apoptosis. *Nature reviews. Molecular cell biology*, 6(4):318–27, 2005.

[124] S Lindquist and E.a. Craig. The heat-shock proteins. *Annual Review of Genetics*, 22:631–677, 1988.

[125] M. P. Mayer and B. Bukau. Hsp70 chaperones: Cellular functions and molecular mechanism. *Cell. Mol. Life Sci.*, 62(6):670–684, 2005.

[126] R Micura, W Pils, C Höbartner, K Grubmayr, M O Ebert, and B Jaun. Methylation of the nucleobases in RNA oligonucleotides mediates duplex-hairpin conversion. *Nucleic acids research*, 29(19):3997–4005, 2001.

[127] Nian Liu, Qing Dai, Guanqun Zheng, Chuan He, Marc Parisien, and Tao Pan. N(6)-methyladenosine-dependent RNA structural switches regulate RNA-protein interactions. *Nature*, 518(7540):560–564, 2015.

[128] Richard R. Meehan, Joe D. Lewis, Stewart McKay, Elke L. Kleiner, and Adrian P. Bird. Identification of a mammalian protein that binds specifically to DNA containing methylated CpGs. *Cell*, 58(3):499–507, 1989.

[129] Xiao Wang, Zhike Lu, Adrian Gomez, Gary C Hon, Yanan Yue, Dali Han, Ye Fu, Marc Parisien, Qing Dai, Guifang Jia, Bing Ren, Tao Pan, and Chuan He. N6-methyladenosine-dependent regulation of messenger RNA stability. *Nature*, 505(7481):117–20, jan 2014.

[130] Dominik Theler, Cyril Dominguez, Markus Blatter, Julien Boudet, and Frédéric H T Allain. Solution structure of the YTH domain in complex with N6-methyladenosine RNA: A reader of methylated RNA. *Nucleic Acids Research*, 42(22):13911–13919, 2014.

[131] Chao Xu, Xiao Wang, Ke Liu, Ian A Roundtree, Wolfram Tempel, Yanjun Li, Zhike Lu, Chuan He, and Jinrong Min. Structural basis for selective binding of m6A RNA by the YTHDC1 YTH domain. *Nature chemical biology*, 10(11):927–9, 2014.

[132] Ujwal Sheth and Roy Parker. Decapping and decay of messenger RNA occur in cytoplasmic processing bodies. *Science (New York, N.Y.)*, 300(5620):805–8, 2003.

[133] M. Brengues. Movement of Eukaryotic mRNAs Between Polysomes and Cytoplasmic Processing Bodies. *Science*, 310(5747):486–489, 2005.

[134] Xiao Wang, Boxuan Simen Zhao, Ian A. Roundtree, Zhike Lu, Dali Han, Honghui Ma, Xiaocheng Weng, Kai Chen, Hailing Shi, and Chuan He. N^6-methyladenosine modulates messenger RNA translation efficiency. *Cell*, 161(6):1388–1399, 2015.

[135] Colin Echeverría Aitken and Jon R Lorsch. A mechanistic overview of translation initiation in eukaryotes. *Nature Structural & Molecular Biology*, 19(6):568–576, 2012.

[136] Ilona Rafalska, Zhaiyi Zhang, Natalya Benderska, Horst Wolff, Annette M Hartmann, Ruth Brack-Werner, and Stefan Stamm. The intranuclear localization and function of YT521-B is regulated by tyrosine phosphorylation. *Human molecular genetics*, 13(15):1535–49, aug 2004.

[137] O. Nayler, a. M. Hartmann, and S. Stamm. The ER Repeat Protein Yt521-B Localizes to a Novel Subnuclear Compartment. *The Journal of Cell Biology*, 150(5):949–962, sep 2000.

[138] Zhaiyi Zhang, Dominik Theler, Katarzyna H Kaminska, Michael Hiller, Pierre de la Grange, Rainer Pudimat, Ilona Rafalska, Bettina Heinrich, Janusz M Bujnicki, Frédéric H-T Allain, and Stefan Stamm. The YTH domain is a novel RNA binding domain. *The Journal of biological chemistry*, 285(19):14701–10, may 2010.

[139] Wen Xiao, Samir Adhikari, Ujwal Dahal, Yu Sheng Chen, Ya Juan Hao, Bao Fa Sun, Hui Ying Sun, Ang Li, Xiao Li Ping, Wei Yi Lai, Xing Wang, Hai Li Ma, Chun Min Huang, Ying Yang, Niu Huang, Gui Bin Jiang, Hai Lin Wang, Qi Zhou, Xiu Jie Wang, Yong Liang Zhao, and Yun Gui Yang. Nuclear m6A Reader YTHDC1 Regulates mRNA Splicing. *Molecular Cell*, 61(4):507–519, 2016.

[140] X D Fu. The superfamily of arginine/serine-rich splicing factors. *RNA (New York, N.Y.)*, 1(7):663–680, 1995.

[141] K Colwill, T Pawson, B Andrews, J Prasad, J L Manley, J C Bell, and P I Duncan. The Clk/Sty protein kinase phosphorylates SR splicing factors and regulates their intranuclear distribution. *The EMBO journal*, 15(2):265–75, 1996.

[142] Paul J Mintz, Scott D Patterson, Andrew F Neuwald, Chris S Spahr, and David L Spector. Purification and biochemical characterization of interchromatin granule clusters. 18(15):4308–4320, 1999.

[143] Angus I Lamond and David L Spector. Nuclear speckles: a model for nuclear organelles. *Nature reviews. Molecular cell biology*, 4(8):605–612, 2003.

[144] C David Allis and Thomas Jenuwein. The molecular hallmarks of epigenetic control. *Nature reviews. Genetics*, 17(8):1–14, 2016.

[145] Thomas Gerken, Christophe a Girard, Yi-Chun Loraine Tung, Celia J Webby, Vladimir Saudek, Kirsty S Hewitson, Giles S H Yeo, Michael a McDonough, Sharon Cunliffe, Luke a McNeill, Juris Galvanovskis, Patrik Rorsman, Peter Robins, Xavier Prieur, Anthony P Coll, Marcella Ma, Zorica Jovanovic, I Sadaf Fa-

rooqi, Barbara Sedgwick, Inês Barroso, Tomas Lindahl, Chris P Ponting, Frances M Ashcroft, Stephen O'Rahilly, and Christopher J Schofield. The obesity-associated FTO gene encodes a 2-oxoglutarate-dependent nucleic acid demethylase. *Science (New York, N.Y.)*, 318(5855):1469–72, nov 2007.

[146] Luis Sanchez-Pulido and Miguel a Andrade-Navarro. The FTO (fat mass and obesity associated) gene codes for a novel member of the non-heme dioxygenase superfamily. *BMC biochemistry*, 8(Ii):23, jan 2007.

[147] Guifang Jia, Cai-Guang Yang, Shangdong Yang, Xing Jian, Chengqi Yi, Zhiqiang Zhou, and Chuan He. Oxidative demethylation of 3-methylthymine and 3-methyluracil in single-stranded DNA and RNA by mouse and human FTO. *FEBS letters*, 582(23-24):3313–9, oct 2008.

[148] Zhifu Han, Tianhui Niu, Junbiao Chang, Xiaoguang Lei, Mingyan Zhao, Qiang Wang, Wei Cheng, Jinjing Wang, Yi Feng, and Jijie Chai. Crystal structure of the FTO protein reveals basis for its substrate specificity. *Nature*, 464(7292):1205–9, apr 2010.

[149] Timothy M. Frayling, Nicholas J. Timpson, Michael N. Weedon, Eleftheria Zeggini, Rachel M. Freathy, Cecilia M. Lindgren, John R. B. Perry, Katherine S. Elliott, Hana Lango, Nigel W. Rayner, Beverley Shields, Lorna W. Harries, Jeffrey C. Barrett, Sian Ellard, Christopher J. Groves, Bridget Knight, Ann-Marie Patch, Andrew R. Ness, Shah Ebrahim, Debbie a. Lawlor, Susan M. Ring, Yoav Ben-Shlomo, Marjo-Riitta Jarvelin, Ulla Sovio, Amanda J. Bennett, David Melzer, Luigi Ferrucci, Ruth J. F. Loos, Inês Ines Barroso, Nicholas J. Wareham, Fredrik Karpe, Katharine R. Owen, Lon R. Cardon, Mark Walker, Graham a. Hitman, Colin N a Palmer, Alex S. F. Doney, Andrew D Morris, George Davey Smith, Andrew T. Hattersley, Mark I. McCarthy, Z. Frayling, T. M., Nicholas, J. T., Michael, N. W., Eleftheria, S. E. Rachel, M. F., Cecilia, M. L., John, R. B. P., Katherine, C. B. Hana, L., Nigel, W. R., Beverley, S., Lorna, W. H., Jeffrey, R. N. Sian, E., Christopher, J. G., Bridget, K., Ann-Marie, P., Andrew, B. Shah, E., Debbie, A. L., Susan, M. R., Yoav, M. Marjo-Riitta, J., Ulla, S., Amanda, J. B., David, K. Luigi, F., Ruth, J. F. L., Inês, B., Nicholas, J. W., Fredrik, a. H. Katharine, R. O., Lon, R. C., Mark, W., Graham, D. S. Colin, N. A. P., Alex, S. F. D., Andrew, D. M., George, and I. M. The Wellcome Trust Case Control Consortium, Andrew, T. H. & Mark. A Common Variant in the FTO Gene Is Associated with Body Mass Index and Predisposes to Childhood and Adult Obesity. *Science*, 316(April):889–894, 2007.

[150] Christian Dina, David Meyre, Sophie Gallina, Emmanuelle Durand, Antje Körner, Peter Jacobson, Lena M S Carlsson, Wieland Kiess, Vincent Vatin, Cecile Lecoeur, Jérome Delplanque, Emmanuel Vaillant, François Pattou, Juan Ruiz, Jacques Weill, Claire Levy-Marchal, Fritz Horber, Natascha Potoczna, Serge Hercberg, Catherine Le Stunff, Pierre Bougnères, Peter Kovacs, Michel Marre, Beverley

Balkau, Stéphane Cauchi, Jean-Claude Chèvre, and Philippe Froguel. Variation in FTO contributes to childhood obesity and severe adult obesity. *Nature Genetics*, 39(6):724–726, 2007.

[151] Julia Fischer, Linda Koch, Christian Emmerling, Jeanette Vierkotten, Thomas Peters, Jens C Brüning, and Ulrich Rüther. Inactivation of the Fto gene protects from obesity. *Nature*, 458(7240):894–8, apr 2009.

[152] Pawan Gulati, Man Ka Cheung, Robin Antrobus, Chris D Church, Heather P Harding, Yi-Chun Loraine Tung, Debra Rimmington, Marcella Ma, David Ron, Paul J Lehner, Frances M Ashcroft, Roger D Cox, Anthony P Coll, Stephen O'Rahilly, and Giles S H Yeo. Role for the obesity-related FTO gene in the cellular sensing of amino acids. *Proceedings of the National Academy of Sciences of the United States of America*, 110(7):2557–62, feb 2013.

[153] Xu Zhao, Ying Yun-Gui Yang, Bao-Fa Sun, Yue Shi, Xin Yang, Wen Xiao, Ya-Juan Hao, Xiao-Li Ping, Yu-Sheng Chen, Wen-Jia Wang, Kang-Xuan Jin, Xing Xiu-Jie Wang, Chun-Min Huang, Yu Fu, Xiao-Meng Ge, Shu-Hui Song, Hyun Seok Jeong, Hiroyuki Yanagisawa, Yamei Niu, Gui-Fang Jia, Wei Wu, Wei-Min Tong, Akimitsu Okamoto, Chuan He, Jannie M Rendtlew Danielsen, Xing Xiu-Jie Wang, and Ying Yun-Gui Yang. FTO-dependent demethylation of N6-methyladenosine regulates mRNA splicing and is required for adipogenesis. *Cell research*, 24(12):1403–19, 2014.

[154] Thomas Peters, Katrin Ausmeier, and Ulrich Rüther. Cloning of Fatso (Fto), a novel gene deleted by the fused toes (Ft) mouse mutation. *Mammalian Genome*, 10(10):983–986, 1999.

[155] Predrag Vujovic, Stefan Stamenkovic, Nebojsa Jasnic, Iva Lakic, Sinisa F Djurasevic, Gordana Cvijic, and Jelena Djordjevic. Fasting induced cytoplasmic Fto expression in some neurons of rat hypothalamus. *PloS one*, 8(5):e63694, jan 2013.

[156] Mamta Tahiliani, Kian Peng Koh, Yinghua Shen, William A Pastor, Hozefa Bandukwala, Yevgeny Brudno, Suneet Agarwal, Lakshminarayan M Iyer, David R Liu, L Aravind, and Anjana Rao. Conversion of 5-methylcytosine to 5-hydroxymethylcytosine in mammalian DNA by MLL partner TET1. *Science (New York, N.Y.)*, 324(5929):930–5, 2009.

[157] Myunggon Ko, Yun Huang, Anna M Jankowska, Utz J Pape, Mamta Tahiliani, Hozefa S Bandukwala, Jungeun An, Edward D Lamperti, Kian Peng Koh, Rebecca Ganetzky, X Shirley Liu, L Aravind, Suneet Agarwal, Jaroslaw P Maciejewski, and Anjana Rao. Impaired hydroxylation of 5-methylcytosine in myeloid cancers with mutant TET2. *Nature*, 468(7325):839–43, 2010.

[158] Junjie U. Guo, Yijing Su, Chun Zhong, Guo Li Ming, and Hongjun Song. Hydroxylation of 5-methylcytosine by TET1 promotes active DNA demethylation in the adult brain. *Cell*, 145(3):423–434, 2011.

[159] Mark Wossidlo, Toshinobu Nakamura, Konstantin Lepikhov, C Joana Marques, Valeri Zakhartchenko, Michele Boiani, Julia Arand, Toru Nakano, Wolf Reik, and Jörn Walter. 5-Hydroxymethylcytosine in the mammalian zygote is linked with epigenetic reprogramming. *Nature communications*, 2:241, 2011.

[160] Shinsuke Ito, Li Shen, Qing Dai, Susan C Wu, Leonard B Collins, James A Swenberg, Chuan He, and Yi Zhang. Tet Proteins Can Convert 5-Methylcytosine to 5-Formylcytosine and 5-Carboxylcytosine. *Science*, 333(6047):1300–1303, 2011.

[161] Ye Fu, Guifang Jia, Xueqin Pang, Richard N Wang, Xiao Wang, Charles J Li, Scott Smemo, Qing Dai, Kathleen a Bailey, Marcelo a Nobrega, Ke-Li Han, Qiang Cui, and Chuan He. FTO-mediated formation of N6-hydroxymethyladenosine and N6-formyladenosine in mammalian RNA. *Nature communications*, 4:1798, jan 2013.

[162] Chong Feng, Yang Liu, Guoqiang Wang, Zengqin Deng, Qi Zhang, Wei Wu, Yufeng Tong, Changmei Cheng, and Zhongzhou Chen. Crystal structures of the human RNA demethylase alkbh5 reveal basis for substrate recognition. *Journal of Biological Chemistry*, 289(17):11571–11583, 2014.

[163] WeiShen Aik, John S Scotti, Hwanho Choi, Lingzhi Gong, Marina Demetriades, Christopher J Schofield, and Michael A McDonough. Structure of human RNA NâĄű-methyladenine demethylase ALKBH5 provides insights into its mechanisms of nucleic acid recognition and demethylation. *Nucleic acids research*, 42(7):4741–54, 2014.

[164] Weizhong Chen, Liang Zhang, Guanqun Zheng, Ye Fu, Quanjiang Ji, Fange Liu, Hao Chen, and Chuan He. Crystal structure of the RNA demethylase ALKBH5 from zebrafish. *FEBS Letters*, 588(6):892–898, 2014.

[165] Yanan Yue, Jianzhao Liu, and Chuan He. RNA N6-methyladenosine methylation in post-transcriptional gene expression regulation. *Yue, Y., Liu, J., & He, C. (2015). RNA N6-methyladenosine methylation in post-transcriptional gene expression regulation. Genes and Development, 29, 1343âĂŞ1355. doi:10.1101/gad.262766.115.GENESGenes and Development*, 29:1343–1355, 2015.

[166] Joseph A Bokar, Mary Eileen Rath-shambaugh, Rachael Ludwiczak, Prema Narayann, and Fritz Rottmanll. Characterization and Partial Purification of mRNA N6-Adenosine Methyltransferase from

HeLa Cell Nuclei. *The Journal of biological chemistry*, 1994.

[167] J A Bokar, M E Shambaugh, and D Polayes. Purification and cDNA cloning of the AdoMet-binding subunit of the human mRNA (N6-adenosine)-methyltransferase. pages 1233–1247, 1997.

[168] Jianzhao Liu, Yanan Yue, Dali Han, Xiao Wang, Ye Fu, Liang Zhang, Guifang Jia, Miao Yu, Zhike Lu, Xin Deng, Qing Dai, Weizhong Chen, and Chuan He. A METTL3-METTL14 complex mediates mammalian nuclear RNA N6-adenosine methylation. *Nature chemical biology*, 10(2):93–5, feb 2014.

[169] Yang Wang, Yue Li, Julia I Toth, Matthew D Petroski, Zhaolei Zhang, and Jing Crystal Zhao. N6-methyladenosine modification destabilizes developmental regulators in embryonic stem cells. *Nature cell biology*, 16(2):191–8, feb 2014.

[170] Xiao-Li Ping, Bao-Fa Sun, Lu Wang, Wen Xiao, Xin Yang, Wen-Jia Wang, Samir Adhikari, Yue Shi, Ying Lv, Yu-Sheng Chen, Xu Zhao, Ang Li, Ying Yang, Ujwal Dahal, Xiao-Min Lou, Xi Liu, Jun Huang, Wei-Ping Yuan, Xiao-Fan Zhu, Tao Cheng, Yong-Liang Zhao, Xinquan Wang, Jannie M Rendtlew Danielsen, Feng Liu, and Yun-Gui Yang. Mammalian WTAP is a regulatory subunit of the RNA N6-methyladenosine methyltransferase. *Cell research*, 24(2):177–89, mar 2014.

[171] Shay Geula, Sharon Moshitch-Moshkovitz, Dan Dominissini, Abed AlFatah Mansour, Nitzan Kol, Mali Salmon-Divon, Vera Hershkovitz, Eyal Peer, Nofar Mor, Yair S Manor, Moshe Shay Ben-Haim, Eran Eyal, Sharon Yunger, Yishay Pinto, Diego Adhemar Jaitin, Sergey Viukov, Yoach Rais, Vladislav Krupalnik, Elad Chomsky, Mirie Zerbib, Itay Maza, Yoav Rechavi, Rada Massarwa, Suhair Hanna, Ido Amit, Erez Y Levanon, Ninette Amariglio, Noam Stern-Ginossar, Noa Novershtern, Gideon Rechavi, and Jacob H Hanna. Stem cells. m6A mRNA methylation facilitates resolution of naïve pluripotency toward differentiation. *Science (New York, N.Y.)*, 347(6225):1002–6, 2015.

[172] Cintia F Hongay and Terry L Orr-Weaver. Drosophila Inducer of MEiosis 4 (IME4) is required for Notch signaling during oogenesis. *Proceedings of the National Academy of Sciences of the United States of America*, 108(36):14855–60, sep 2011.

[173] Silin Zhong, Hongying Li, Zsuzsanna Bodi, James Button, Laurent Vespa, Michel Herzog, and Rupert G Fray. MTA is an Arabidopsis messenger RNA adenosine methylase and interacts with a homolog of a sex-specific splicing factor. *The Plant cell*, 20(5):1278–88, may 2008.

[174] Pedro J Batista, Benoit Molinie, Cosmas C Giallourakis, Y Howard, Jinkai Wang, Kun Qu, Jiajing Zhang, Lingjie Li, Donna M Bouley, Peter Dedon, Marius Wernig, Alan C Mullen, Yi Xing, and Howard Y Chang. m 6 A RNA Modification Controls Cell Fate Transition in Mammalian Embryonic Stem Cells Article m

6 A RNA Modification Controls Cell Fate Transition in Mammalian Embryonic Stem Cells. pages 707–719, 2014.

[175] Jacob Hanna, Styliani Markoulaki, Maisam Mitalipova, Albert W. Cheng, John P. Cassady, Judith Staerk, Bryce W. Carey, Christopher J. Lengner, Ruth Foreman, Jennifer Love, Qing Gao, Jongpil Kim, and Rudolf Jaenisch. Metastable Pluripotent States in NOD-Mouse-Derived ESCs. *Cell Stem Cell*, 4(6):513–524, 2009.

[176] Jamie A. Hackett and M. Azim Surani. Regulatory principles of pluripotency: From the ground state up, 2014.

[177] Boxuan Simen Zhao and Chuan He. Fate by RNA methylation: m6A steers stem cell pluripotency. *Genome biology*, 16:43, 2015.

[178] Mary J Clancy, Mary Eileen Shambaugh, Candace S Timpte, and Joseph A Bokar. Induction of sporulation in Saccharomyces cerevisiae leads to the formation of N6-methyladenosine in mRNA: a potential mechanism for the activity of the IME4 gene. *Nucleic acids research*, 30(20):4509–18, oct 2002.

[179] Zsuzsanna Bodi, James D Button, Donald Grierson, and Rupert G Fray. Yeast targets for mRNA methylation. *Nucleic acids research*, 38(16):5327–35, sep 2010.

[180] Holger Dinkel, Kim Van Roey, Sushama Michael, Norman E. Davey, Robert J. Weatheritt, Diana Born, Tobias Speck, Daniel Krüger, Gleb Grebnev, Marta Kubań, Marta Strumillo, Bora Uyar, Aidan Budd, Brigitte Altenberg, Markus Seiler, Lucía B. Chemes, Juliana Glavina, Ignacio E. Sánchez, Francesca Diella, and Toby J. Gibson. The eukaryotic linear motif resource ELM: 10 years and counting. *Nucleic Acids Research*, 42(D1), 2014.

[181] Holger Dinkel, Kimvan Roey, Sushama Michael, Manjeet Kumar, Bora Uyar, Brigitte Altenberg, Vladislava Milchevskaya, Melanie Schneider, Helen Kühn, Annika Behrendt, Sophie Luise Dahl, Victoria Damerell, Sandra Diebel, Sara Kalman, Steffen Klein, Arne C. Knudsen, Christina Mäder, Sabina Merrill, Angelina Staudt, Vera Thiel, Lukas Welti, Norman E. Davey, Francesca Diella, and Toby J. Gibson. ELM 2016 - Data update and new functionality of the eukaryotic linear motif resource. *Nucleic Acids Research*, 44(D1):D294–D300, 2016.

[182] Janusz M. Bujnicki, Marcin Feder, Monika Radlinska, and Robert M. Blumenthal. Structure prediction and phylogenetic analysis of a functionally diverse family of proteins homologous to the MT-A70 subunit of the human mRNA:m6A methyltransferase. *Journal of Molecular Evolution*, 55(4):431–444, 2002.

[183] a Lupas, M Van Dyke, and J Stock. Predicting coiled coils from protein sequences. *Science (New York, N.Y.)*, 252(5010):1162–4, 1991.

[184] René E M A Van Herpen, Jorrit V. Tjeertes, Susan A M Mulders, Ralph J A Oude Ophuis, Bé Wieringa, and Derick G. Wansink. Coiled-coil interactions modulate multimerization, mitochondrial binding and kinase activity of myotonic dystrophy protein kinase splice isoforms. *FEBS Journal*, 273(6):1124–1136, 2006.

[185] Barbara Ciani, Saša Bjelic, Srinivas Honnappa, Hatim Jawhari, Rolf Jaussi, Aishwarya Payapilly, Thomas Jowitt, Michel O Steinmetz, and Richard a Kammerer. Molecular basis of coiled-coil oligomerization-state specificity. *Proceedings of the National Academy of Sciences of the United States of America*, 107(46):19850–19855, 2010.

[186] J. Jefferson P Perry, Aroumougame Asaithamby, Adam Barnebey, Foad Kiamanesch, David J. Chen, Seungil Han, John A. Tainer, and Steven M. Yannone. Identification of a coiled coil in Werner syndrome protein that facilitates multimerization and promotes exonuclease processivity. *Journal of Biological Chemistry*, 285(33):25699–25707, 2010.

[187] Allison Lange, Ryan E. Mills, Christopher J. Lange, Murray Stewart, Scott E. Devine, and Anita H. Corbett. Classical nuclear localization signals: Definition, function, and interaction with importin ??, 2007.

[188] M. Latimer, M.K. Ernst, L.L. Dunn, M. Drutskaya, and N.R. Rice. The N-terminal domain of IκBα masks the nuclear localization signal(s) of p50 and c-Rel homodimers. *Molecular and Cellular Biology*, 18(5), 1998.

[189] Lili Gu, Takahiro Tsuji, Mohamed Ali Jarboui, Geok P Yeo, Noreen Sheehy, William W Hall, and Virginie W Gautier. Intermolecular masking of the HIV-1 Rev NLS by the cellular protein HIC : Novel insights into the regulation of Rev nuclear import. *Retrovirology*, 8(17):1–13, 2011.

[190] Jean-Michel Fustin, Masao Doi, Yoshiaki Yamaguchi, Hayashi Hida, Shinichi Nishimura, Minoru Yoshida, Takayuki Isagawa, Masaki Suimye Morioka, Hideaki Kakeya, Ichiro Manabe, and Hitoshi Okamura. RNA-methylation-dependent RNA processing controls the speed of the circadian clock. *Cell*, 155(4):793–806, nov 2013.

[191] Ping Wang, Katelyn A. Doxtader, and Yunsun Nam. Structural Basis for Cooperative Function of Mettl3 and Mettl14 Methyltransferases, 2016.

[192] Xiang Wang, Jing Feng, Yuan Xue, Zeyuan Guan, Delin Zhang, Zhu Liu, Zhou Gong, Qiang Wang, Jinbo Huang, Chun Tang, Tingting Zou, and Ping Yin. Structural basis of N6-adenosine methylation by the METTL3-METTL14 complex. *Nature*, pages 1–15, 2016.

[193] Andrea Sinz. Chemical cross-linking and mass spectrometry to map three-dimensional protein structures and protein-protein interactions. *Mass Spectrometry Reviews*, 25(4):663–682, 2006.

[194] Alexander Leitner, Thomas Walzthoeni, Abdullah Kahraman, Franz Herzog, Oliver Rinner, Martin Beck, and Ruedi Aebersold. Probing Native Protein Structures by Chemical Cross-linking, Mass Spectrometry, and Bioinformatics. *Molecular & Cellular Proteomics : MCP*, 9(8):1634–1649, 2010.

[195] S S Szegedi and R I Gumport. DNA binding properties in vivo and target recognition domain sequence alignment analyses of wild-type and mutant RsrI [N6-adenine] DNA methyltransferases. *Nucleic acids research*, 28:3972–3981, 2000.

[196] Yoshikazu Furuta, Mikihiko Kawai, Ikuo Uchiyama, and Ichizo Kobayashi. Domain movement within a gene: A novel evolutionary mechanism for protein diversification. *PLoS ONE*, 6(4), 2011.

[197] Deepak P. Patil, Chun-Kan Chen, Brian F. Pickering, Amy Chow, Constanza Jackson, Mitchell Guttman, and Samie R. Jaffrey. m6A RNA methylation promotes XIST-mediated transcriptional repression. *Nature*, pages 1–25, 2016.

[198] Hairui Su, Yanyan Liu, and Xinyang Zhao. Split End Family RNA Binding Proteins: Novel Tumor Suppressors Coupling Transcriptional Regulation with RNA Processing. *Cancer Translational Medicine*, pages 21–25, 2015.

[199] Tina Lence, Junaid Akhtar, Marc Bayer, Katharina Schmid, Laura Spindler, Cheuk Hei Ho, Nastasja Kreim, Miguel A. Andrade-Navarro, Burkhard Poeck, Mark Helm, and Jean-Yves Roignant. m6A modulates neuronal functions and sex determination in Drosophila. *Nature*, 540(7632):242–247, 2016.

[200] Jody M. Mason and Katja M. Arndt. Coiled coil domains: Stability, specificity, and biological implications. *ChemBioChem*, 5(2):170–176, 2004.

[201] Kurt Wagschal, Brian Tripet, Colin Mant, Robert S. Hodges, and Pierre Lavigne. The role of position a in determining the stability and oligomerization state of Îś-helical coiled coils: 20 amino acid stability coefficients in the hydrophobic core of proteins. *Protein Science*, 8(11):2312–2329, 1999.

[202] Brian Tripet, Kurt Wagschal, Pierre Lavigne, Colin T. Mant, and Robert S. Hodges. Effects of side-chain characteristics on stability and oligomerization state of a de Novo-designed model coiled-coil:

20 amino acid substitutions in position âĂIJdâĂİ. *Journal of Molecular Biology*, 300(2):377–402, 2000.

[203] K T O'Neil and W F DeGrado. A thermodynamic scale for the helix-forming tendencies of the commonly occurring amino acids. *Science (New York, N.Y.)*, 250(4981):646–51, 1990.

[204] D Kalderon, W D Richardson, a F Markham, and a E Smith. Sequence requirements for nuclear location of simian virus 40 large-T antigen. *Nature*, 311:33–38, 1984.

[205] Elena Conti and John Kuriyan. Crystallographic analysis of the specific yet versatile recognition of distinct nuclear localization signals by karyopherin α. *Structure*, 8(3):329–338, 2000.

[206] M R Fontes, T Teh, and B Kobe. Structural basis of recognition of monopartite and bipartite nuclear localization sequences by mammalian importin-alpha. *Journal of molecular biology*, 297(5):1183–94, 2000.

[207] Fa Ann Ran, Patrick D Pd Patrick D Hsu, Jason Wright, Vineeta Agarwala, David a Scott, and Feng Zhang. Genome engineering using the CRISPR-Cas9 system. *Nature protocols*, 8(11):2281–308, 2013.

[208] Shuibin Lin, Junho Choe, Peng Du, Robinson Triboulet, and Richard I. Gregory. The m6A Methyltransferase METTL3 Promotes Translation in Human Cancer Cells. *Molecular Cell*, 62(3):335–345, 2016.

[209] Tanja La Cour, Lars Kiemer, Anne Mølgaard, Ramneek Gupta, Karen Skriver, and Søren Brunak. Analysis and prediction of leucine-rich nuclear export signals. *Protein Engineering, Design and Selection*, 17(6):527–536, 2004.

[210] Shunichi Kosugi, Masako Hasebe, Masaru Tomita, and Hiroshi Yanagawa. Nuclear export signal consensus sequences defined using a localization-based yeast selection system. *Traffic*, 9(12):2053–2062, 2008.

[211] Darui Xu, Alicia Farmer, and Yuh Min Chook. Recognition of nuclear targetin signals by Karyopherin-b proteins. *Current Opinion in Structural Biology*, 20(6):782–790, 2011.

[212] Daniel Schraivogel, Susann G. Schindler, Johannes Danner, Elisabeth Kremmer, Janina Pfaff, Stefan Hannus, Reinhard Depping, and Gunter Meister. Importin-βfacilitates nuclear import of human GW proteins and balances cytoplasmic gene silencing protein levels. *Nucleic Acids Research*, 43(15):7447–7461, 2015.

[213] D A Jans, T Moll, K Nasmyth, and P Jans. Cyclin-dependent kinase site-regulated signal-dependent nuclear localization of the SW15 yeast transcription factor in mammalian cells. *J Biol Chem*, 270(29):17064–17067, 1995.

[214] Chong Yun Xiao, Stefan Hübner, and David A. Jans. SV40 large tumor antigen nuclear import is regulated by the double- stranded DNA-dependent protein kinase site (Serine 120) flanking the nuclear localization sequence. *Journal of Biological Chemistry*, 272(35):22191–22198, 1997.

[215] David S. Goldfarb, Anita H. Corbett, D. Adam Mason, Michelle T. Harreman, and Stephen A. Adam. Importin α: A multipurpose nuclear-transport receptor, 2004.

[216] Ivan K H Poon and David a Jans. Regulation of nuclear transport: central role in development and transformation? *Traffic (Copenhagen, Denmark)*, 6:173–186, 2005.

[217] Stefan Jäkel and Dirk Görlich. Importin β, transportin, RanBP5 and RanBP7 mediate nuclear import of ribosomal proteins in mammalian cells. *EMBO Journal*, 17(15):4491–4502, 1998.

[218] Yuh Min Chook and Katherine E. Süel. Nuclear import by karyopherin-βs: Recognition and inhibition, 2011.

[219] Joseph A. Bokar, Mary Eileen Rath-Shambaugh, Rachael Ludwiczak, Prema Narayan, and Fritz Rottman. Characterization and partial purification of mRNA N6-adenosine methyltransferase from HeLa cell nuclei: Internal mRNA methylation requires a multisubunit complex. *Journal of Biological Chemistry*, 269(26):17697–17704, 1994.

[220] H. Berghammer and B. Auer. "Easypreps": fast and easy plasmid minipreparation for analysis of recombinant clones in E. coli. *Biotechniques*, Apr; 14(4):524, 528, 1993.

[221] David B Friedman, Sjouke Hoving, and Reiner Westermeier. Isoelectric focusing and two-dimensional gel electrophoresis. *Methods in enzymology*, 463(09):515–40, 2009.

[222] U K Laemmli. Cleavage of structural proteins during the assembly of the head of bacteriophage T4. *Nature*, 227(5259):680–685, 1970.

[223] H Blum, H Beier, and H J Gross. Improved silver staining of plant proteins, RNA and DNA in polyacrylamide gels, 1987.

[224] F. Herzog, A. Kahraman, D. Boehringer, R. Mak, A. Bracher, T. Walzthoeni, A. Leitner, M. Beck, F.-U. Hartl, N. Ban, L. Malmstrom, and R. Aebersold. Structural Probing of a Protein Phosphatase 2A Network by Chemical Cross-Linking and Mass Spectrometry. *Science*, 337(6100):1348–1352, 2012.

[225] Thomas Walzthoeni, Manfred Claassen, Alexander Leitner, Franz Herzog, Stefan Bohn, Friedrich Förster, Martin Beck, and Ruedi Aebersold. False discovery rate estimation for cross-linked peptides identified by mass spectrometry. *Nat Methods*, 9(9):901–903, 2012.

[226] Daniel W A Buchan, Federico Minneci, Tim C O Nugent, Kevin Bryson, and David T. Jones. Scalable web services for the PSIPRED Protein Analysis Workbench. *Nucleic acids research*, 41(Web Server issue), 2013.

Acknowledgments

First of all, I would like to thank Prof. Dr. Gunter Meister for allowing me to complete my doctoral thesis at his institute. I want to express my thanks for allowing me to follow my scientific curiosity and to have a chance to work on cutting-edge projects. I also want to thank Prof. Dr. Joachim Griesenbeck for evaluating this work as a second referee and being part of my PhD examination committee. Down the same line, I also want thank Prof. Dr. Klaus Grasser, Prof. Dr. Herbert Tschochner and Prof. Dr. Wolfgang Seufert for being members of the same examination committee.

I want to address a big thank-you to the whole Biochemistry I department for the very interesting four and a half years. I want to thank Dr. Thomas Treiber and Dr. Nora Treiber for their great help during the practical part of this work. I also would like to thank Franzi, Eva, Dani and Danner for the amusing moments in the department and for creating an enjoyable and lively atmosphere while working at the bench. Besides the AG Meister, I would like to thank all the members of the AG Medenbach and AG Kretz for being great colleagues (both personally as well as professionally). I would like to especially thank Markus for his efforts in mentoring me during my time in Regensburg, for the great scientific discussions and for the very interesting kicker-matches (go panda-agility!).

I also want to thank my dearest friend Pascal Hermes for his unceasing friendship over the last 20 years. The stimulating conversations after a hard day in the lab always helped me when I needed a fresh perspective. Great thanks also goes to Alicia Lis for her loyalty and friendship. I very much appreciate the advice and patient she has provided me over the recent years.

My biggest thanks goes to my mother Ursula. Thank you for your limitless love and support that I have experienced throughout my whole life. I also thank you for the tremendous efforts you have made over the last 20 years that enabled me to reach my goals and made me the person that I am today.